

Spring 1988

Chemical and mineralogical transformations accompanying the weathering of retorted oil shale

Irene Elizabeth McGee
University of New Hampshire, Durham

Follow this and additional works at: <https://scholars.unh.edu/dissertation>

Recommended Citation

McGee, Irene Elizabeth, "Chemical and mineralogical transformations accompanying the weathering of retorted oil shale" (1988).
Doctoral Dissertations. 1539.
<https://scholars.unh.edu/dissertation/1539>

This Dissertation is brought to you for free and open access by the Student Scholarship at University of New Hampshire Scholars' Repository. It has been accepted for inclusion in Doctoral Dissertations by an authorized administrator of University of New Hampshire Scholars' Repository. For more information, please contact nicole.hentz@unh.edu.

INFORMATION TO USERS

The most advanced technology has been used to photograph and reproduce this manuscript from the microfilm master. UMI films the original text directly from the copy submitted. Thus, some dissertation copies are in typewriter face, while others may be from a computer printer.

In the unlikely event that the author did not send UMI a complete manuscript and there are missing pages, these will be noted. Also, if unauthorized copyrighted material had to be removed, a note will indicate the deletion.

Oversize materials (e.g., maps, drawings, charts) are reproduced by sectioning the original, beginning at the upper left-hand corner and continuing from left to right in equal sections with small overlaps. Each oversize page is available as one exposure on a standard 35 mm slide or as a 17" × 23" black and white photographic print for an additional charge.

Photographs included in the original manuscript have been reproduced xerographically in this copy. 35 mm slides or 6" × 9" black and white photographic prints are available for any photographs or illustrations appearing in this copy for an additional charge. Contact UMI directly to order.



Accessing the World's Information since 1938

300 North Zeeb Road, Ann Arbor, MI 48106-1346 USA

Order Number 8816694

**Chemical and mineralogical transformations accompanying the
weathering of retorted oil shale**

McGee, Irene Elizabeth, Ph.D.

University of New Hampshire, 1988

U·M·I
300 N. Zeeb Rd.
Ann Arbor, MI 48106

PLEASE NOTE:

In all cases this material has been filmed in the best possible way from the available copy. Problems encountered with this document have been identified here with a check mark .

1. Glossy photographs or pages _____
2. Colored illustrations, paper or print _____
3. Photographs with dark background
4. Illustrations are poor copy
5. Pages with black marks, not original copy
6. Print shows through as there is text on both sides of page _____
7. Indistinct, broken or small print on several pages
8. Print exceeds margin requirements _____
9. Tightly bound copy with print lost in spine _____
10. Computer printout pages with indistinct print _____
11. Page(s) _____ lacking when material received, and not available from school or author.
12. Page(s) _____ seem to be missing in numbering only as text follows.
13. Two pages numbered _____. Text follows.
14. Curling and wrinkled pages _____
15. Dissertation contains pages with print at a slant, filmed as received
16. Other _____



CHEMICAL AND MINERALOGICAL TRANSFORMATIONS ACCOMPANYING
THE WEATHERING OF RETORTED OIL SHALE

BY

IRENE E. MCGEE
B.S. College of Mount Saint Vincent, 1982

DISSERTATION

Submitted to the University of New Hampshire
in Partial Fulfillment of
the Requirements for the Degree of

Doctor of Philosophy

in

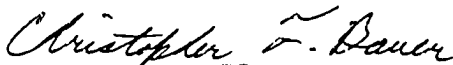
Chemistry

May, 1988

This dissertation has been examined and approved.



Dissertation Director, C. L. Grant
Professor of Chemistry



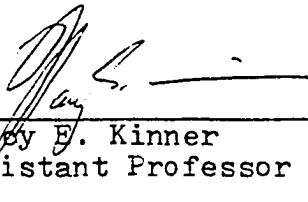
Christopher F. Bauer
Associate Professor of Chemistry



Louise H. Foley
Assistant Professor of Chemistry



Colin D. Hubbard
Professor of Chemistry



Nancy E. Kinner
Assistant Professor of Civil Engineering

7/24/87

Date

TABLE OF CONTENTS

	Page
ACKNOWLEDGEMENTS	iv
LIST OF TABLES	v
LIST OF FIGURES	vi
ABSTRACT	viii
SECTION	
I. INTRODUCTION	1
History	2
Oil Generation And Waste Disposal	3
Retorted Oil Shale (ROS)	5
Leaching Studies	8
Design Of This Study	11
II. EXPERIMENTAL	14
Materials And Reagents	14
Methods	16
Procedures	19
III. RESULTS AND DISCUSSION	23
Introduction	23
Homogeneity Of Rulison Samples	26
Particle Surface Characteristics	30
Bulk Composition Studies	38
X-Ray Diffraction Analysis	38
Differential Thermal Analysis	41
Dissolution Rate Experiments	49
Paraho ROS	52
Rulison ROS	56
IV. CONCLUSIONS	70
Summary Of Results	70
Recommendations For Future Work	71
V. APPENDICES	73
Appendix A . Sampling Experiment	74
Appendix B Differential Thermal Analysis	76
Appendix C Dissolution Rate Experiments	82
VI. REFERENCES	104

ACKNOWLEDGEMENTS

I would like to acknowledge the United States Geological Survey, Denver, Colorado, for the use of a Dionex Model 10 Ion Chromatograph for the research reported here. I would also acknowledge the Cold Regions Research and Engineering Laboratory, Hanover, New Hampshire, for financial support in the form of a research assistantship.

LIST OF TABLES

	Page
Table 1. Composition of unweathered Paraho ROS.	9
Table 2. Summary of experimental conditions for atomic absorption analysis.	17
Table 3. Percent composition of Rulison core 2 ROS.	24
Table 4. Percent composition of Rulison core 6 ROS.	25
Table 5. Estimate of subsampling error for core 7 ROS, 4.7-5.7 ft.	29
Table 6. Summary of DTA results for cores 1,2,3 and 6	46
Table 7. Total anion and cation concentrations in Rulison ROS leachates.	62
Table 8. Percentage of an element extracted from core 2 and core 6 ROS.	63
Table 9. Ratio of leachate concentrations from samples at depth to surface samples after 1 hour.	66

LIST OF FIGURES

	Page
Figure 1. Distribution of oil shale deposits in Colorado, Wyoming and Utah.	4
Figure 2. Hypothetical structure of oil shale.	6
Figure 3. Rulison, Colorado project site showing location of sampling cores.	15
Figure 4. Experimental design of sampling experiment.	28
Figure 5. Scanning electron micrographs of Paraho ROS.	31
Figure 6. Scanning electron micrographs of Core 2 ROS, 5000X.	32
Figure 7. Scanning electron micrographs of Core 2 ROS, 10000X.	33
Figure 8. EDAX Ca maps of Rulison ROS samples.	36
Figure 9. EDAX Ca maps of Rulison ROS samples and Paraho samples.	37
Figure 10. X-ray diffractograms of Paraho unweathered ROS and laboratory weathered ROS.	39
Figure 11. DTA results for pure calcite, and two forms of laboratory precipitated calcite.	43
Figure 12. DTA results for Core 6 ROS.	45
Figure 13. Correlation of peak width/area to % calcite.	47
Figure 14. Correlation of peak width/area to extractable Na.	48
Figure 15. Correlation of % calcite to extractable Na.	50
Figure 16. Sodium dissolution rate curve for Paraho unweathered ROS.	53
Figure 17. Sulfate dissolution rate curve for Paraho unweathered ROS.	54
Figure 18. Magnesium dissolution rate curve for Paraho unweathered ROS.	55
Figure 19. Sodium dissolution rate curves: Core 2 samples.	57

Figure 20. Magnesium dissolution rate curves: Core 2 samples.	59
Figure 21. Sulfate dissolution rate curves: Core 2 samples.	60
Figure 22. Ratio of Na to Mg in leachate with time, Core 2 samples.	67
Figure 23. Ratio of Na to Mg in leachate with time, Core 6 samples.	68

ABSTRACT

CHEMICAL AND MINERALOGICAL TRANSFORMATIONS ACCOMPANYING THE WEATHERING OF RETORTED OIL SHALE

BY

Irene E. McGee
University of New Hampshire, May, 1988

The development of western oil shale reserves will present major environmental problems due to the generation of huge quantities of mineral waste (retorted oil shale). The goals of this study are to investigate the extent of weathering within a retorted oil shale (ROS) spoil pile, in order to better understand the long term environmental impact of the material.

The U. S. Bureau of Mines operated a pilot scale retort facility in Rulison, Colorado from 1926 to 1929. Core samples from the spoil pile associated with this project were obtained by the U. S. Geological Survey, and serve as the basis for this work. The effects of over 50 years of natural weathering were investigated by using batch equilibration studies to characterize the aqueous dissolution rates of analytes from samples obtained at different depths in the spoil pile. In support of the dissolution studies, differential thermal analysis and scanning electron microscopy with energy dispersive x-ray analysis were used to examine changes in the composition and morphologies of the particles.

Dissolution rate curves, in conjunction with scanning electron microscopy, suggest the existence of different phases of an ROS particle. A highly weathered surface sample consists of two phases; the bulk silicate mineral matrix which is only very slowly soluble, and a second

phase external to the bulk which consists primarily of readily soluble salts. In contrast, subsurface samples which are not highly weathered, often contain a third phase, formed from the translocation and redeposition of material at various depths. Rates of dissolution depend on the phase from which the analyte originates, although solubility and ion exchange equilibria contribute to the shapes of the dissolution curves.

Weathering processes have not significantly altered the major mineral composition of ROS as yet. The mineral matrix itself has remained largely intact. However, laboratory weathering studies and x-ray diffraction analysis suggest that accelerated weathering of the silicate mineral matrix will occur in the presence of these highly alkaline leachates.

INTRODUCTION

Development of an oil shale industry will require the solution of many environmental problems. Of primary concern is retorted oil shale (ROS), the mineral waste produced during oil shale pyrolysis. Disposal of this waste presents a formidable problem due to the huge quantities involved, and the expected adverse environmental impact caused by leaching of soluble constituents from spoil piles into surface and groundwaters. A mature oil shale industry producing one million barrels of oil per day will generate 1.2 million tons per day of ROS (Tang and Yen, 1979). Disposal and stabilization of this potentially toxic spent shale is possibly the greatest challenge facing the industry today.

Geochemical weathering proceeds in response to the local chemical environment. Minerals exposed to the atmosphere are vulnerable to attack by water, oxygen, and carbon dioxide primarily because some of their constituents are dissolved and effectively removed from the immediate environment. As these processes advance with time, the residue is progressively enriched in less soluble constituents as well as in oxygen and hydroxyl groups. Ultimately, recrystallization of the residue produces new mineral phases which are in equilibrium with prevailing atmospheric conditions (Loughnan, 1969).

Undoubtedly, the most important factor controlling the rate of breakdown of parent minerals and the formation of secondary products is the quantity of water leaching through the weathering environment, in this case, a mineral spoil pile. Percolation of rain and snowmelt will remove the soluble constituents released by hydrolysis at mineral

surfaces, and permit weathering reactions to proceed toward completion (Loughnan, 1969). Soluble constituents either move downward through the spoil pile or they are carried in surface runoff, ultimately reaching subsurface waters.

It is important for predictive purposes to understand the mechanisms of solubilization, redistribution, and transformation of inorganic and organic constituents of ROS after disposal. Specifically, we require an understanding of: 1) the factors which control the rate and extent of leaching; 2) the chemical composition of ROS leachates; 3) the environmental lifetimes of leachate constituents and their degradation products; and 4) possible modes of impact on the environment.

Many factors will affect leachate chemistry and transport in ROS spoil piles. These include: 1) identities, concentrations, and solubilities of the minerals present; 2) size distributions and physical forms of these minerals; 3) the prevalent solution equilibria; 4) seasonal precipitation patterns; 5) the degree of surface runoff and/or run-in, which is related to the degree of compaction of the pile; 6) plant cover; 7) frequency and duration of freeze-thaw and wet-dry cycles (Skogerboe et.al., 1979). Clearly, characterization of transformation and transport behavior of constituents of an ROS spoil pile, and identification of long-term weathering effects, is a complex problem. However, its investigation is essential to the development of an environmentally acceptable oil shale industry.

History

Oil shale represents one of the largest undeveloped fossil energy resources in the United States. It is estimated that high grade shale

(25 gallons of syncrude per ton of shale) capable of providing over 600 billion barrels of oil exists in the Green River Formation of Colorado, Wyoming and Utah. The richest of these deposits are located in the Piceance Creek Basin of western Colorado (Figure 1). In addition, 1600 billion barrels are estimated to exist in low grade (25 gallons per ton) shale in the continental U.S. (Ettinger, 1981).

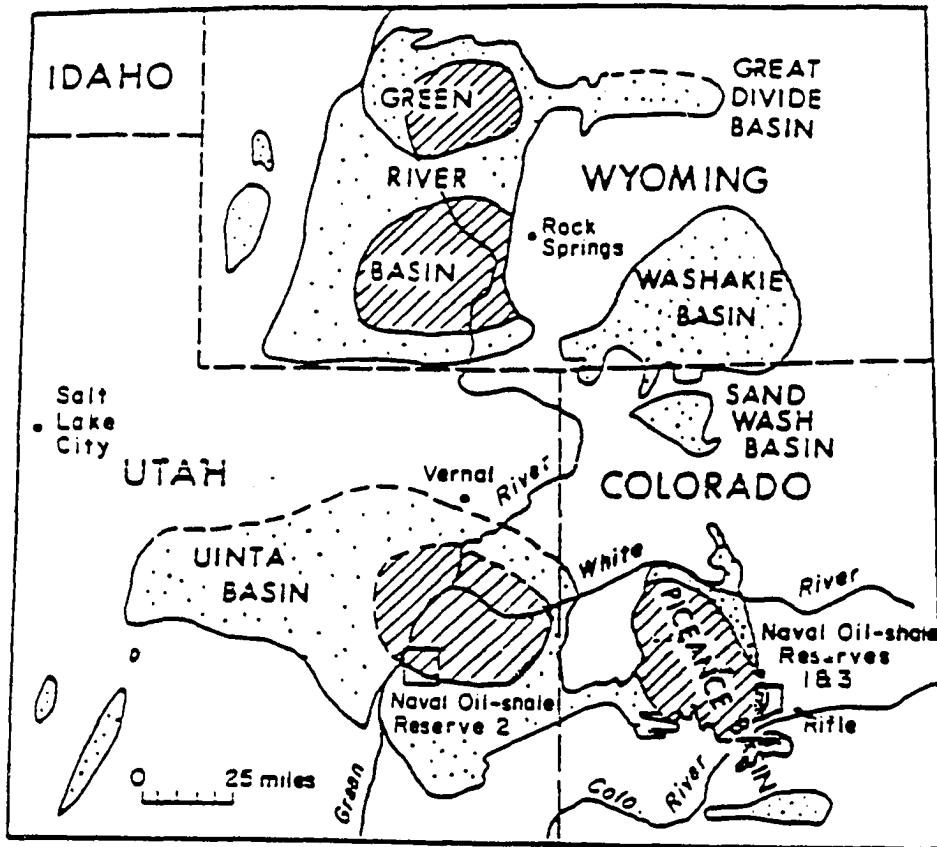
Research on oil shale technology has been conducted in the U. S. since 1916, largely under the leadership of the U. S. Bureau of Mines. Improved mining, retorting, and reclamation technology has been developed under industrial and government sponsorship. The 1970's saw renewed interest in oil shale, and in 1974, the U. S. Department of the Interior leased federal oil shale tracts to several commercial developers.

Despite the current hiatus in development of western oil shale reserves, most informed observers are convinced that these deposits will be tapped within a few years. The Department of Energy recently forecasted a 20% increase in U. S. petroleum consumption by 1995, and a 70% increase in imports in the same period (Haggin, 1984). Failure to increase and develop alternative energy options now could lead to serious problems in the near future.


Oil Generation and Waste Disposal


Oil shale is a rock in which the mineral portion and high molecular weight hydrocarbons are associated in a complex manner. The mineral fraction, classified as a marlstone, makes up about 86% by weight of raw oil shale. Dolomite, feldspar, quartz and illite predominate, with smaller amounts of albite, calcite and pyrite. The remaining 14% is principally the high molecular weight solid hydrocarbon kerogen, with small amounts of bitumen. The minerals are dispersed throughout the

Figure 1. Distribution of Oil Shale Deposits in Colorado, Wyoming and Utah



EXPLANATION

 Area Underlain by the Green River Formation in which the Oil-shale is unappraised or low grade

 Area Underlain Oil-shale more than 10 feet Thick, which Yields 25 gallons or More per ton of Shale

kerogen network (Yen, 1979). A hypothetical structure is shown in Figure 2.

Recovery of oil from shale is accomplished by retorting (thermal decomposition) of the kerogen and bitumen in situ or above ground, followed by separation of syncrude from mineral matter by distillation or solvent extraction. Large quantities of ROS will be produced by both above-ground and in situ retorting. A portion of the retorted shale may be returned below ground, but because of the increase in volume during pyrolysis, surface disposal will be required even where some below ground disposal is feasible.

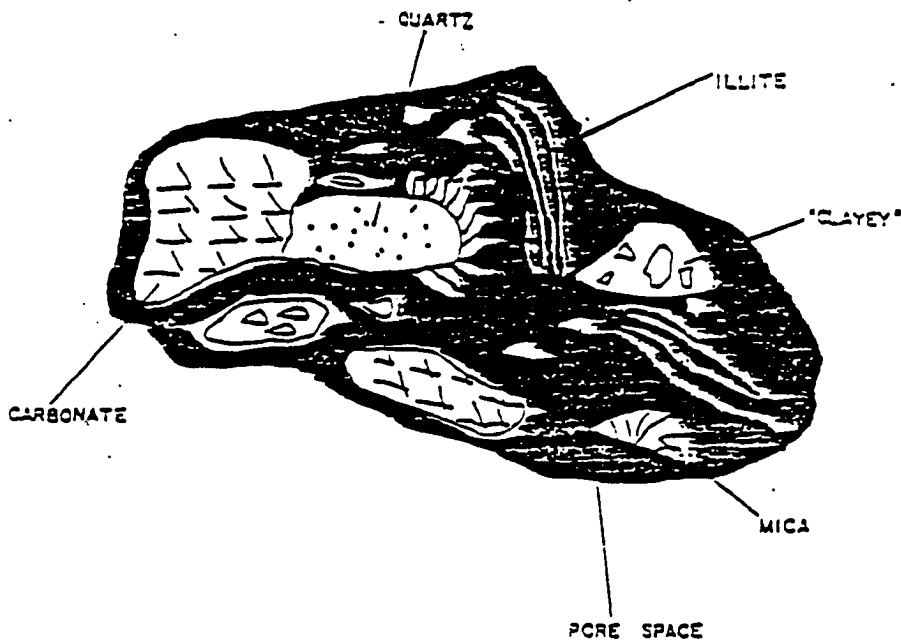
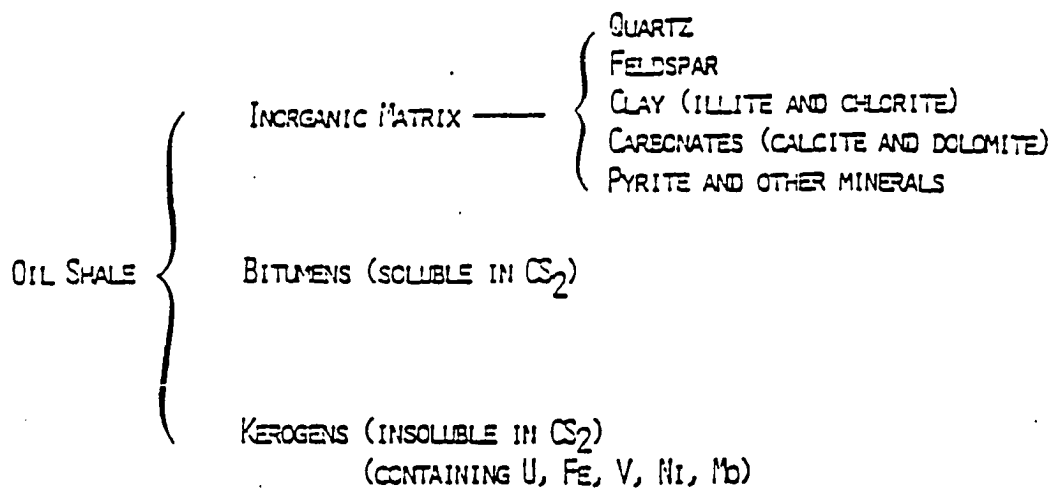
Surface disposal of ROS may result in serious contamination of surface and groundwater as a result of erosion, runoff and percolation through a spoil pile. During high intensity summer storms or spring snowmelt, large quantities of soluble salts are mobilized. When a wetting episode has ceased, evaporation and plant roots will remove moisture from the upper shale layers. Evapotranspiration may cause movement of soluble salts from the moist middle shale layers to the dry upper layers, where salts may be deposited and/or carried away by overland flow, or wind.

Surface stabilization of exposed ROS surfaces has been attempted by establishing vegetation directly on shale or on soil overlaying shale (Harbert et al., 1978; Kilkelly et al., 1982; Stark and Redente, 1986). Concerns are that toxic concentrations of trace elements and salts will migrate toward the soil surface by diffusion or capillary action, and prevent adequate vegetative growth. Stark and Redente noted movement of Na and F salts both upward and downward in topsoil-covered ROS testplots.

Retorted Oil Shale (ROS)

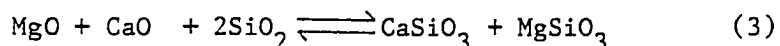
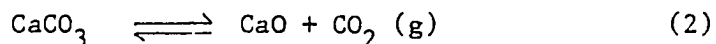
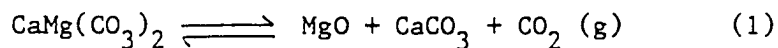
The physical and chemical characteristics of ROS depend on the raw

Figure 2. Hypothetical Structure of Oil Shale (Yen, 1977)



shale mineralogy, the degree to which the raw shale was crushed prior to retorting, and the retorting process itself. For example, aqueous extracts of spent shales retorted at a temperature of 500°C have pH's of 8 to 9, but shales retorted at temperatures of 650°C - 800°C yield extracts with pH's of 11-12 (Richardson et al., 1981).

The elevated temperatures used in oil shale retorting cause mineral transformations. Reactions may initially lead to the formation of water soluble, amorphous oxides, such as CaO and Mg(OH)₂, and subsequently to secondary crystalline mineral phases if requisite temperature and atmospheric conditions are met (Wildung and Zachara, 1981). Reddy and Lindsay used x-ray diffraction analysis to identify different mineral phases of ROS (1985). Results indicate that the processing of oil shales at high temperature destroys carbonate minerals and forms silicate minerals:

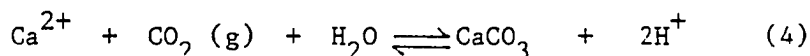


Ca(OH)₂ and MgO minerals were identified in spent shale, but these compounds were absent after equilibrating with water. Their studies suggest that when contacted with water, these minerals dissolve and precipitate as more stable minerals, such as CaMg(SiO₃)₂.

Unweathered ROS particles can be considered to consist of at least two major phases. The bulk silicate mineral matrix is relatively insoluble, but there is a second phase external to the fundamental matrix which consists primarily of readily soluble salts. Weathered ROS may contain a third phase, formed from the translocation and redeposition of material at various depths.

Typical chemical composition data for two size fractions of Paraho unweathered ROS are given in Table 1. Retorted oil shale is highly saline and alkaline as a result of the mineral transformations which occur during retorting. The soluble fraction of ROS which may be up to 10% by weight, is dominated by alkali and alkaline earth salts, mainly sodium and magnesium sulfates (Trujillo et al., 1981). Most of the trace elements in raw shale are conserved in the ROS (Wildung and Zachara, 1981). A major environmental concern is the potential increase in solubility of macro and trace elements as a consequence of the elevated pH. Anionic trace metals such as selenate, arsenate, borate and molybdate can be expected to accompany the dominant soluble salts as serious environmental contaminants. In addition, some retorted oil shales contain up to 5% residual organic carbon by weight. Part of this organic matter is composed of polycyclic compounds and various water soluble metal complexing agents.

Several studies have dealt with recarbonation of retorted shales, which can be expected to occur over time via contact with the atmosphere and groundwater. Reddy et al. (1986) found that recarbonation caused Ca^{2+} to be released from the dissolution of silicate minerals, with the subsequent precipitation of CaCO_3 .



The drop in pH associated with recarbonation has important implications for the solubility of trace elements, and the potential of vegetative stabilization of ROS spoil piles.

Leaching Studies

Investigations of leachate composition have been performed using

Table 1. Composition of Unweathered Paraho ROS (Trujillo et.al., 1981)

<u>Constituent</u>	<u>Percent by Weight</u>	
	18-30 mesh (1.0-0.6 mm)	60-100 mesh (0.25-0.15 mm)
SiO ₂	37.19	37.47
Al ₂ O ₃	8.62	8.61
Fe ₂ O ₃	3.26	3.37
MgO	7.29	7.19
CaO	16.93	15.97
Na ₂ O	3.09	3.30
K ₂ O	2.10	1.98
TiO ₂	0.33	0.34
P ₂ O ₅	0.43	0.27
MnO	0.03	0.03
Loss on Ignition	18.68	18.48
C (total)	6.81	6.98
S (total)	0.71	0.89

both laboratory batch and column studies, and field lysimeter studies (Richardson et al., 1981; Fransway and Wagenet, 1981; Stollenwerk and Runnells, 1981; Trujillo et al., 1981; Bell et al., 1982; Bell et al., 1986). Laboratory leaching studies are not easily compared due to wide variations in experimental variables such as solid/solution ratio, vigor of agitation, and contact time. These variables will affect leachate composition in a complex fashion. However, there are many observations which are common to these studies. The most abundant ions in all ROS leachates are Na^+ , Mg^{2+} , Ca^{2+} , K^+ , and SO_4^{2-} . A major fraction of these constituents is readily leached in the first batch equilibration or first few pore volumes through a column, although there can be large composition modifications due to solubility limitations and ion exchange. Slow release of most constituents continues over several washings or pore volumes.

While laboratory leaching studies are accelerated simulations of what occurs in the field, lysimeter studies may offer a more realistic picture of natural weathering processes. However field studies are expensive, and will probably require many years for full validation. In addition, the installation of drains needed to collect leachates may actually disrupt natural drainage and leaching patterns. Although laboratory simulations cannot mimic all field variables, they offer rapid, economic methods for obtaining information on mobility and transformation of leachate constituents.

The leaching of organic matter from spent shale has been investigated (Pereira et al., 1981; Amy et al., 1980; Leenheer and Stuber, 1981). Pereira et al. identified polynuclear aromatic hydrocarbons, saturated fatty acids, aromatic carboxylic acids, 2-alkanones, aromatic amines, and others in surface samples of the 50

year old Rulison, Colorado spoil pile. Endersen (1983) observed the translocation and redeposition of organic compounds at depth in the same spoil pile.

A model of leachate generation has been constructed using x-ray photoelectron spectroscopy (Ferrer et al., 1986; Ramirez et al., 1985). They concluded that pore diffusion and mineral dissolution reactions are the dominant mechanisms controlling leachate release. The model assumes an initially porous particle in which the leachate diffuses out through interconnecting pores throughout the interior of the particle. The concentration of a solid species at the surface of the particle is nearly constant. This is in contrast to a model proposed by Skogerboe et al. (1979) which features a porous layer from which minerals have been dissolved, surrounding an unreacted core of low porosity. The rate of leaching is initially dependent on the surface area of soluble species, and ultimately on the kinetic and equilibrium chemistry of the unreacted core. The two models represent extremes, and a realistic model of leachate generation will quite likely include aspects of each.

Design of This Study

Preliminary studies used unweathered ROS, generated by the Paraho Oil Shale Project operated at Anvil Points, Colorado. The Paraho semi-works facility operated an above-ground directly heated retort (Wen and Yen, 1979). Paraho ROS has never been exposed to field conditions, having been collected immediately after generation.

Most investigations were performed using weathered ROS, originally generated by the U. S. Bureau of Mines Rulison, Colorado Project between 1925 and 1929 (Gavin and Desmond, 1930). The Bureau of Mines began operation of this pilot plant in 1925. Oil shale was mined, crushed, and the oil extracted in two above-ground retorts; the Pumpherson retort

used indirect heating from an external source, usually recycled process gas, while the NTU retort was directly heated with hot gases from the combustion of a portion of the carbonaceous material in the shale. A total of 6173 tons of shale was retorted before competition from east Texas oil fields discontinued the project in 1929.

Samples were obtained from the spoils pile associated with this project in 1981 by the U. S. Geological Survey. These core samples have been exposed to over 50 years of natural weathering. Previous studies (Endersen, 1983) of these samples have demonstrated that 1) both organic and inorganic compounds are mobile in the ROS spoil pile; 2) a large percentage of the leachate was derived from highly soluble salts external to the fundamental ROS particles; 3) it is likely that some dissolved material originated in the bulk mineral matrix, as evidenced by slow decreases in leachate concentrations during serial extractions. The proportionate contribution of the mineral matrix was greatest for surface samples where extensive leaching had removed much of the highly soluble material.

The Rulison site presented an opportunity to study the effects of long term weathering on ROS, prior to the establishment of a full scale oil shale industry. This is a unique opportunity, because environmental impact studies must usually be done by modeling field conditions in the lab, or by observing effects in the field over a very short term.

One of the principal goals of this work was to develop a laboratory test which would permit determination of the extent to which the natural weathering of an ROS sample had progressed. Laboratory tests were designed to characterize the aqueous dissolution rate of this material. Rates of dissolution should depend primarily on the characteristics of the phase from which the analyte originates. For example, material taken

from the subsurface of the Rulison spoil pile has not been extensively weathered, but it has received translocated solutes from surface material. It was hypothesized that this material might exhibit three successive rates in a dissolution curve. The fastest rate would be attributed to solubilization of translocated and recrystallized material; an intermediate rate would be associated with salts other than the major mineral matrix; and finally, there would be a slow rate of dissolution of the mineral matrix. In contrast, an extensively weathered surface sample should be nearly devoid of highly soluble salts, and therefore, slow dissolution of the mineral matrix should dominate.

The contribution of such factors as solubility, ion exchange, adsorption equilibria, mineralogical dissolution, and weathering, to the shapes of the dissolution curves is not easily predicted because of interactions between these phenomena. In order to elucidate the operational processes which control leachate composition, extensive anion and cation determinations have been performed. In support of the dissolution studies, differential thermal analysis (DTA), scanning electron microscopy and energy dispersive x-ray analysis (SEM-EDAX) were used to examine changes in the composition and morphologies of the particles.

It was hoped that differences in the dissolution curves of weathered ROS, in conjunction with DTA and SEM-EDAX data, could be correlated with differences in the extent of weathering as represented by different depths in the spoil pile. These studies should also provide increased understanding of the kinds of physical and chemical alterations occurring during weathering processes. Such knowledge will aid in the production of models of environmental impact associated with ROS disposal.

EXPERIMENTAL

Materials and Reagents

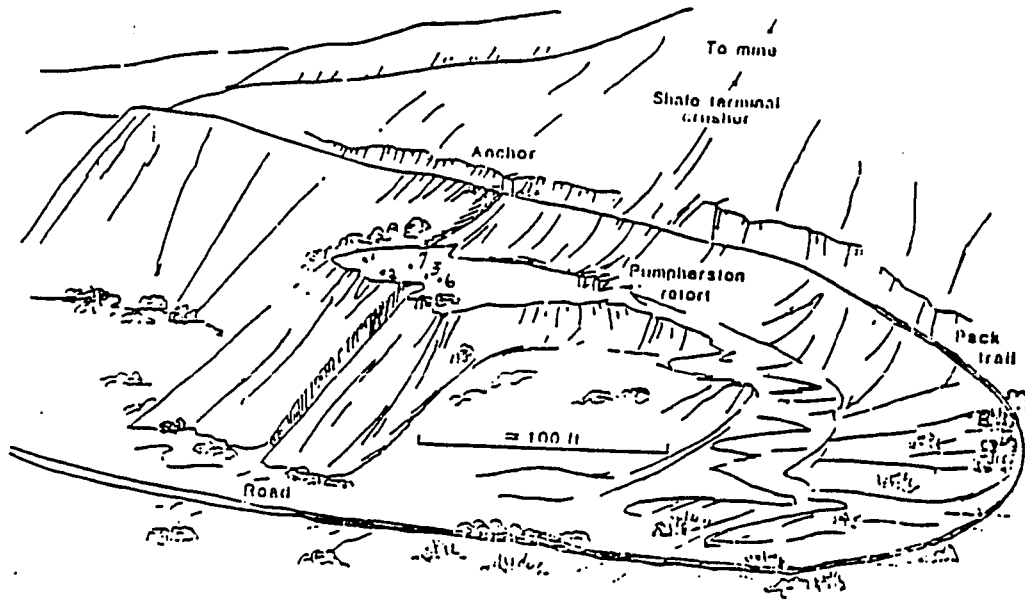
Preliminary experiments to develop test protocols were done on unweathered ROS produced at the Paraho pilot scale operation at Anvil Points, Colorado. "Paraho" ROS was collected immediately after retorting during Spring, 1977, and stored in sealed, polyethylene lined drums.

Weathered ROS was generated by the U. S. Bureau of Mines pilot scale operation in Rulison, Colorado, between 1926 and 1929. Core samples used in this study were obtained by the U. S. Geological Survey in 1981 from the Rulison project's spoil pile. A general layout of the project site appears in Figure 3. Cores were sectioned according to depth and stored in individual containers.

All samples were sized using standard screens to give 3 size fractions: 42-60 mesh, 60-100 mesh and 100-200 mesh. If more of a particular size fraction was needed, larger particles were ground in a Spex mixer/mill (Catalog No. 8000), and dry sieved using the standard screens. These samples were well mixed with those remaining from the original sieving before subsampling. For a given fine particle size, such as 60/100 mesh, leachate composition is not dependent on whether the ROS particles are obtained from the original sieving, or from grinding larger particles to produce a smaller size (Trujillo et al., 1981).

Deionized water from a research grade mixed bed demineralizer cartridge (Barnstead D0809) was used in all leaching experiments and analyses, except for ion chromatographic (IC) analysis, which used distilled deionized water. Distillation was conducted in a Kontes WS-2

Figure 3. Rulison, Colorado Project Site Showing Location of Sampling Cores



continuous water still.

Working standards of Na^+ , K^+ , Ca^{2+} , and Mg^{2+} for atomic absorption analyses were prepared from Baker Instra-Analyzed Atomic Spectral Standards (J. T. Baker). Fresh standards were prepared for each experiment by diluting concentrated standards with water. A 10,000 ppm La^{3+} solution was prepared from $\text{LaCl}_3 \cdot 7\text{H}_2\text{O}$ (Ultrapure, Alfa Products) as a spectroscopic buffer for calcium and magnesium determinations. A 10,000 ppm Cs^+ solution was prepared from CsCl (Suprapur, Merck) as an ionization buffer for sodium and potassium determinations.

Stock solutions of 1000 ppm F^- , Cl^- , NO_3^- , and SO_4^{2-} were prepared from analytical reagent grade sodium or potassium salts. Working standards for IC analysis were prepared just prior to use by diluting concentrated standards with water. They covered a concentration range of 0.10 - 10.0 ppm. The working eluent was prepared from a concentrated solution of NaHCO_3 (Baker Reagent Grade) and Na_2CO_3 (Fisher ACS Grade), and allowed to equilibrate overnight in the instrument.

Methods

Atomic absorption analysis (AA) of leachates was carried out using an Instrumentation Laboratories Model 951 AA/AE spectrophotometer. Calcium, magnesium, sodium and potassium were determined using an air-acetylene flame. Leachates were diluted and buffers were added just prior to analysis. Concentrations were obtained from absorbance vs. concentration calibration curves. In most cases, a linear least squares calibration curve was applicable. Table 2 summarizes the experimental conditions under which the samples were analyzed.

Ion chromatographic analysis (IC) of leachates was performed using a

Table 2. Summary of Experimental Conditions for Atomic Absorption Analyses

<u>Element</u>	<u>Wavelength</u>	<u>Standard Matrix</u>	<u>Calibration Range</u>
Na	5890 Å	0.3% HNO ₃ ; 1000 ppm Cs ⁺	0-0.8 ppm
K	7665 Å	0.3% HNO ₃ ; 1000 ppm Cs ⁺	0-0.6 ppm
Ca	2852 Å	0.3% HNO ₃ ; 1000 ppm La ³⁺	0-2.8 ppm
Mg	4227 Å	0.3% HNO ₃ ; 1000 ppm La ³⁺	0-0.28 ppm

Dionex Model 10 Ion Chromatograph with conductivity detection. Fluoride, chloride, sulfate and nitrate were determined using the Dionex AS-3 Anion HPIC Guard and Separator Columns and Dionex ASC-1 Anion Packed-Bed Suppressor. A Spectraphysics SP4270 Computing Integrator was used for data collection. Samples were diluted just prior to analysis with distilled deionized water. The eluent was 0.0028 M NaHCO_3 /0.0024 M Na_2CO_3 at a flow rate of 0.2 mL/min. Concentrations of ions were obtained from integrator signal vs. concentration or peak height vs concentration calibration curves.

Differential thermal analysis (DTA) of ROS particles was performed using a Dupont 900 Differential Thermal Analyzer equipped with a 1600°C High Temperature Cell and a platinum-platinum 13% rhodium control thermocouple. Analyses were conducted on 100-200 mesh particles that had been oven-dried at 80°C. Calcined alumina was used as the reference, and also to prepare 1:1 dilutions of all samples. The heating rate was 15°C/min, and the furnace atmosphere was static air.

Two synthetic samples of calcite were prepared for the DTA studies; one with coprecipitated impurities and one with impurities around a pure calcite core (Okumura and Kitano, 1986). A $\text{Ca}(\text{HCO}_3)_2$ solution was prepared by bubbling $\text{CO}_2(\text{g})$ through a calcium carbonate suspension and then filtering out the remaining suspension. Sodium sulfate (0.300 g), sodium chloride (2.54 g), potassium chloride (0.38 g) and magnesium sulfate (3.22 g) were dissolved in the $\text{Ca}(\text{HCO}_3)_2$ solution. Coprecipitation was initiated via degassing of CO_2 by stirring the solution with a magnetic stirrer at 25°C until approximately 90% of the calcium ions precipitated. The precipitate was filtered off, washed with deionized water, and then air dried at room temperature. An "adsorbed" sample was prepared from an identical $\text{Ca}(\text{HCO}_3)_2$ salt solution, except

0.500 g of CaCO_3 was added prior to degassing.

Scanning electron microscopic analysis (SEM) of ROS particles was performed on the University of New Hampshire's AMR-1000 scanning electron microscope and AMR energy dispersive x-ray analyzer (EDAX) system. Samples were mounted on aluminum SEM stubs using doubly sided tape. Samples for SEM analysis were sputter coated with Au-Pd while samples for SEM-EDAX analysis were coated with carbon.

X-ray diffraction analysis of ROS particles was performed on the General Electric XRD-3 at the Materials Laboratory, Mechanical Engineering Dept., University of New Hampshire. Samples were ground to fine powders, then scanned using $\text{CuK}\alpha$ radiation generated at 40kV and 10mA.

Three samples of Paraho ROS were artificially weathered in preparation for X-ray diffraction analysis. Simulated weathered samples were obtained by equilibrating 1 gram Paraho ROS in 20 mL of water on a reciprocating shaker. Triplicate samples were prepared. One sample was removed after 5 minutes, filtered and air-dried. A second sample was removed after 24 hours, filtered and air-dried. The third sample was removed after 24 hours and not filtered; the leachate, still in contact with the ROS, was allowed to evaporate slowly at room temperature.

Procedures

1. Sampling Experiment

These experiments were designed to investigate the effect of varying the size of subsamples taken directly from bulk samples of Rulison ROS on sampling uncertainty. A large sample of ROS from Core 7, at a depth of 4.7-5.7 ft., served as the bulk sample. This original sample was sized using standard screens, and two size fractions were retained for the experiments: 100-200 mesh (0.15-0.075 mm) and 42-60 mesh (0.354-0.250

mm). Each sized sample was well mixed prior to subsampling. Three subsample weights were chosen for each size fraction: 0.050 g, 0.500 g, and 2.000 g. Subsamples were obtained via random sampling by spatula from the bulk sample. Acid leach trials were run on eight replicate subsamples for each sample size.

Weighed samples were transferred into 25 or 50 mL beakers. To each sample was added 15-20 mL of 10% HCl (25-30 mL to the 2.000 g samples). The samples were gently heated until CO₂ evolution ceased. Solutions were allowed to cool, then gravity filtered (Whatman 541 filter paper) into volumetric flasks and brought to volume with water. The solutions were analyzed for Na and K by AA.

2. Dissolution Rate Experiments

In these experiments, samples were withdrawn from an ROS-water slurry (solids-to-solution ratio = 1 gram/100 mL) at times ranging from 15 seconds to 30 hours after initial contact of the ROS with water. The samples were rapidly filtered, and the leachate (filtrate) analyzed by AA and IC. Alkalinity and pH were also determined.

A typical experiment used 2.00 grams of air dried 60-100 mesh (0.25 mm-0.15 mm) ROS added all at once to 200.0 mL of stirred water in a 250 mL polypropylene beaker. The temperature of the mixture was thermostatted at $20 \pm 1^\circ\text{C}$ for the first three hours of the experiment by means of a water bath; then allowed to vary with room temperature. The slurry was stirred using a stainless steel three-bladed paddle stirrer (Talboys Engineering Corp. T-Line Laboratory Stirrer) under variac control. Experiments were run in duplicate, the stirring rates of the paddle stirrers being matched using a stroboscope (General Radio Co. Strobotac 631-BL). All experiments were run at 1060 RPM, which was

sufficient to suspend the entire 2.00 g of ROS in 200 mL of water. Reaction vessels were open to the atmosphere.

At periodic intervals, 3 to 4 mL samples were removed from the slurry using a 10 mL plastic syringe (Beckton-Dickinson), and then rapidly filtered. Sampling from the stirred solution removed both solution and solid, and allowed the solids-to-solution ratio to remain fairly constant throughout the course of the experiment.

For contact times of less than 5 minutes, filtration was accomplished with a Nuclepore Swin-Lok filter apparatus. A 25 mm diameter, 0.4 micron polycarbonate filter (Nuclepore) and a 22 mm diameter glass fiber prefilter (Whatman GF/A) were placed in the filter holder, which was attached directly to the syringe containing the sample. Leachates were collected in carefully cleaned 30 mL polypropylene bottles. This sampling-filtration procedure took less than 4 seconds. For contact times greater than 5 minutes, where filtration rate was not as critical, samples were processed by vacuum filtration through 0.4 micron polycarbonate filters (Nuclepore) using a 47 mm plastic support. This sampling and filtration procedure took less than 12 seconds. Again leachates were collected in 30 mL polypropylene beakers. All filters were presoaked in water, and then rinsed well with water before use. Glass fiber filters were rinsed with hot water, as this was found to be more efficient in removing sodium contaminants from the filters.

Both pH and alkalinity measurements were made on the leachates as soon as possible after collection. An Orion Research model 701/A digital ionanalyzer and Fisher micro-combination pH electrode (No. 13-639-270) were used to determine the pH of a 0.3 mL portion of the leachate. Alkalinity measurements used a 0.50 mL portion of leachate. A microburet with 0.2 mL maximum delivery was used to titrate the samples with

0.002100 M HCl to the phenolphthalein and bromocresol green-methyl orange endpoints. Volumes were recorded to the nearest 0.001 mL. The remaining leachate was stored at 4°C until further analysis by AA and IC.

RESULTS AND DISCUSSION

Introduction

Since the bulk composition of ROS obtained at interval sampling depths in the Rulison spoil pile has been reported by Akerman et al. (1983), it seemed worthwhile to examine these data for any evidence of translocation of soluble constituents from surface to depth. Results are presented in Tables 3 and 4 for Core 2 and Core 6 samples. Cores 2 and 6, selected for this study, were previously studied by Endersen (1983). Previous work has shown that these cores are quite different, and would therefore provide valuable comparisons. Four depths are reported for each core, chosen so as to provide a useful cross-sectional representation of the spoil pile.

The chemical composition of ROS in different sections of the ROS spoil pile varies with the source of the raw shale, and the retort operating conditions when the ROS was generated. Because the Rulison project was a pilot scale operation, experimental process conditions were frequently manipulated in order to increase both product yield and thermal efficiency. Thus it is not surprising to find variations in the bulk composition of ROS from different sections of the spoil pile. Nonetheless, the average composition is very similar to the composition of the Paraho ROS as seen in Table 1.

One might expect that the translocation of soluble salts from surface to depth in the spoil pile would be reflected in the bulk composition data. However, four elements expected to be mobile, Na, K, Mg and Ca, show no consistent pattern of translocation. Apparently the

Table 3. Percent composition of Rulison core 2 ROS (Akerman, 1981)

	<u>0.75-1.6 ft.</u>	<u>4.2-5.3 ft.</u>	<u>6.8-7.9 ft.</u>	<u>13.1-14.1 ft.</u>
SiO ₂	38.7	36.3	33.4	37.6
Al ₂ O ₃	9.0	8.1	7.6	8.8
Fe ₂ O ₃	3.7	3.3	3.0	3.6
MgO	8.3	8.3	6.8	7.6
CaO	19.1	24.4	23.4	20.7
Na ₂ O	2.2	2.4	3.0	2.7
K ₂ O	2.2	1.7	1.6	2.3
TiO ₂	0.33	0.27	0.26	0.32
P ₂ O ₅	0.22	0.25	0.40	0.42
MnO	0.04	0.03	0.03	0.04
LOI*	14.7	12.7	18.4	13.8

* Loss on Ignition

Table 4. Percent composition of Rulison core 6 ROS (Akerman, 1981)

	<u>0.0-0.5 ft.</u>	<u>6.5-7.7 ft.</u>	<u>11.7-12.5 ft.</u>	<u>14.4-15.4 ft.</u>
SiO ₂	40.0	30.3	36.6	34.5
Al ₂ O ₃	9.1	6.7	8.5	8.0
Fe ₂ O ₃	3.7	3.4	3.8	3.3
MgO	6.9	7.6	7.4	7.7
CaO	20.1	20.7	15.3	20.1
Na ₂ O	2.9	2.1	2.1	2.2
K ₂ O	2.1	1.7	2.8	2.6
TiO ₂	0.32	0.23	0.31	0.29
P ₂ O ₅	0.44	0.22	0.19	0.22
MnO	0.04	0.03	0.03	0.03
LOI*	12.9	26.1	21.3	19.8

* Loss on Ignition

soluble fraction is small enough compared to the bulk ROS, that translocation of soluble salts does not significantly alter bulk composition. Heterogeneity in the spoil pile is apparently the predominant cause of variations in bulk composition.

Homogeneity of Rulison Samples

It has long been recognized by analysts that the probability of obtaining a particulate sample which perfectly represents the parent distribution is remote. It is also generally recognized that several subsampling steps are normally involved in reducing a bulk sample to an actual laboratory analysis sample. Very often a laboratory sample is subsampled in two steps: a portion is ground to a finer mesh size, and this is subsampled for analysis. Sampling errors involved in reducing a laboratory sample of a pound or less can be as large as those involved in representative sampling of ton quantities.

The error in a determination of an element in a laboratory subsample of a rock or mineral depends on the analytical error, the weight of the sample analyzed and the nature and history of the laboratory sample. Particle to particle composition variations arise due to the fact that trace constituents often reside in isolated mineral grains. The chance of equivalent numbers of such mineral grains appearing in each analyzed subsample becomes more remote as the sample weight decreases. Fine grinding of the laboratory sample is the most effective way of reducing heterogeneity. Larger samples also give more particles and therefore less heterogeneity from sample to sample.

Because it was expected that a wide variety of techniques requiring various sample sizes would be applied to the Rulison ROS, there was a need to explore the subsampling characteristics and its contribution to overall experimental error. The sampling experiment was designed using

two particle size fractions of Core 7 ROS. Figure 4 illustrates the experimental design. Dilution and analysis of each of the 48 extracts were performed in duplicate in order to estimate analysis error. Results are expressed in mg of Na (or K) extracted per gram ROS (mg/g). All results are included in Appendix A. It is interesting to note that extraction efficiency decreased for both Na and K as sample size increased. This trend was most apparent for the finer particles. However, this difference should not significantly alter the reproducibility estimates.

The observed scatter within each of the six sets of replicates includes both analytical and subsampling variability. Analysis of variance provides the means of separately estimating $S(\text{anal})$, the standard deviation of analysis, and $S(\text{samp})$, the standard deviation of sampling. A summary of these standard deviation estimates is presented in Table 5.

For small sample size (0.050 g), subsampling error was never greater than analytical error. For larger samples (0.500 g and 2.000 g), sampling error was approximately 2.5 times analytical error in all but one case. Because the estimate of analytical error contains only the analysis error, and not the error associated with the acid extraction steps, it is likely that $S(\text{anal})$ has been underestimated. It appears that for the particle sizes and sample weights chosen, Rulison core samples are quite homogeneous after grinding and sieving. The contribution of subsampling error in the various experiments using these sample weights is likely to be acceptably small, averaging less than 2% relative standard deviation.

Figure 4. Design of experiment for subsampling characteristics

Core 7 ROS (4.7-5.7 ft.)						
	42-65 mesh			100-200 mesh		
	0.050 g	0.500 g	2.000 g	0.050 g	0.500 g	2.000g
*	12345678	12345678	12345678	12345678	12345678	12345678
**	aaaaaaaa	aaaaaaaa	aaaaaaaa	aaaaaaaa	aaaaaaaa	aaaaaaaa
	bbbbbbbb	bbbbbbbb	bbbbbbbb	bbbbbbbb	bbbbbbbb	bbbbbbbb

* Numbers 1-8 represent replicate extracts of each subsample weight

** a and b represent duplicate dilutions and analyses of extracts

Table 5. Estimate of subsampling error for core 7 ROS (4.7-5.7 ft.)

<u>Standard Deviation Estimates (mg/g ROS)</u>						
	42-65 mesh			100-200 mesh		
	<u>0.050 g</u>	<u>0.500 g</u>	<u>2.000 g</u>	<u>0.050 g</u>	<u>0.500 g</u>	<u>2.000 g</u>
<u>Na</u>						
S _{anal}	1.40	0.35	0.59	0.41	0.20	0.36
S _{samp}	1.14	0.76	1.50	0.21	0.01	0.59
<u>K</u>						
S _{anal}	0.77	0.14	0.01	0.41	0.10	0.11
S _{samp}	0.60	0.34	0.09	0.21	0.02	0.30

Particle Surface Characteristics

Paraho ROS and Rulison ROS samples from different sections of the spoil pile were examined using scanning electron microscopy with x-ray detection capability (SEM-EDAX). It was hoped that morphological characteristics in combination with x-ray analytical data could be used to identify specific features on a particle.

In Figure 5, SEM micrographs of Paraho unweathered ROS are presented. The surface morphology is quite irregular, and demonstrates the porous nature of the material. The inclusions on the surface of the particle are likely tiny crystallites or deposits from thermal processes. It is believed that these inclusions are the source of readily soluble material in leachates of these samples. Attempts were made to identify the composition of surface features using SEM-EDAX analysis. Based on earlier batch extraction studies (Trujillo *et.al.*, 1981), it was believed that these surface deposits were sodium salts, but they could not be specifically identified using SEM-EDAX.

Samples taken at 0.3-0.8 ft and at 12.5-13.5 ft from Core 2 in the Rulison spoil pile are shown in Figure 6. Both particles show surface morphologies which are irregular and porous. Figure 7 shows higher magnification views of the same two particles, where differences in the morphologies are clearer. The particle from depth is covered with small needle-like crystals. The particle from the surface is void of these crystals, and is less flaky and irregular in appearance.

The SEM micrographs appear consistent with the models proposed for material obtained at different depths in the spoil pile. The needle-like crystals observed on the particle taken from depth are most likely a result of translocation and recrystallization of readily soluble material from above. The highly weathered surface particle has no regular

Figure 5. Scanning electron micrographs of Paraho ROS
Top: 5000X
Bottom: 10000X

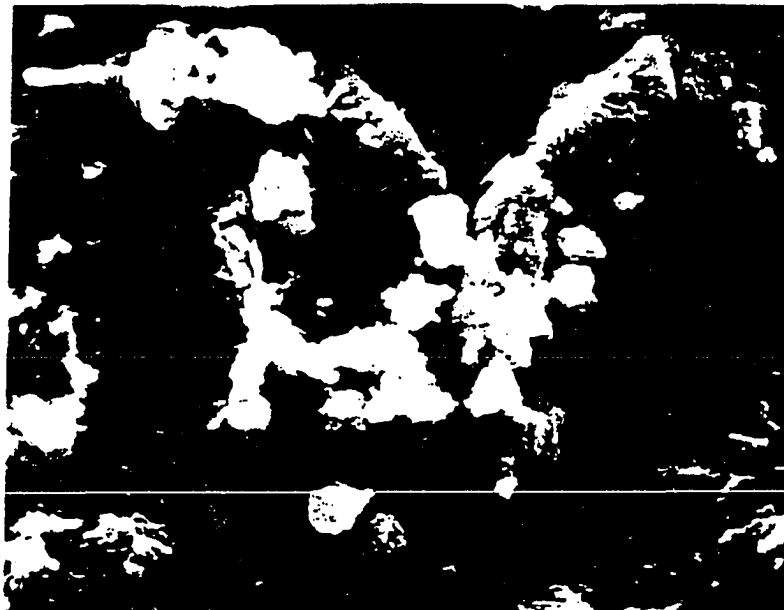


Figure 6. Scanning electron micrographs of core 2 ROS, 5000X
Top: 0.3-0.8 ft.
Bottom: 12.5-13.5 ft.

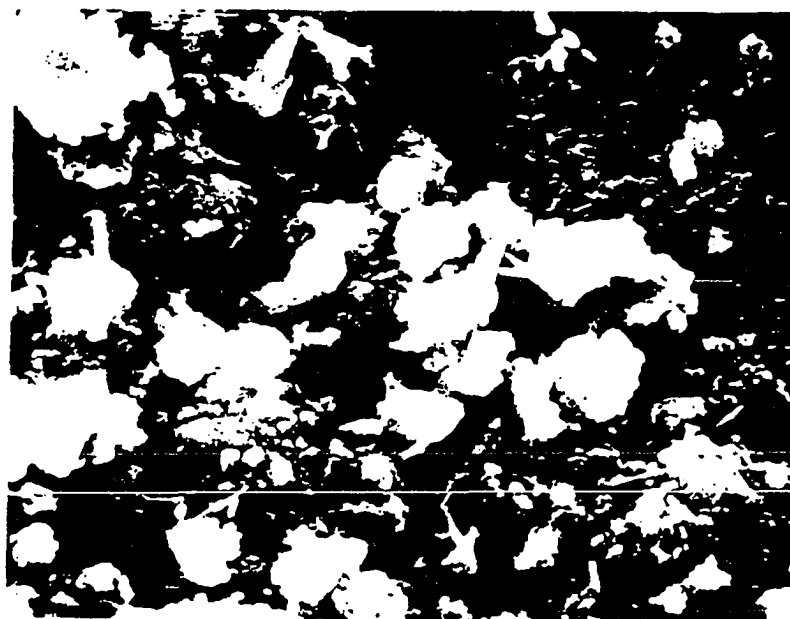
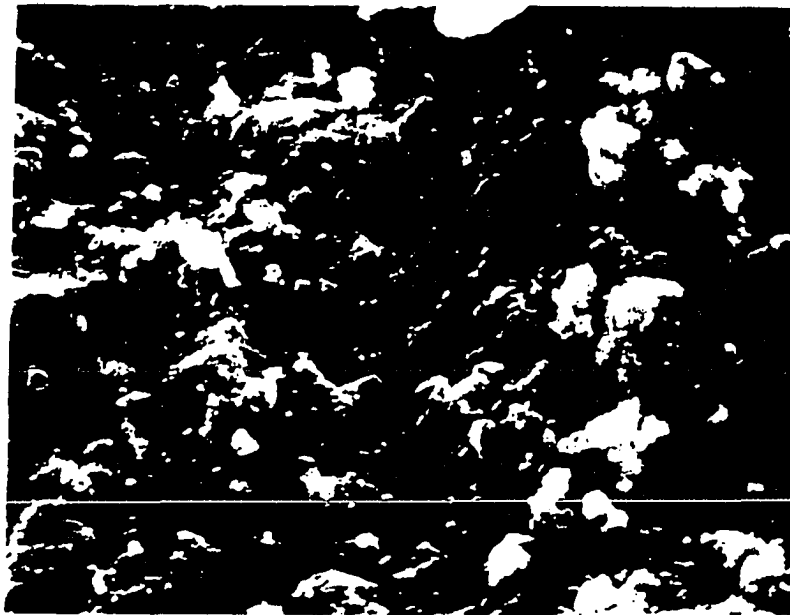
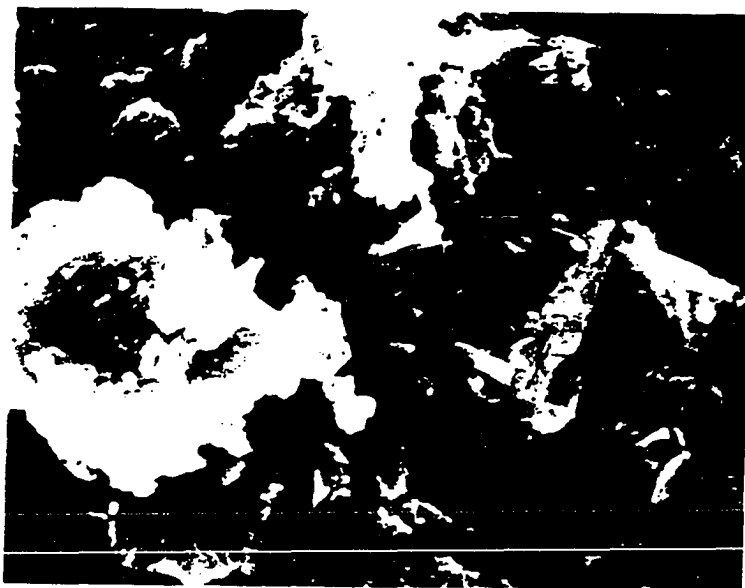
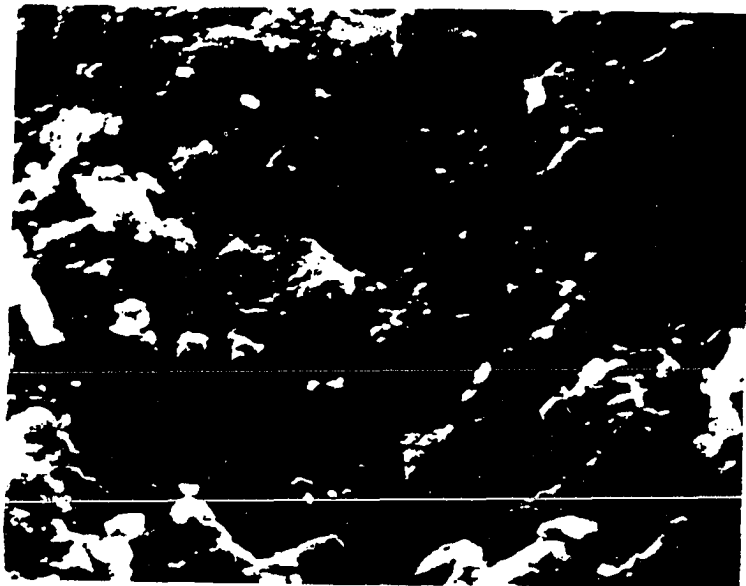


Figure 7. Scanning electron micrographs of core 2 ROS, 10000X
Top: 0.3-0.8 ft.
Bottom: 12.5-13.5 ft.



crystalline features. The readily soluble material has been leached, and it is primarily the bulk mineral matrix of the particle which remains.

It was hoped that SEM-EDAX analysis of the samples taken from different depths in the spoil pile would provide evidence of the presence of translocated recrystallized material. For example, a distribution map of Na for a highly weathered surface sample would show a fairly homogeneous distribution, with signals originating from the surface of the bulk mineral matrix of the particle. In contrast, a sample from deep in the spoil pile would exhibit heterogeneity due to the presence of translocated and recrystallized material on its surface.

Distribution maps of Na and S x-rays were obtained for samples at surface and depth in the spoil pile. Although previous studies demonstrated that Na has accumulated at depth (Endersen, 1983), dramatic differences were not observed in the distribution maps of samples from surface and depth. Similarly, sulfur maps showed few differences.

The lack of distinctive differences between surface and deep samples might be explained by considering the depth from which the x-rays originate. The scanning electron microscope bombards the sample with a focused beam of electrons. Secondary electrons employed in SEM image formation are low energy electrons ejected from the sample by the primary electron beam. Because these are low energy electrons, only those formed within the top 50-100 Å of the surface have enough energy to escape and be detected. Thus the SEM image reveals information about the sample surface. The primary electron beam also causes emission of x-rays by which the EDAX map is formed. The x-rays have a greater penetrating ability, so they will probably escape from the sample even at the point of maximum electron penetration. Therefore, the x-ray data are characteristic of the composition of the top few microns of the sample

surface. Since translocation of soluble salts does not significantly alter bulk composition, it is possible that the x-ray energies are great enough to show Na and S from the underlying bulk matrix. Thus, translocated material on particle surfaces cannot be distinguished from the bulk in the x-ray maps.

Distribution maps of calcium for three Core 2 ROS samples are presented in Figures 8 and 9. Heterogeneity of Ca distribution increases with increasing depth in the spoil pile. For comparison, a Ca map of Paraho unweathered ROS is also included in Figure 9. It has been argued that the depth of x-ray origination precludes distinguishing bulk material from translocated material, in which case the heterogeneity cannot be attributed solely to the presence of translocated calcium. Bulk composition data do not reveal large differences in calcium content of these samples. An explanation for the homogeneity of surface and subsurface samples compared to samples at depth may be that the surface samples have undergone recarbonation. Recarbonation causes Ca^{2+} to be released from the dissolution of silicate minerals, with the subsequent precipitation of calcite. The reduced pH of aqueous leachates of surface samples indicates that recarbonation may have occurred. The samples at depth still contain large amounts of alkaline material, as evidenced by the elevated pH of leachates. The calcium present in the recarbonated form may result in a more homogeneous distribution. Calcium at depth, where recarbonation has not occurred, gives rise to a heterogeneous distribution, similar to that observed for unweathered Paraho ROS. This hypothesis was further investigated in the next section, where differential thermal analysis was used in an attempt to distinguish calcite present as a result of recarbonation.

Figure 8. EDAX Ca maps of Rulison ROS samples, 2000X
Top: core 2, 0.3-0.8 ft.
Bottom: core 2, 6.4-7.4 ft.

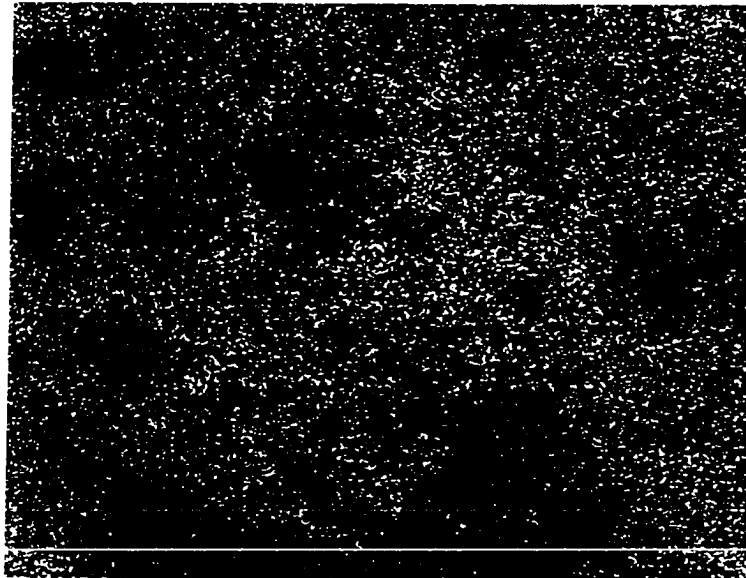
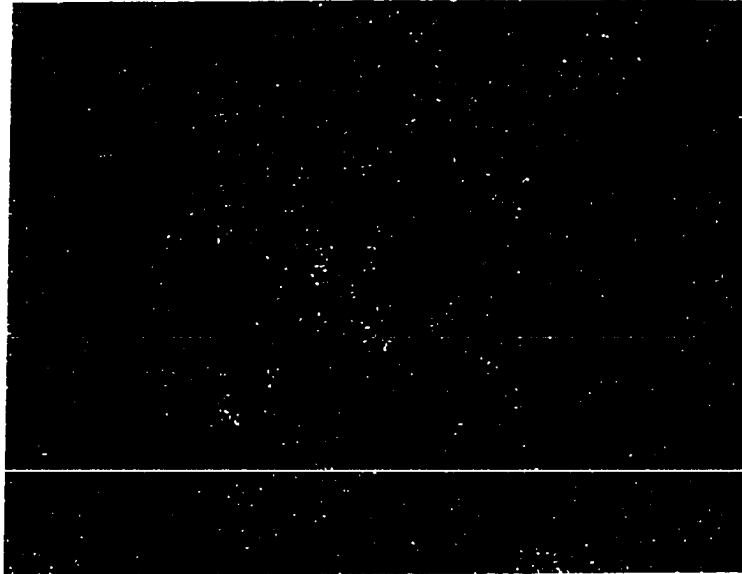
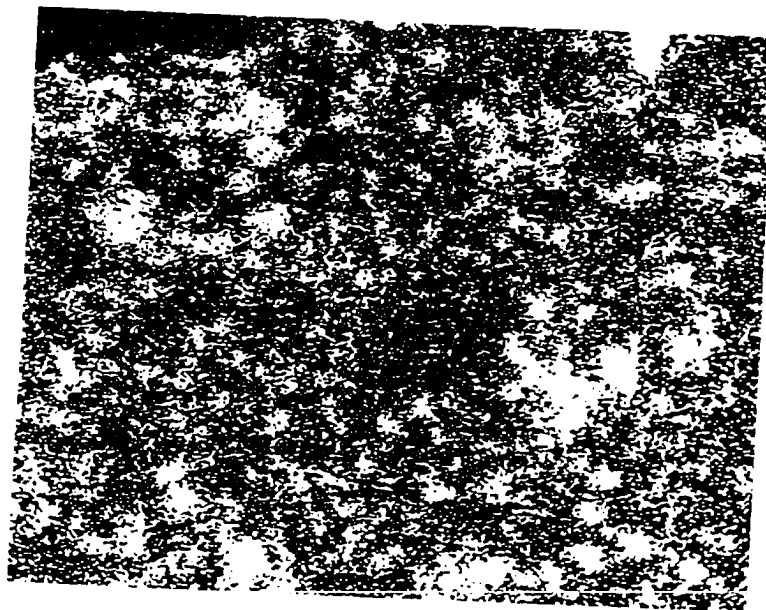
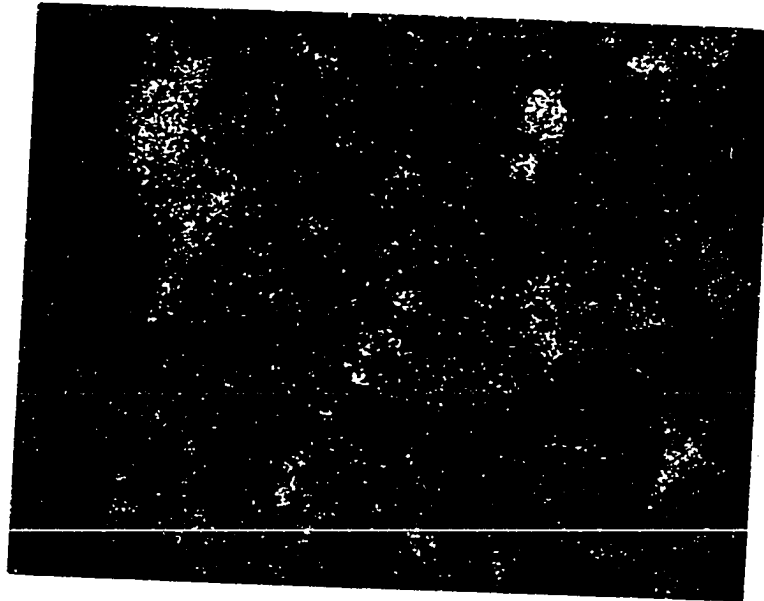


Figure 9. Edax Ca maps of Rulison and Paraho samples, 2000X
Top: Rulison core 2, 12.5-13.5 ft.
Bottom: Paraho unweathered



Bulk Composition Studies

Previously a physical description of weathering effects was presented using SEM and SEM-EDAX analysis of Paraho and Rulison ROS. In this section, bulk composition studies are discussed based on x-ray diffraction and differential thermal analysis.

X-ray Diffraction Analysis

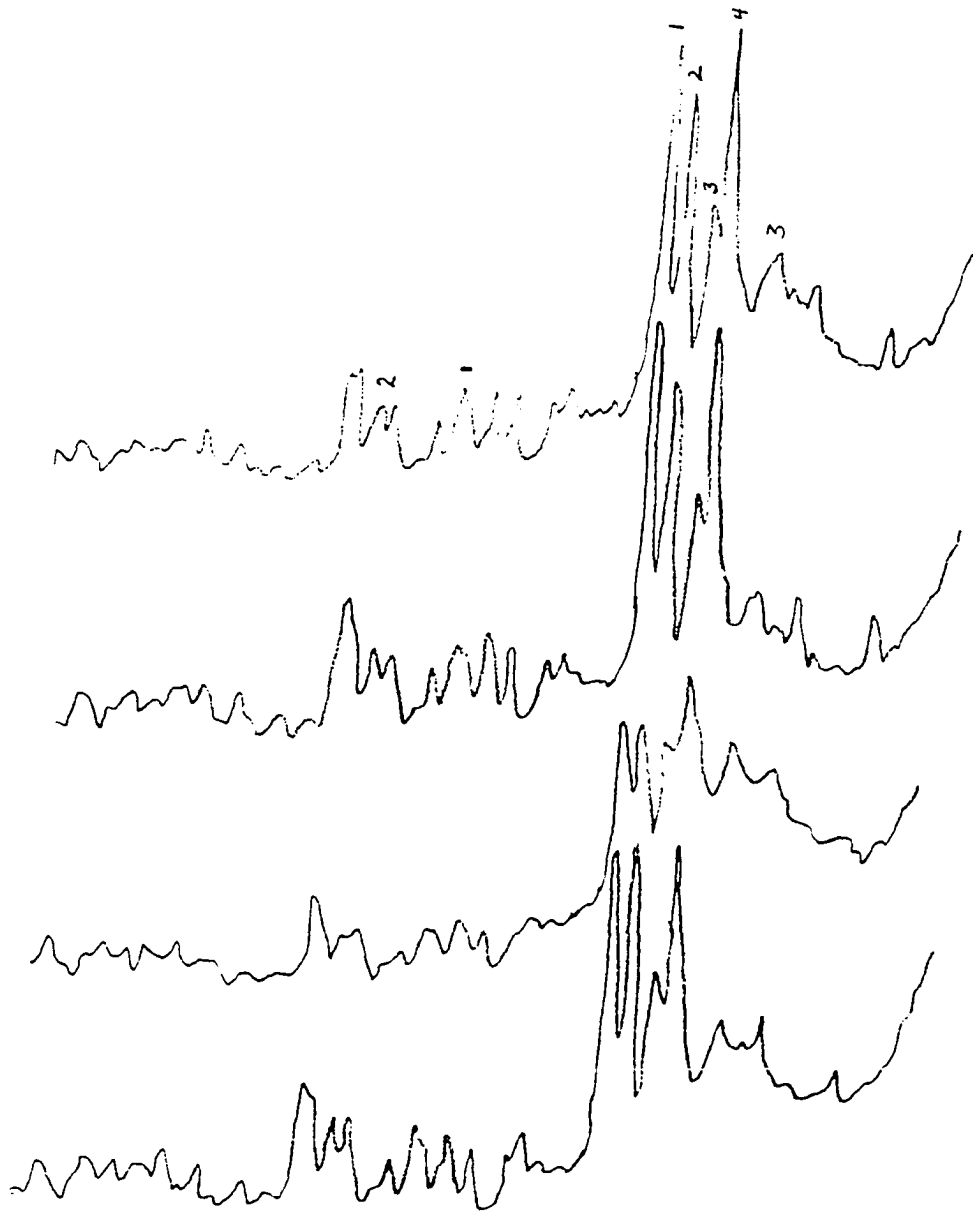
Determination of mineralogical changes caused by leaching is of interest in ascertaining the source of the leached constituents. X-ray diffractograms of Paraho unweathered ROS and three types of laboratory weathered Paraho ROS, are shown in Figure 10. The x-ray patterns produced were compared with the American Society for Testing Materials file (ASTM, 1974). Four major peaks were identified in each pattern, corresponding to d-spacings for dolomite, calcite, albite and quartz, numbered 1 to 4 in Figure 10.

The patterns for unweathered Paraho ROS, and Paraho ROS weathered for 5 minutes are similar in both line location and intensity. There is slightly better definition of peaks for the weathered sample, and a small increase in the intensity of the dolomite peak relative to quartz. This may be a result of surface cleaning, but it may also be normal variability.

The sample weathered for 24 hours and filtered shows a greatly reduced total diffraction intensity. In addition, the peaks for dolomite and calcite are reduced relative to quartz. These minerals have apparently been partially solubilized. The sample from which the leachate slowly evaporated produced a pattern which is similar to that for the unweathered sample, except that the calcite peak has increased relative to quartz.

Similar results were obtained by Reddy et al. (1986) and Reddy and

Figure 10. X-ray diffractograms of Paraho unweathered ROS and laboratory weathered ROS: (a) unweathered (b) lab weathered: 5 minutes leaching, filtered (c) lab weathered: 24 hours leaching, filtered (d) lab weathered: 24 hours leaching, evaporate to dryness at room temperature. Numbered peaks are 1) dolomite, 2) calcite 3) albite and 4) quartz



Lindsay (1986) using ROS generated by the Los Alamos National Laboratory (LANL) and Lurgi-Ruhr gas (Lurgi) processes. The pH of leachates from LANL and Lurgi ROS using a solid to solution ratio of 1:20 were as high as 12.4, which was attributed to the dissociation of silicate minerals, including wollastonite, clinoenstatite and diopside. The pH obtained for leachates of Paraho ROS using a solid to solution ratio of 1:20 was 11.8. Wollastonite, clinoenstatite and diopside were not identified in Paraho ROS. However, differences in the mineralogy for the three types of ROS are not surprising considering they were generated using different processes and different sources of oil shale. The high alkalinity associated with Paraho ROS may be a result of hydrolysis of MgO and $\text{Ca}(\text{OH})_2$.

Reddy et al. (1986) performed recarbonation studies on LANL and Lurgi ROS, and reported that during recarbonation, Ca^{2+} released by the dissolution of silicate minerals combined with added $\text{CO}_2(\text{g})$ to precipitate calcite. The studies performed here using Paraho ROS demonstrated that silicate minerals are solubilized under vigorous extraction conditions; significant concentrations of Si were present in leachates. The increase in intensity of the calcite peak after evaporation of the leachate is consistent with the earlier recarbonation studies of Reddy et al.

Examination of mineralogical data for the Rulison core samples (Akerman, 1983) does not reveal dramatic differences in silicate mineral concentrations between samples which are highly weathered, i.e. surface samples, and samples at depth that are not highly weathered. The extraction conditions used in artificial weathering of the Paraho samples, and the LANL and Lurgi samples, are apparently much more severe than conditions in the field. However, highly alkaline leachates might

be produced in the field, depending on seasonal precipitation patterns, the degree of surface runoff and/or run-in, and the compaction of the spoil pile. Production of highly alkaline leachates may lead to accelerated weathering of the silicate minerals in ROS, as observed under the more vigorous laboratory conditions.

Differential Thermal Analysis

In early studies of oil shale carbonates (Park et al., 1979), it was found that decomposition reactions began at temperatures lower than those observed for the corresponding pure phases. The decomposition of dolomite occurred below 565°C, while the decomposition of calcite began at 620°C. Both of these temperatures are more than 200°C lower than those observed for the corresponding pure minerals.

A number of factors influence decomposition temperatures of oil shale carbonates, including particle size, structure, and composition of the surrounding atmosphere. The rate of decomposition increases with a decrease in particle size because of the shorter time needed for heat to penetrate, and carbon dioxide to diffuse from, the reaction zone of the particle. Crystalline varieties of carbonates that have more closely packed molecules than amorphous varieties, decompose somewhat more slowly (Jukkola et al., 1953). Bischoff's work with gases (1949) showed that practically no decomposition occurred in an atmosphere of carbon dioxide as a result of the effect on the equilibrium $\text{CaCO}_3 \rightleftharpoons \text{CaO} + \text{CO}_2$. The presence of certain salts has also been shown to lower the decomposition temperatures of carbonate minerals. Schwab (1947) showed that alkali metal salts caused a premature decomposition of the dolomitic structure. Esin et al. (1949) noted that sodium and potassium chloride, sodium nitrate, sodium fluoride, sodium oxalate and sodium carbonate, when

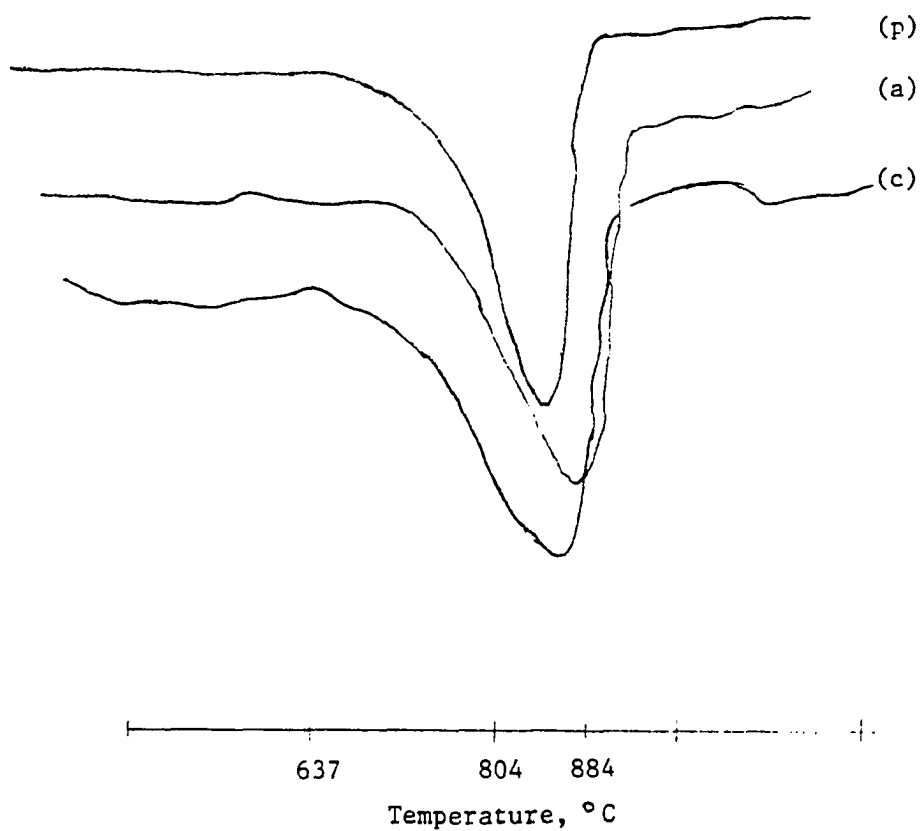
placed in contact with dolomite, shifted the decomposition of dolomite to lower temperatures.

It was hypothesized that CaCO_3 present in the ROS spoil pile as a result of recarbonation might have thermal decomposition characteristics different from CaCO_3 which is part of the bulk mineral matrix of the ROS. Recarbonation and precipitation of calcite would occur in the presence of soluble salts. The precipitated calcite would also likely have different particle size from the native material. Differential thermal analysis (DTA) was used in an attempt to distinguish between the two forms of calcite which may be present in the spoil pile.

To test the hypothesis, laboratory samples of calcite were prepared in the presence of dissolved salts. One sample was prepared by coprecipitation from a $\text{Ca}(\text{HCO}_3)_2$ solution containing dissolved Na_2SO_4 , NaCl , KCl and MgSO_4 ("coprecipitated"). A second sample was prepared in a similar fashion, except that the coprecipitation occurred in the presence of solid calcium carbonate ("adsorbed"). Details are provided in the experimental section. In Figure 11, DTA results are presented for pure calcite, and the two forms of laboratory precipitated calcite designed to represent possible extremes in the natural setting. The coprecipitated sample was expected to exhibit a lower decomposition temperature than adsorbed calcite, and both should decompose at lower temperature than the pure calcite.

The results indicate a slightly lower initial decomposition temperature for both laboratory prepared samples compared to pure calcite, resulting in wider peaks. These results suggest that analysis of the core samples might show differences in the temperature range of peaks depending on the extent of recarbonation, and the extent of translocation and recrystallization of soluble salts.

Figure 11. DTA results for pure calcite (p), coprecipitated calcite (c), and adsorbed calcite (a)



In Figure 12, DTA thermograms are presented for Core 6 samples from the surface and at depth in the spoil pile. Results for Cores 1, 2 and 3 are included in Appendix B. The width at half height was obtained for each peak in a consistent manner, and is included in Table 6. Also included in Table 6 are the areas of each peak expressed as the weight in milligrams of chart paper tracings, the % calcite in each sample as reported by Akerman (1983), and the concentration of Na in 24 hour batch extractions of the sample.

The size of each sample was kept as consistent as possible. However, because the amount of calcite in a sample varied, it was reasonable to assume that the shape of a peak might be correlated with the % calcite. In Figure 13, the width of each peak at half height divided by the area of the peak is correlated with the corresponding % calcite in the sample. One sample point was excluded (Core 1 7.0-8.0 ft) from the correlation as an unusually low value for % calcite was reported. The correlation coefficient, r , obtained for 11 data points is 0.560, which is significant at the 90% confidence level ($r_{(0.10),9}=0.521$). Although this demonstrates a weak correlation, it is important not to attribute a cause-effect relationship to weathering and increasing peak width. Variations in calcite concentrations may be caused by mineralogical or processing variations.

In Figure 14, the peak width/area ratio is plotted versus extractable sodium. One data point is excluded as before. Cores 2,3 and 6 all show an increasing peak width/area ratio with increased Na in the leachate. The sample from 13.0-14.0 ft. in Core 1 is a soil sample, which may explain the anomaly in the Core 1 results. The correlation coefficient, r , obtained excluding all of the Core 1 results is 0.799, which is significant at the 90% confidence level ($r_{(0.10),6}=0.621$). The

Figure 12. DTA results for core 6 ROS: (a) 0.3-0.8 ft. (b) 14.8-15.8 ft.

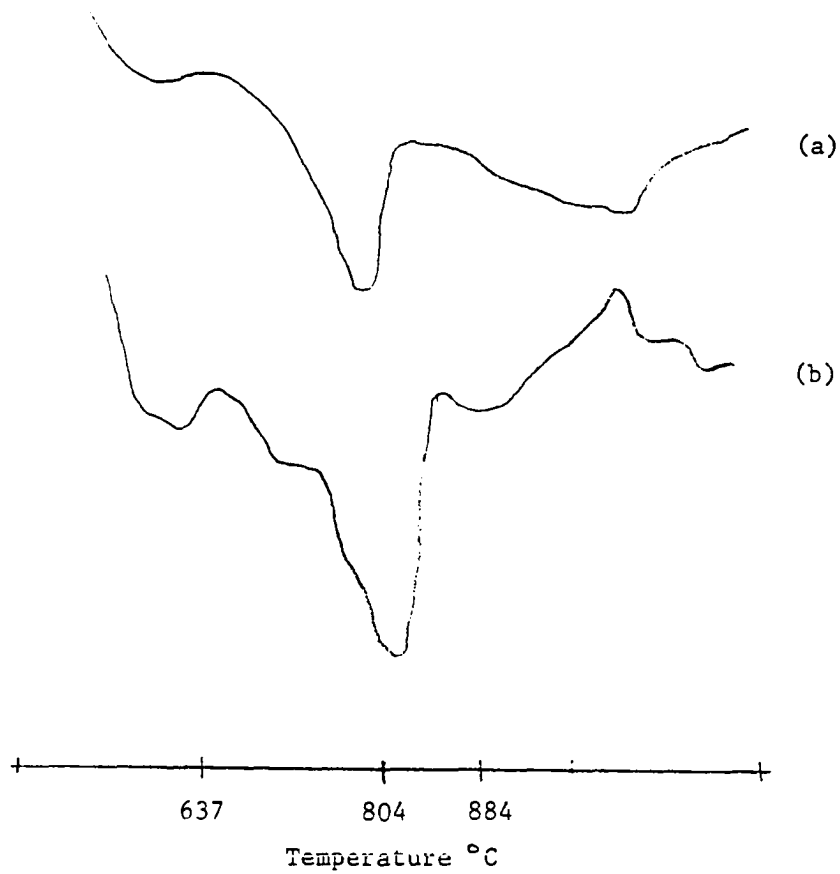


Table 6. Summary of DTA results for cores 1,2,3 and 6

	Width ¹	Peak Area ²	%Calcite ³	Extractable Na, ppm
<u>Core 1</u>				
0.5-1.0 ft.	2.2	22.9	41	2.7 *
7.0-8.0 ft.	2.2	14.1	21	106 *
13.0-14.0 ft.	2.3	28.3	42	227 *
<u>Core 2</u>				
0.3-0.8 ft.	1.8	33.4	36	13.4 **
6.4-7.4 ft.	2.6	28.5	39	346 **
9.0-10.0 ft.	2.2	24.7	38	
12.5-13.5 ft.	1.8	24.6	30	209 **
<u>Core 3</u>				
0.4-1.4 ft.	1.9	30.4	34	50 *
5.0-6.0 ft.	2.0	33.2	21	34 *
13.0-13.7 ft.	2.4	26.5	36	136 *
<u>Core 6</u>				
0.3-0.8 ft.	1.5	20.0	27	28.9 **
14.8-15.8 ft.	2.2	26.6	48	214 **

1 peak width at half height, cm

2 peak area expressed as weight in mg of chart paper tracing

3 Akerman, 1981

* Maynard, unpublished data

** Endersen, 1983

Figure 13. Correlation of peak width at half height to % calcite in sample

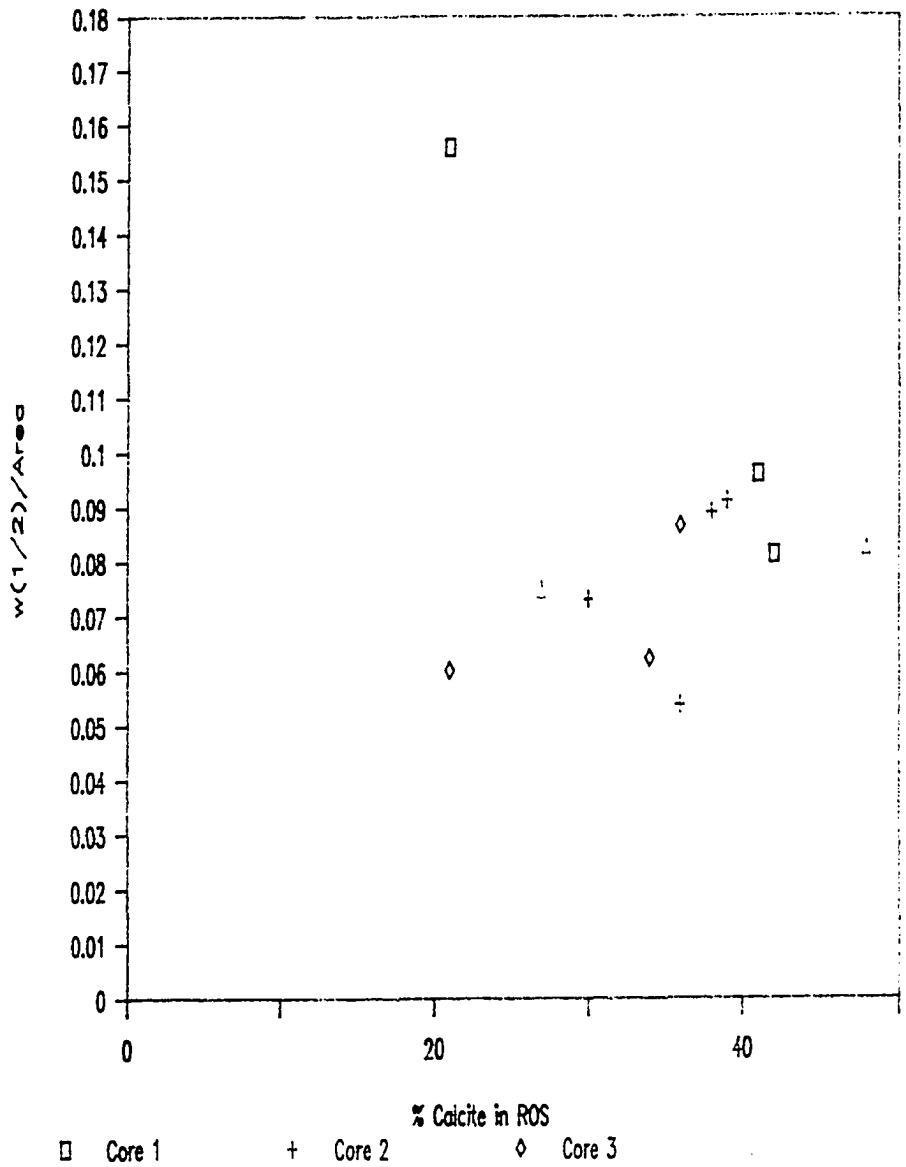
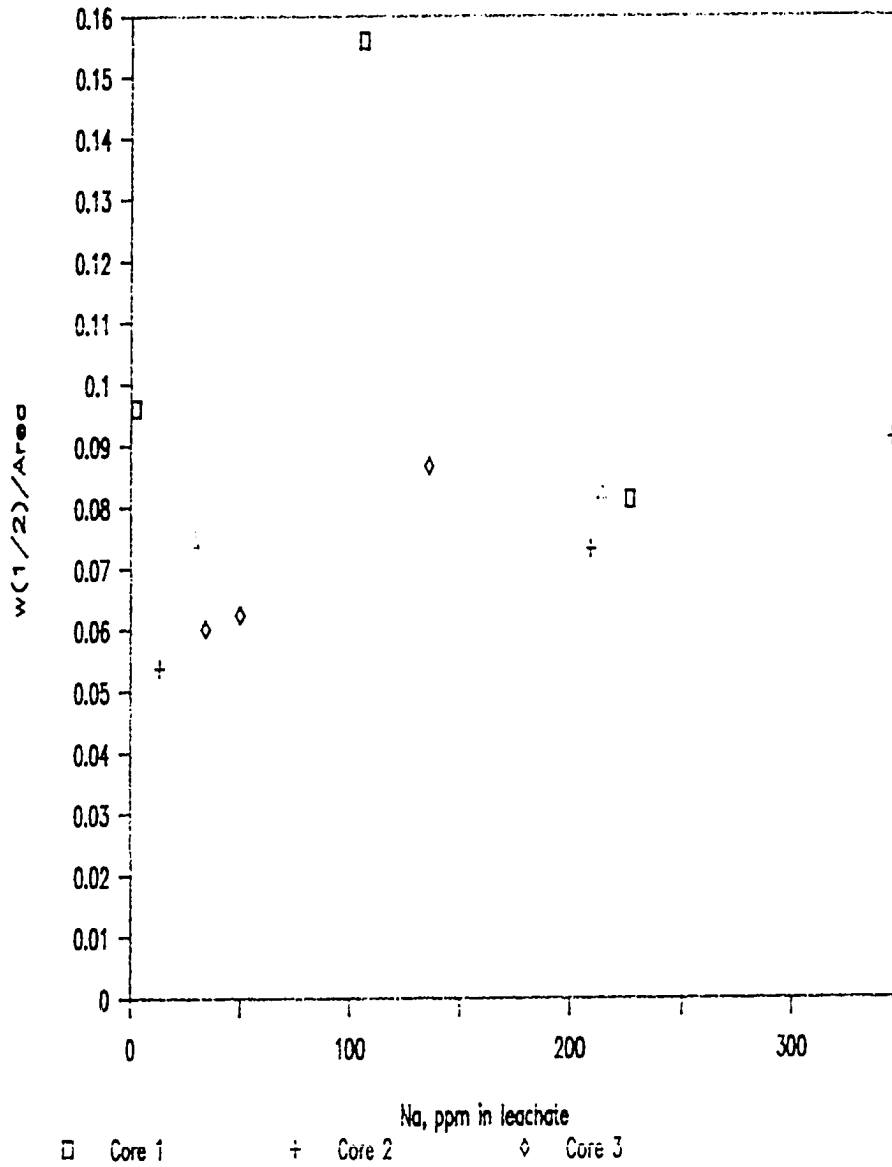


Figure 14. Correlation of (peak width at half height/area) to extractable Na



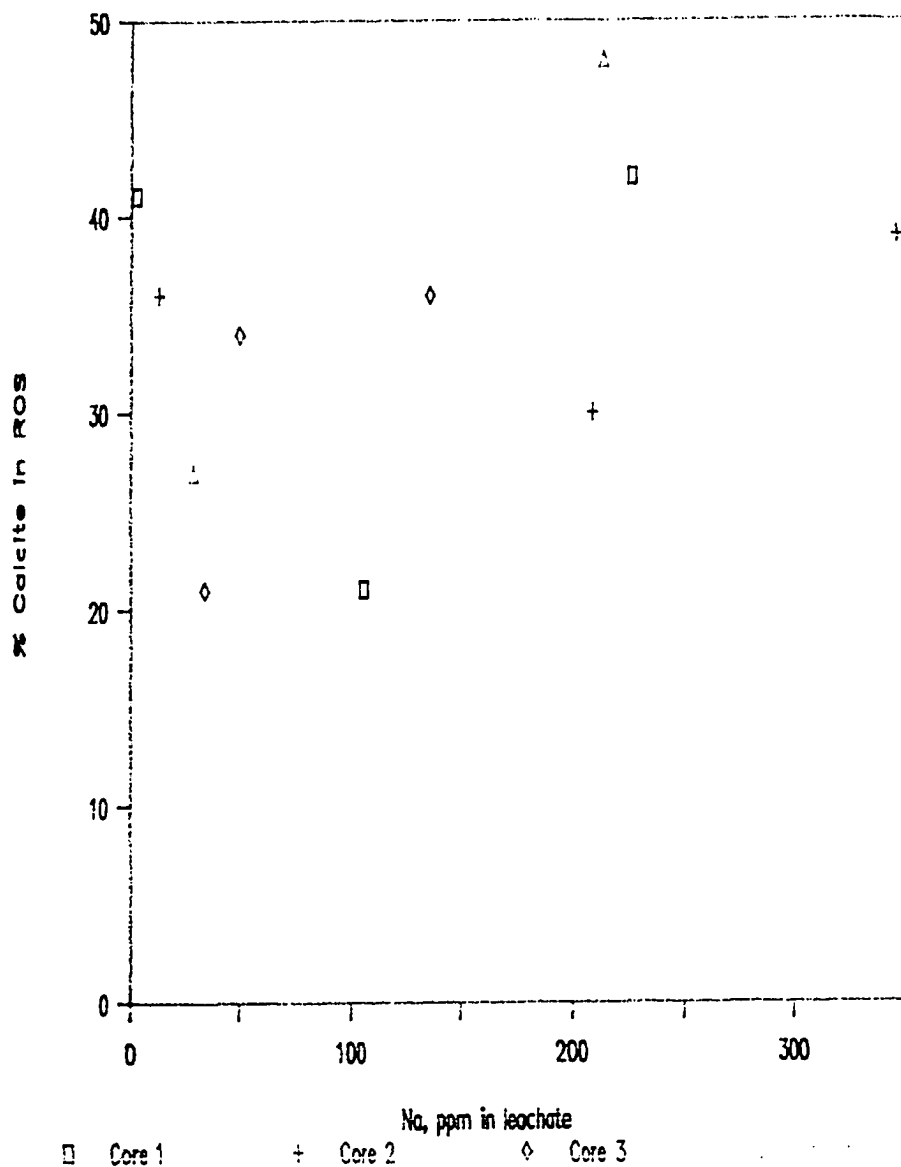
increase in peak width/area with increasing amounts of extractable sodium in a leachate is consistent with recarbonation of ROS followed by precipitation in the presence of alkali metal salts. The relationship of peak width/area to extractable sodium is enhanced by the absence of a significant correlation between % calcite in a sample and extractable sodium (Figure 15). One sample, Core 1 7.0-8.0 ft., was excluded as was done previously. The correlation coefficient, r , obtained for 10 data points is 0.434, which is not significant at the 90% confidence level ($r_{(0.10),8}=0.549$). Had extractable sodium been correlated with % calcite, the relationship of peak width/area to extractable sodium would just be another reflection of this correlation. Even in the absence of a significant correlation between % calcite and extractable sodium, the relationship of DTA peak shape and weathering is tenuous at best.

The DTA results indicate that the presence of translocated alkali metal salts may affect the thermal decomposition characteristics of calcite in ROS. However, the differences observed were too small to permit quantitative evaluation of the amount of calcite present as a result of recarbonation. Perhaps translocation of soluble salts does not significantly alter thermal decomposition characteristics of recarbonated calcite, because it does not significantly alter total concentration of the alkali metals.

Dissolution Rate Experiments

In batch equilibration studies using water as the extractant, leachate composition depends on many factors. Variables such as solid to solution ratio, vigor of agitation, and contact time interact in a complex fashion to control concentrations of dissolved species in the leachate. A high solid to solution ratio often closely mimics leaching conditions in an ROS spoil pile. When rain or snowmelt contacts ROS, a

Figure 15. Correlation of % calcite to extractable Na



highly alkaline leachate is produced within minutes. With increasing contact time, this solution develops still higher pH and salt content. On the other hand, a low solid to solution ratio would more closely mimic field conditions such as overland flow.

Previous studies of the Rulison spoil pile used a solid to solution ratio of 1:10 (Endersen, 1983; Trujillo et al., 1981). A high solid to solution ratio imposes severe solubility constraints on leachate composition, and makes interpretation of actual species mobility difficult. For example, at a solid to solution ratio of 1:10, magnesium concentration in leachates can be limited by solubility, with precipitation of $Mg(OH)_2$ at high pH dominating. However it is expected that magnesium would become mobile in the spoil pile as alkaline materials are removed by weathering, and pH drops below about 9.

Batch equilibration experiments conducted for this study used a solid to solution ratio of 1:100 to avoid serious solubility constraints on leachate composition. Additional information can be inferred about species mobility during the different stages of weathering of the ROS spoil pile. In addition, the low solid to solution ratio facilitates the study of the rate of dissolution of a species, by accommodating rapid sampling and filtering from the ROS-water slurry.

It was hypothesized that different rates of dissolution would be observed for different solid phase species, and for material taken from different sections of the spoil pile. It was hoped that changes in the rate of dissolution could be associated with the presence of various species in separate phases of the ROS particles. By combining results from dissolution curves with data from solid phase characterizations, it was thought that conclusions could be drawn as to the extent of weathering of the spoil pile.

Paraho ROS

Preliminary work used unweathered ROS. Results were in agreement with those predicted for a two phase model for unweathered material. Some analytes, such as sodium and potassium, exhibited dissolution behavior typical of a highly soluble phase. The sodium dissolution curve obtained for Paraho ROS at a solid to solution ratio of 1:100 is shown in Figure 16. After 2 minutes, the concentration of Na in the leachate was 0.74 meq/L. Sodium reached a high concentration in solution rapidly, followed by a very slow increase over time. The concentration of sodium in the leachate after 30 hours had only increased to 0.82 meq/L. The slow rate at longer times is attributed to dissolution of Na from the bulk mineral matrix of the particles. In experiments run at a solid to solution ratio of 1:10, the concentration of Na and K was approximately ten times the concentration in the 1:100 experiment, indicating a lack of any solubility constraints on concentration in the leachate.

The sulfate dissolution curve obtained for Paraho ROS is shown in Figure 17. Sulfate typifies an ion which dissolves slowly, but continues to increase in concentration at a slow, but significant rate throughout the duration of the experiment. After 5 minutes, the concentration was 0.56 meq/L; after 30 hours, it had reached 1.19 meq/L. In experiments run at a solid to solution ratio of 1:10, the concentration of sulfate in the leachate was approximately ten times the concentration in the 1:100 experiment, again indicating a lack of solubility constraints on concentration in the leachate. Clearly much of the sulfate is associated with other than alkali metals, most likely alkaline earth sulfates.

The magnesium dissolution curve obtained for Paraho ROS at a solid to solution ratio of 1:100 is shown in Figure 18. Magnesium illustrates an ion which responds dramatically to changes in leachate composition.

Figure 16. Sodium dissolution rate curve for Paraho unweathered ROS

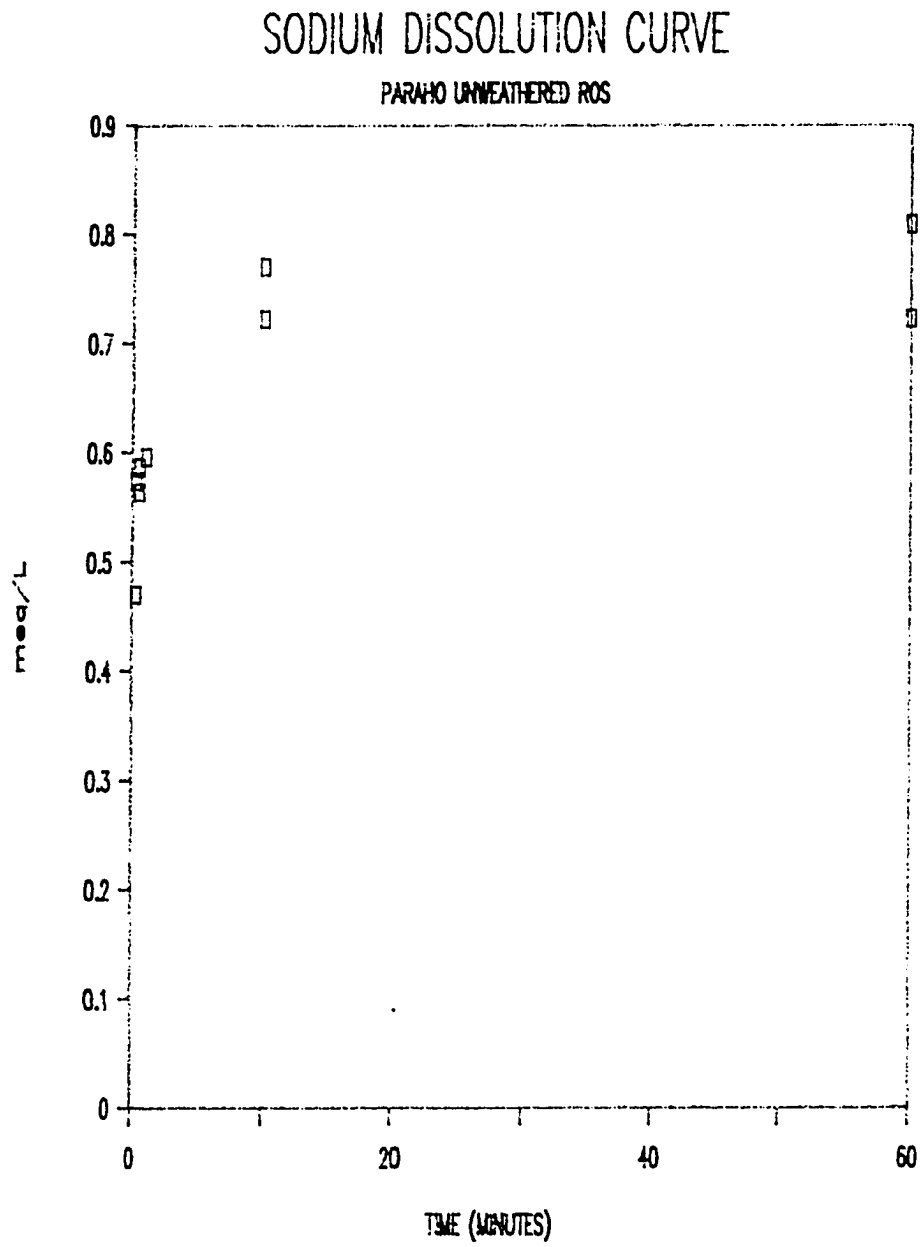


Figure 17. Sulfate dissolution rate curve for Paraho unweathered ROS

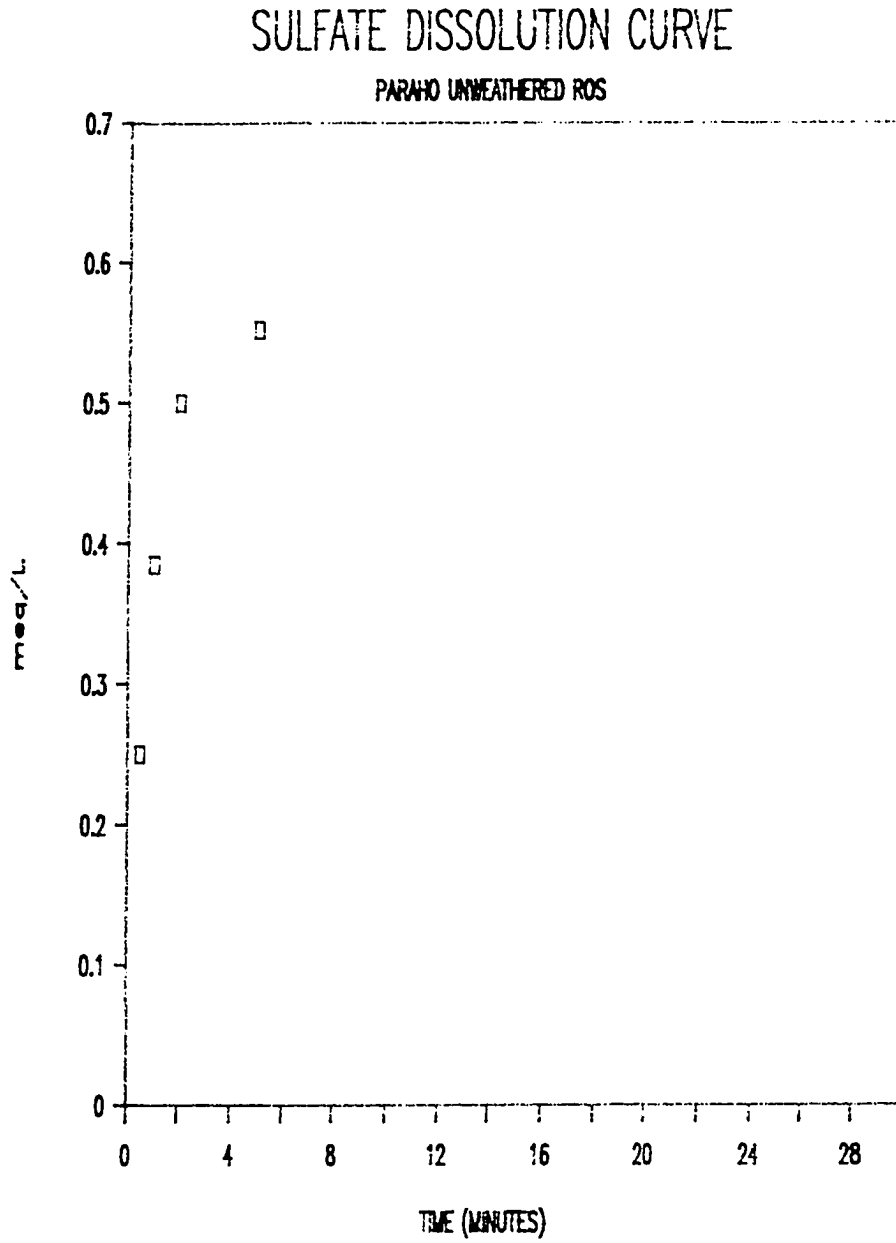
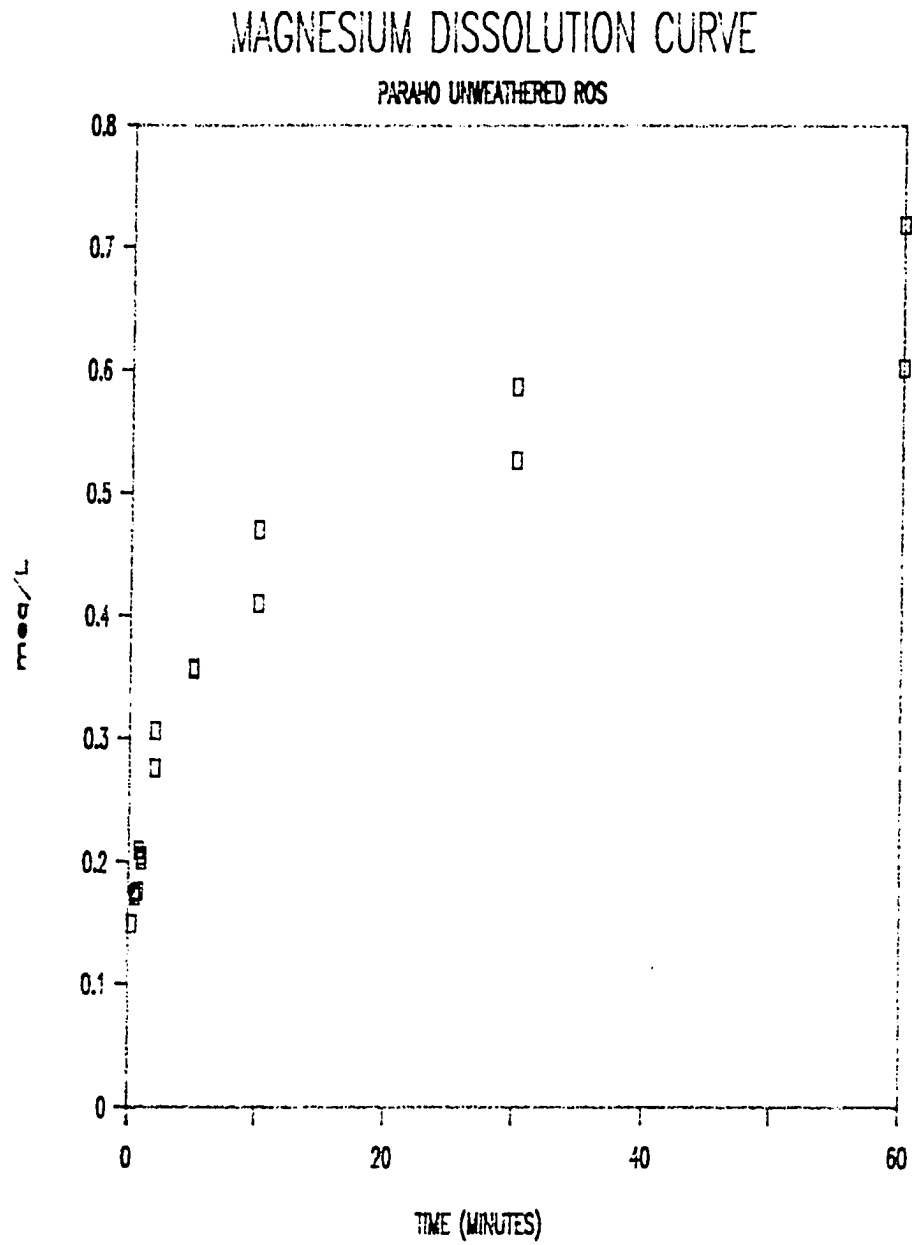


Figure 18. Magnesium dissolution rate curve for Paraho unweathered ROS



At a ratio of 1:100, the concentration of Mg in solution was 0.66 meq/L after one hour. The concentration continued to rise and after 30 hours it was 5.8 meq/L. The dissolution curve shape is very similar to that of sulfate. In contrast, for the experiment run at a ratio of 1:10, the concentration of Mg was only 0.12 meq/L after one hour, and it dropped to 0.06 meq/L after 30 hours. The behavior of magnesium can be readily explained considering the pH attained in the different experiments. At the low ratio of 1:100, the pH after 30 hours was 8.5, whereas it was 11.5 after 30 hours at the high ratio of 1:10. As the pH approached 11, concentration of Mg decreased due to $Mg(OH)_2$ precipitation. These results clearly demonstrate the importance of considering all experimental variables when comparing results from different studies.

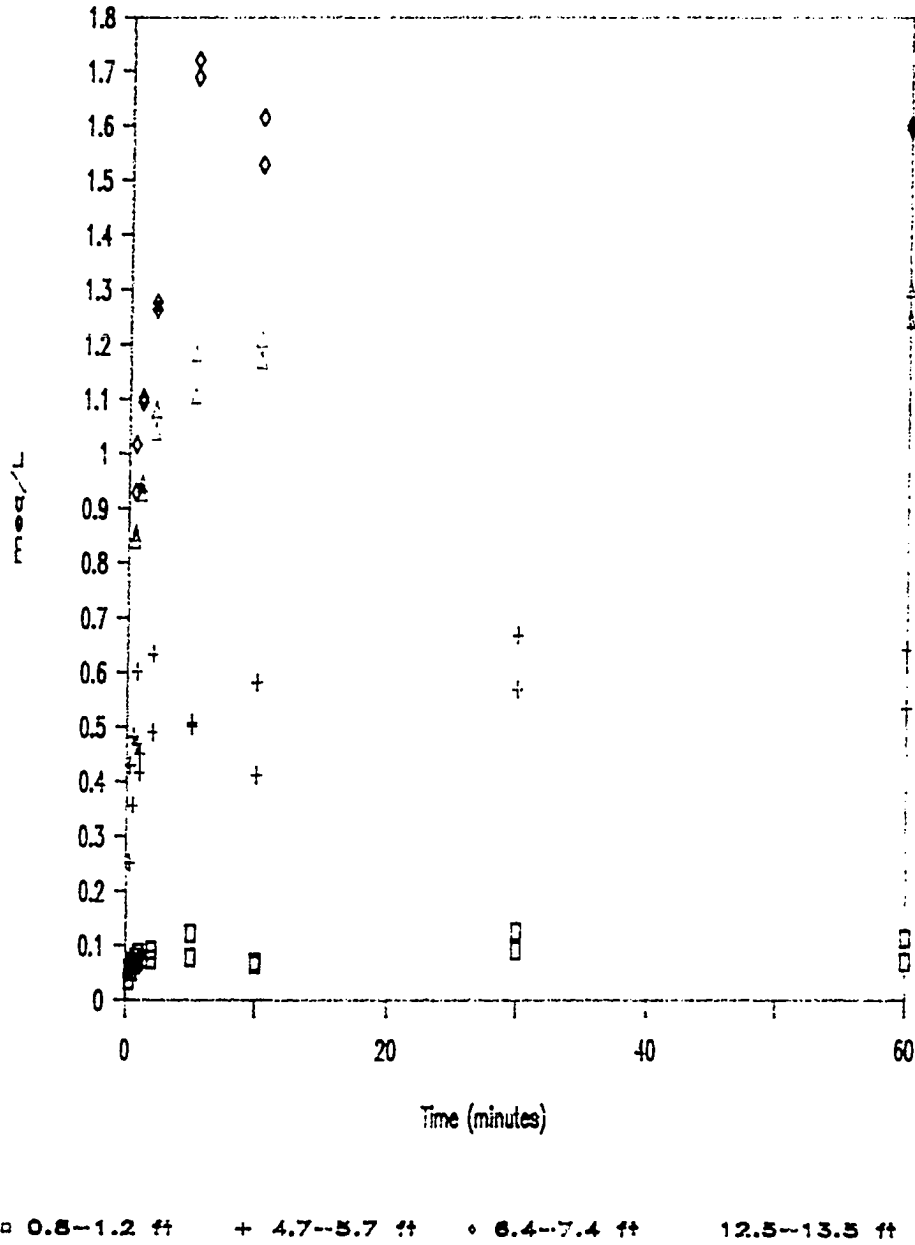
Rulison ROS

Most dissolution rate experiments were performed on Core 2 and Core 6 samples from the Rulison spoil pile. Appendix C contains tabulated and graphical results for all core samples investigated. A summary of results will be presented for discussion.

Sodium dissolution rate curves for Core 2 samples are shown in Figure 19. The surface sample, which is highly weathered, exhibits only a slow rate of dissolution and a low maximum concentration. Sodium in the leachate presumably originates from the bulk mineral phase, which is only sparingly soluble. Three successive rates are suggested for the samples from intermediate depths. For the first two minutes, the concentration increases rapidly. Between two and ten minutes, dissolution continues, but at a slower rate. Only a small increase in Na concentration is observed after ten minutes. The fastest rate may be associated with translocated and recrystallized material. The

Figure 19. Na dissolution rate curves: Rulison core 2 samples

Na Dissolution Curves: Core 2 Samples



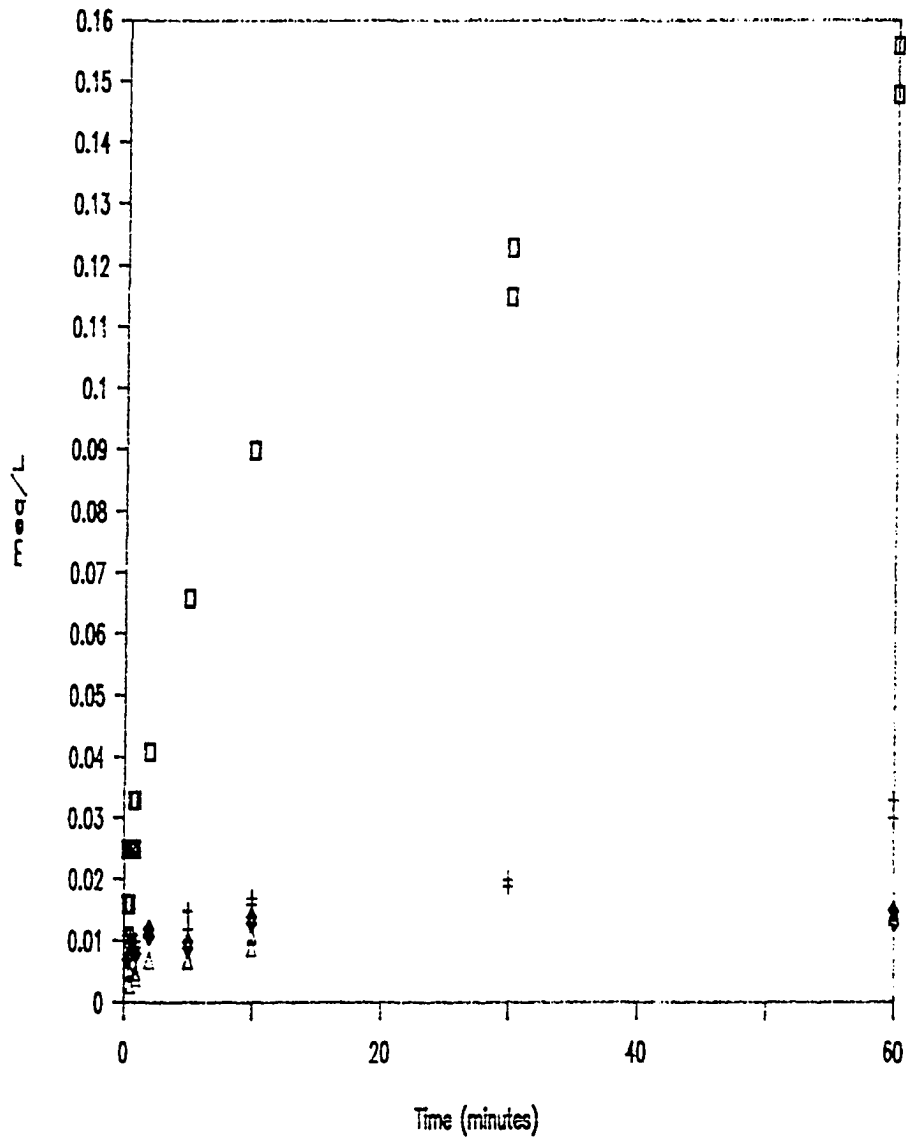
needle-like crystals observed in SEM micrographs of Core 2 samples at depth are most likely the source of the readily soluble material. The intermediate rate may be associated with redeposited material which is occluded in recarbonized calcite or gypsum. Finally there is the slow dissolution of the mineral matrix. The sample from the greatest depth produces the steepest dissolution curve. It is believed that the material at the greatest depth is most like Paraho ROS in its dissolution behavior. There may be a very small amount of translocated and redeposited material at this depth, but the material is largely unweathered.

Magnesium dissolution curves for Core 2 samples are presented in Figure 20. In contrast to Na, the fastest rate of dissolution and the highest concentration is observed for the surface sample. Samples at depth exhibit only a slow rate of dissolution and low final concentration. Solubility equilibria can be used to interpret the shapes of these curves. The pH of the leachate from the surface sample does not go above 7, while the samples at depth develop pH as high as 9.4. The high pH of the samples at depth limits magnesium mobility, however mobility increases for the surface samples where alkaline material has been removed by weathering. The behavior of magnesium has implications for other metals forming insoluble hydroxides at elevated pH, e.g. copper.

Sulfate dissolution curves for Core 2 samples are presented in Figure 21. Sulfate, like sodium, should not be subject to solubility constraints in the leachate. However, dissolution curves indicate that sulfate behaves quite differently from sodium. Sodium dissolution curves for surface samples exhibited only a slow rate of dissolution and very low final concentration. Sulfate dissolution curves indicate continued

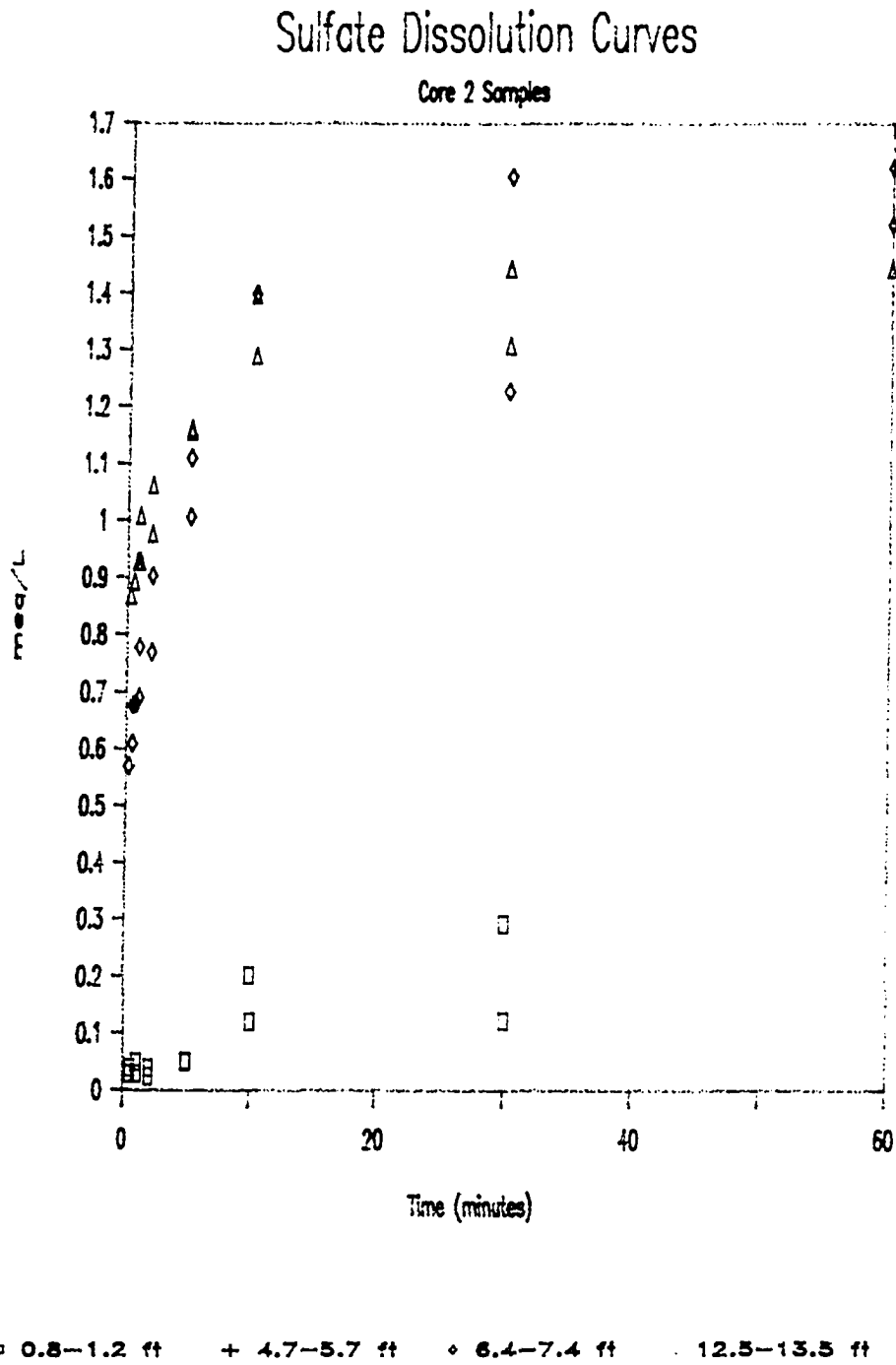
Figure 20. Magnesium dissolution rate curves: Rulison core 2 samples

Mg Dissolution Curves: Core 2 Samples



□ 0.8-1.2 ft + 4.7-5.7 ft ♦ 6.4-7.4 ft △ 12.5-13.5 ft

Figure 21. Sulfate dissolution rate curves: Rulison core 2 samples



slow release from the highly weathered surface sample. Dissolution curves of sulfate for mid-depth and deep samples are similar, although the deep sample may exhibit a slightly faster initial rate of dissolution. Sodium dissolution curves for Core 2 samples suggested a zone of accumulation at about 6.4-7.4 ft., but there is little evidence of sulfate accumulation at this depth. The lower mobility of sulfate in the spoil pile is not surprising considering the results obtained for Paraho ROS. Sulfate dissolved slowly from the Paraho ROS, but continued to increase in concentration at a slower, but significant rate throughout the experiment. The lower mobility of sulfate in the core samples is most likely due to its association with other than alkali metals.

Because fairly complete anion and cation analyses were obtained (Appendix C), the electroneutrality of the leachate solutions could be examined. Table 7 lists the total anion concentration and the total cation concentration in a leachate, after one hour contact with ROS. Results are expressed in meq/L. Fairly good agreement is observed between total anion content and total cation content. However, for all but one sample, total cation concentration is slightly higher than total anion concentration. Anions which have not been accounted for in the analyses, but which are known to occur in oil shale leachates, include thiosulfate, various silicate species, and anionic trace metals such as arsenate, molybdate, selenate and borate. The individual anions listed were not present at high enough concentration to be conveniently determined, however in combination they may account for the anion deficit.

In Table 8, the percentage of Na, K, Ca and Mg extracted from bulk ROS has been calculated as the respective oxides. Only a small percentage of the total element available in the bulk ROS was extracted

Table 7. Total anion and cation concentrations in Rulison ROS leachates
(results expressed in meq/L)

<u>Core 2</u>	<u>Cation</u>	<u>Anion</u>
0.8-1.2 ft.	0.992	0.932
6.4-7.4 ft.	2.69	2.45
12.5-13.5 ft.	2.43	2.13
 <u>Core 6</u>		
0.3-0.8 ft.	0.564	0.569
7.1-8.1 ft.	1.26	1.04
12.1-12.7 ft.	1.26	1.12
13.8-14.8 ft.	1.85	1.54

Table 8. Percentage of an element extracted from core 2 and core 6 ROS

<u>Core 2</u>	Depth			
	<u>0.8-1.2 ft</u>	<u>4.7-5.7 ft</u>	<u>6.5-7.4 ft</u>	<u>12.5-13.5 ft</u>
Na ₂ O				
2 min	1.2	7.5	13.0	12.6
1 hr	1.7	7.5	17.0	14.8
30 hr	1.8		18.7	18.5
K ₂ O				
2 min	2.6	5.4	11.3	12.2
1 hr	4.3	9.4	15.0	17.0
30 hr	4.4		16.9	30.0
CaO				
2 min	0.32	0.39	0.31	0.22
1 hr	0.68	1.0	0.73	0.48
30 hr	1.9		2.0	2.4
MgO	0.27	0.03	0.005	0.017
2 min	0.63	0.08	0.034	0.039
1 hr	2.4		0.78	0.86
30 hr				

<u>Core 6</u>	Depth			
	<u>0.3-0.8 ft</u>	<u>7.1-8.1 ft</u>	<u>12.1-12.7 ft</u>	<u>13.8-14.8 ft</u>
Na ₂ O				
2 min	2.1	2.4	4.9	14.3
1 hr	2.1	2.8	5.5	13.3
K ₂ O				
2 min	2.0	3.7	3.7	7.6
1 hr	1.6	4.6	5.2	11.2
CaO				
2 min	0.10	0.18	0.36	0.13
1 hr	0.31	0.30	0.82	0.32
MgO				
2 min	0.10	0.66	0.25	0.04
1 hr	0.39	1.8	0.59	0.16

in most cases. Even where availability is the major factor controlling concentration in the leachate, i.e., no solubility constraints are operating, only a small portion of the ROS is being extracted. This supports the conclusion that most material in solution was originally external to the fundamental ROS particles, and the mineral matrix itself has remained largely intact. For example, in Core 2 a maximum of 17% of the total Na_2O in the bulk ROS has been removed after one hour from the sample at 6.4-7.4 ft., which represents the zone of accumulation of translocated salts. K_2O does not exhibit a maximum over the range of depths investigated. Compared to Na_2O , higher percentages of K_2O are available for extraction from surface and subsurface samples. The Core 2 results suggest that potassium has not been translocated to the same extent as sodium, possibly due to retention on ion exchange sites.

Core 6 results for Na_2O and K_2O do not exhibit a maximum in the same depth region as Core 2. Results for Core 6 suggest that the zone of accumulation may be near 13.8-14.8 ft., which is directly above the soil-ROS boundary. Without deeper core samples, it is impossible to validate this suggestion. It is quite possible that the slope and elevation of the spoil pile in the region of Core 6 or differences in the compaction caused the weathering pattern to differ from Core 2. As observed for Core 2, a higher percentage of K_2O than Na_2O is available from the subsurface sample at 7.1-8.1 ft., suggesting that potassium is less mobile than sodium.

Core 2 shows only small changes in %CaO extracted with depth, but there is a maximum at 4.7-5.7 ft. The maximum % Na_2O extracted was at 6.4-7.4 ft. In Core 6, CaO shows a maximum at 12.1-12.7 ft., and Na_2O may be at a maximum at 13.8-14.8 ft. The actual zone of maximum Na accumulation may be closer to that of Ca in Core 6, between 12.7-13.8 ft.

In any case, CaO relative to Na₂O shows a consistent pattern with apparently deeper translocation in Core 6.

Only a small percentage of the total available MgO is extracted. Larger amounts of magnesium are extracted from surface samples of Core 2 and Core 6, where weathering has reduced alkalinity and increased magnesium mobility.

In Table 9, the ratios of concentrations of analytes in leachates of samples at depth to the concentrations in the leachates of the surface sample are presented. This is an alternative way of viewing the information on % extracted (Table 8). For Core 2, Na⁺ shows a maximum ratio at 6.4-7.4 ft., which indicates a zone of Na⁺ accumulation. A zone of accumulation has not developed for K⁺ and SO₄²⁻, due to a lower mobility of these ions compared to Na. The decreasing ratio for Mg²⁺ reflects the solubility constraints operating in the leachate. As weathering proceeds and alkaline material is removed from samples at depth, this ratio would increase.

The ratio of leachates from Core 6 samples suggests a greater extent of weathering than in Core 2. The maximum ratio for Na⁺, K⁺ and SO₄²⁻ occurs at 13.8-14.8 ft., although the actual zone of accumulation may be between 12.7 and 13.8 ft. The higher ratio for Mg²⁺ at an intermediate depth suggests that alkaline material has been removed from this region, increasing magnesium mobility.

In Figures 22 and 23, the ratio of Na⁺ to Mg²⁺ in a leachate is plotted as a function of time for Core 2 and Core 6 samples. These two ions appear to be the most sensitive indicators of the extent of weathering. Sodium is highly mobile, and translocation should only be limited by the permeability of the spoil pile. Magnesium responds to the solubility constraints operational in the spoil pile. Increased

Table 9. Ratio of Leachate Concentrations from Samples at Depth to Surface Sample After 1 Hour

Depth Ratio: Core 2				
	$\frac{0.8-1.2 \text{ ft}}{0.8-1.2 \text{ ft}}$	$\frac{4.7-5.7 \text{ ft}}{0.8-1.2 \text{ ft}}$	$\frac{6.4-7.4 \text{ ft}}{0.8-1.2 \text{ ft}}$	$\frac{12.5-13.5 \text{ ft}}{0.8-1.2 \text{ ft}}$
Na ⁺	1	6.6	17.8	14.4
Mg ²⁺	1	0.2	0.07	0.07
Ca ²⁺	1	2.0	1.5	0.8
K ⁺	1	2.1	2.6	4.9
SO ₄ ²⁻	1	2.1	2.6	4.9

Depth Ratio: Core 6				
	$\frac{0.3-0.8 \text{ ft}}{0.3-0.8 \text{ ft}}$	$\frac{7.1-8.1 \text{ ft}}{0.3-0.8 \text{ ft}}$	$\frac{12.1-12.7 \text{ ft}}{0.3-0.8 \text{ ft}}$	$\frac{13.8-14.8 \text{ ft}}{0.3-0.8 \text{ ft}}$
Na ⁺	1	1.4	2.6	6.7
Mg ²⁺	1	5.2	1.6	0.5
Ca ²⁺	1	1.0	1.7	1.0
K ⁺	1	2.4	4.3	8.9
SO ₄ ²⁻	1	6.4	10.6	16.2

Figure 22. Ratio of Na to Mg in leachate with time, Rulison core 2 samples

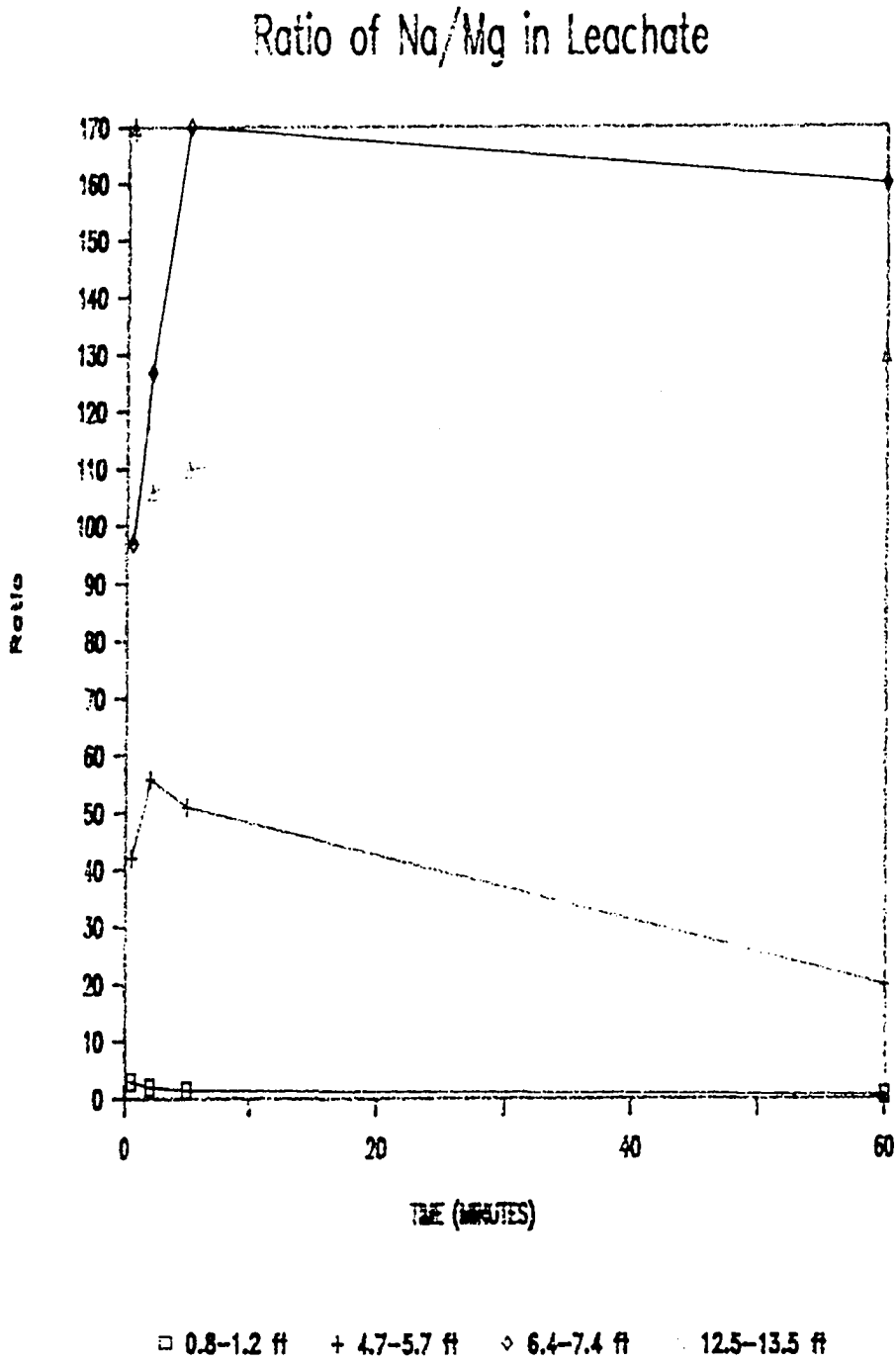
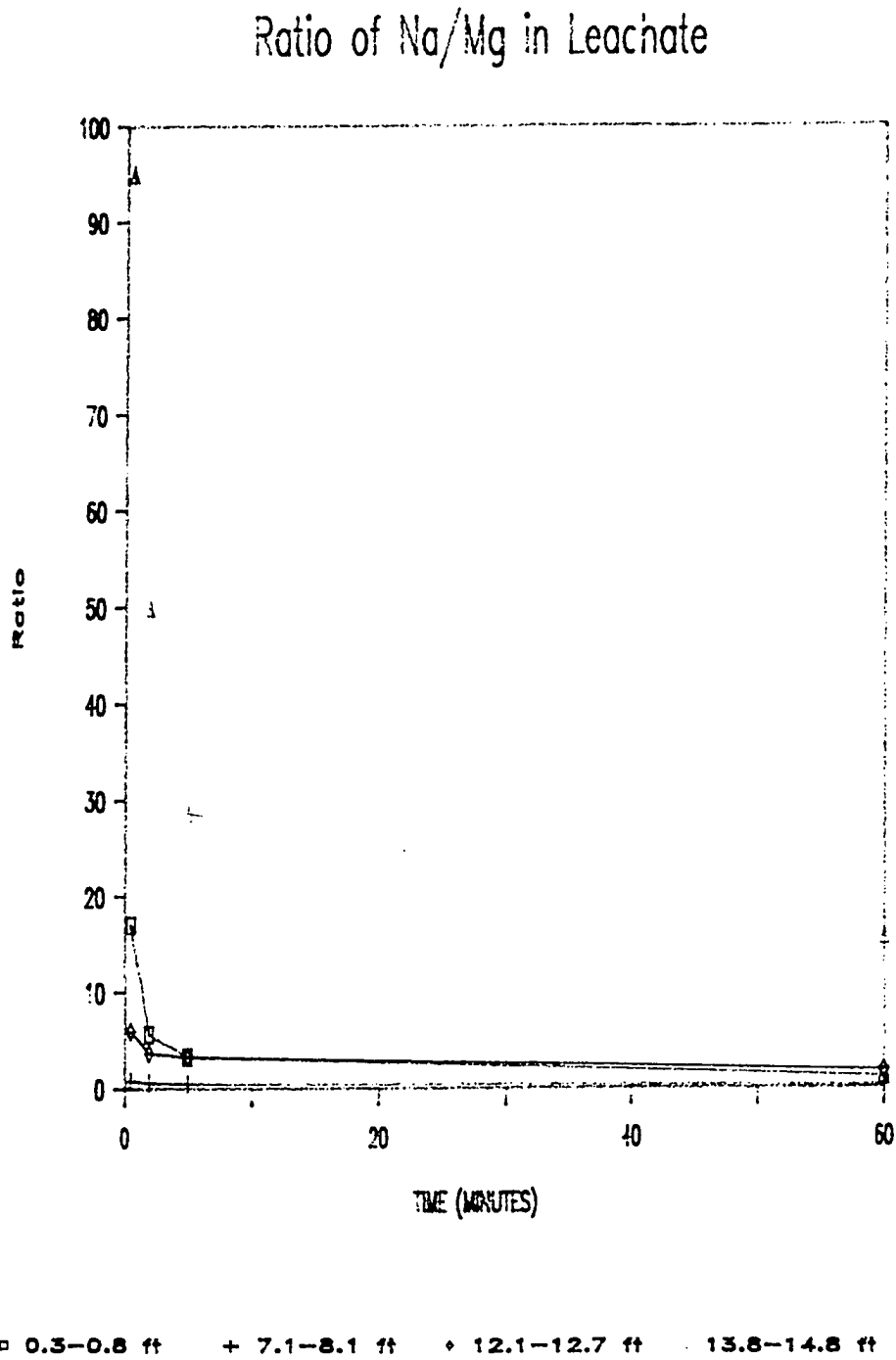


Figure 23. Ratio of Na to Mg in leachate with time, Rulison core 6 samples



magnesium mobility is an indication of increased weathering.

In Core 2 the surface sample is highly weathered, and magnesium mobility has increased. Thus the ratio is very low. A similar curve is produced for the Core 6 surface sample. At intermediate depths in Core 2, Na has accumulated, but Mg concentration is low due to the presence of alkaline material. Therefore the ratio increases. In Core 6, where it is thought that subsurface samples are more highly weathered than in Core 2, the ratio remains low due to the increased mobility of magnesium. Samples at greatest depth in each core exhibit different curves. The differences may be indicative of differences in the extent of weathering undergone by samples at depth.

CONCLUSIONS

Summary of Results

The work reported here has applied both solid phase characterizations and laboratory batch equilibration studies toward a more complete understanding of the effects of long term weathering on ROS.

Laboratory tests were designed to characterize the aqueous dissolution curves of weathered ROS. Differences in the dissolution curves of weathered ROS were observed for material taken from different depths in the spoil pile. The dissolution rate curves, in conjunction with the scanning electron microscopy results, support the models proposed for material obtained at different depths in the spoil pile. However, modifications of the dissolution rate curves occur as a result of competing solution equilibria. Sodium and magnesium appear to be the most sensitive indicators of weathering. For example, a highly weathered surface sample will have an increased magnesium mobility due to decreased alkalinity. The same sample will be largely depleted of sodium, which is highly mobile. The dissolution behavior of other analytes is difficult to elucidate due to complex solubility equilibria.

The leachate chemistry and transport behavior of Core 2 and Core 6 samples is different. Additional information on the physical characteristics of the spoil pile is necessary to explain differences in leachate composition between the two cores.

The translocation of soluble salts from surface to depth in the spoil pile does not significantly alter bulk composition. The mineral matrix itself has remained largely intact. However the x-ray diffraction

work on laboratory weathered ROS indicates that accelerated weathering of the bulk silicate mineral matrix will occur in the presence of highly alkaline leachates (pH 12). Highly alkaline leachates may occur in the field depending on the physical characteristics of the spoil pile.

The extent of recarbonation the spoil pile has undergone is important for successful surface stabilization by vegetative cover over the spoil pile. Differential thermal analysis was not a sensitive enough approach toward quantitative evaluation of the extent of recarbonation as an indicator of weathering. Some recarbonation of the Rulison spoil pile has occurred, as evidenced by the reduced pH of aqueous leachates of surface samples.

Recommendations for Future Work

Based on the data and interpretations presented here, a number of additional routes of investigation are suggested. Continued research on the weathered material is of particular interest, because it eliminates many of the problems of predicting long term stability via laboratory simulations of weathering effects.

Laboratory leaching tests performed here utilized batch extractions at a low solid to solution ratio. Previous studies employed a high solid to solution ratio. A comparison of results points out the importance of variables such as contact time, solid to solution ratio, particle size, and agitation conditions on leachate composition. Column studies of the weathered ROS would be useful, as they may be more appropriate simulations of natural leaching conditions. In addition, more components should be determined for in the leachates. The mobility of trace elements in the Rulison spoil pile has not been extensively investigated. Of particular interest are the anionic trace metals selenate, borate,

molybdate and arsenate, which may become more mobile as weathering proceeds. Additional leaching work using actual groundwater, as well as synthetic leachate solutions, would provide further information on the solubility constraints operational in the natural setting.

The SEM, SEM-EDAX and x-ray diffraction studies provided useful information as to the kinds of physical and chemical alterations which occur as a result of weathering. However, additional work is needed. By further examination of the particle surface characteristics of ROS, the mechanisms of interaction of ROS with groundwater can be more fully characterized, and hopefully better understood.

APPENDICES

Appendix A

Sampling Experiment

Results of Na and K AA analyses. Results expressed in mg Na (or K) extracted per g ROS.

Sodium

Mesh	42-65	42-65	42-65	100-200	100-200	100-200
Sample Weight	0.05g	0.50g	2.00g	0.05g	0.50g	2.00g
1	11.3	11.2	8.8	12.0	9.3	7.4
	10.7	10.7	9.7	11.7	9.7	7.6
2	11.7	9.1	8.7	11.5	9.7	9.1
	16.1	9.1	8.6	11.7	9.2	8.0
3	11.7	10.9	11.9	11.7	9.7	9.4
	14.5	10.5	9.9	12.4	9.4	8.8
4	16.2	9.5	10.1	11.3	9.3	8.2
	15.4	10.5	10.7	11.3	9.4	7.9
5	11.4	9.2	12.1	11.3	9.4	7.3
	12.2	8.6	11.9	11.6	9.2	7.4
6	13.1	9.1	12.2	11.8	9.1	7.5
	11.9	9.1	12.5	11.7	9.5	7.3
7	12.2	9.3	12.8	11.4	9.2	8.2
	12.0	8.9	12.2	10.4	9.1	8.6
8	12.3	9.3	9.2	11.9	9.5	7.6
	11.4	9.3	8.9	10.8	9.4	7.6

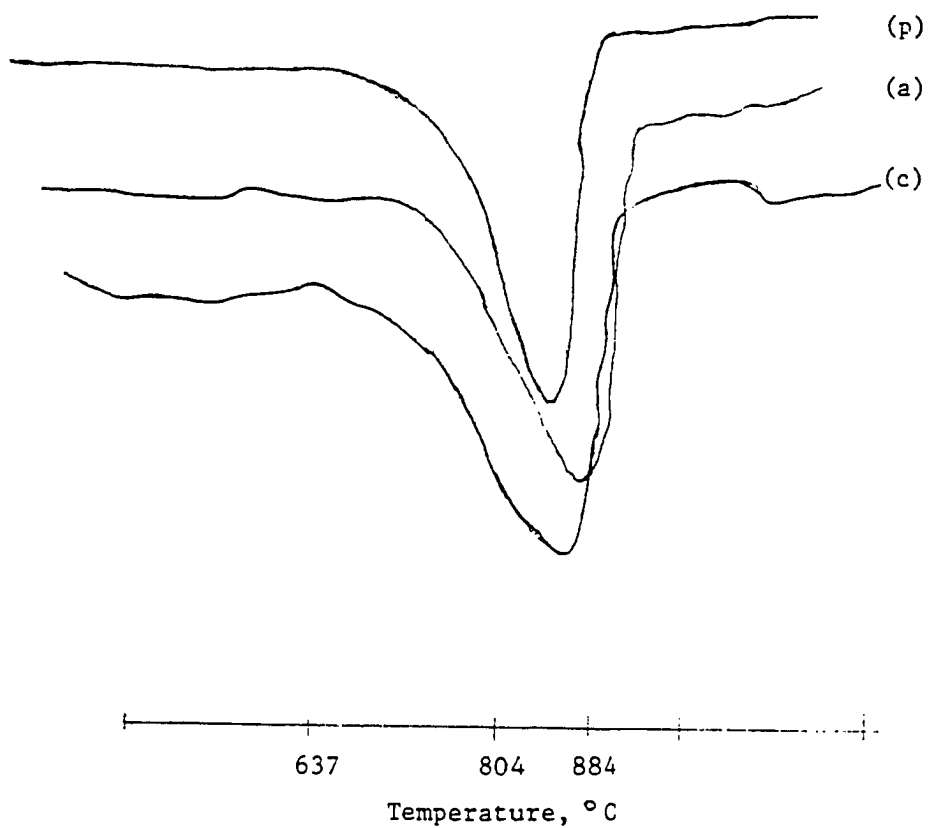
Potassium

Mesh	42-65	42-65	42-65	100-200	100-200	100-200
Sample Weight	0.05g	0.50g	2.00g	0.05g	0.50g	2.00g
1	9.3	7.4	6.2	9.1	6.9	5.5
	8.6	7.3	6.3	9.1	7.1	5.6
2	8.5	6.6	6.1	8.8	7.0	5.9
	8.5	6.5	6.2	9.1	6.8	5.7
3	9.5	7.5	6.6	8.5	6.9	6.4
	8.1	7.4	6.4	8.9	6.8	6.2
4	8.0	6.8	6.5	9.7	6.8	5.8
	7.6	7.1	6.5	9.1	6.9	5.6
5	8.6	6.7	6.4	9.0	6.9	5.4
	9.1	6.5	6.4	9.3	6.9	5.4
6	10.5	6.6	6.2	9.2	6.7	5.4
	8.6	6.8	6.4	8.5	6.9	5.3
7	11.4	6.7	6.4	8.9	6.8	5.8
	9.7	6.5	6.3	8.4	6.8	5.9
8	9.3	6.7	6.3	9.0	6.9	5.4
	9.3	6.7	6.2	8.5	6.9	5.6

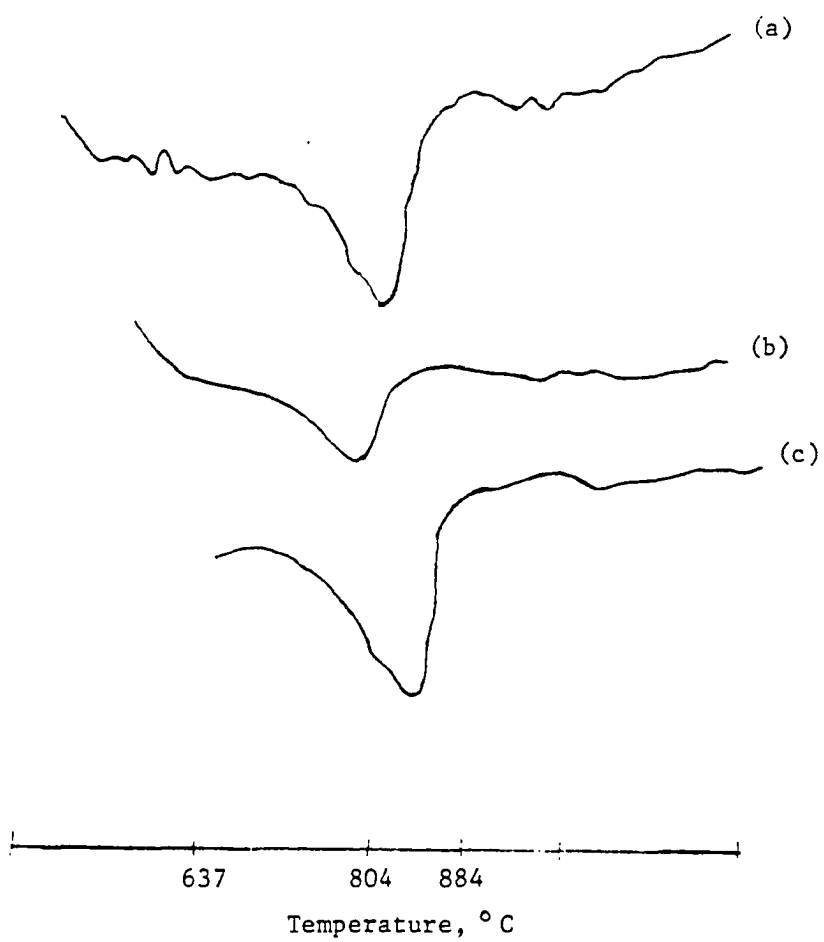
Appendix B

Differential Thermal Analysis

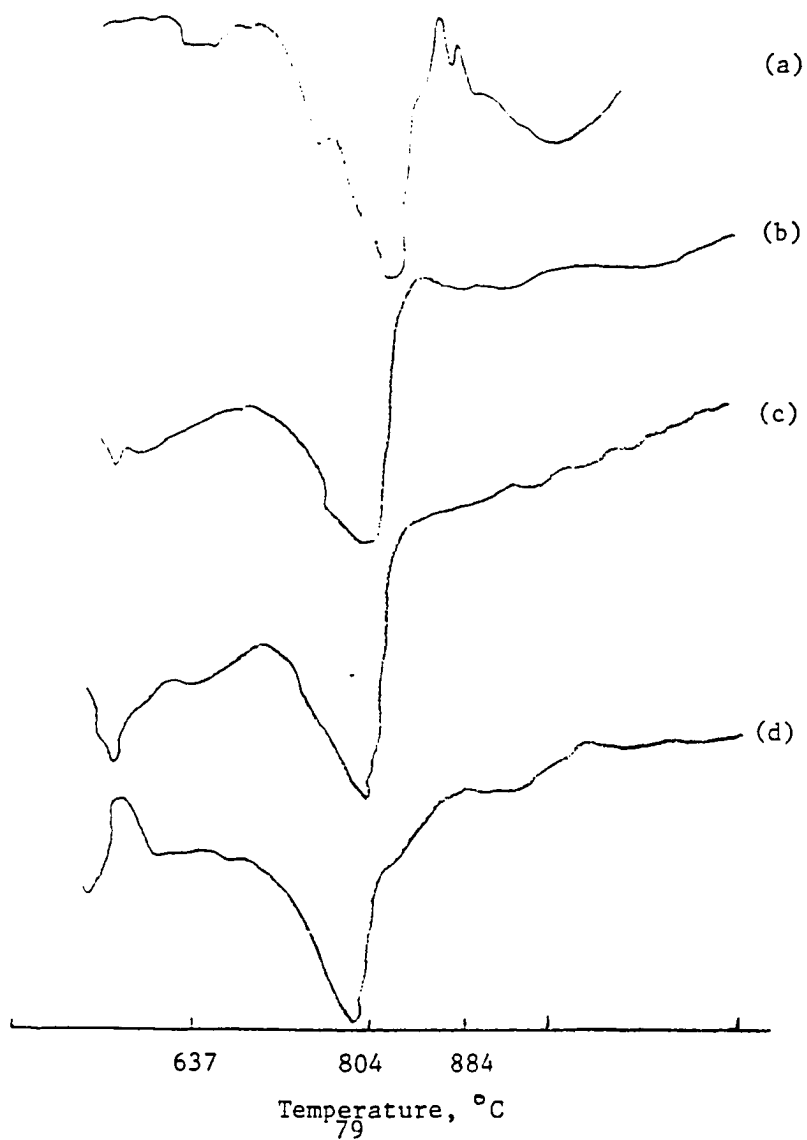
DTA Results for pure calcite (p), coprecipitated calcite (c), and adsorbed calcite (a).



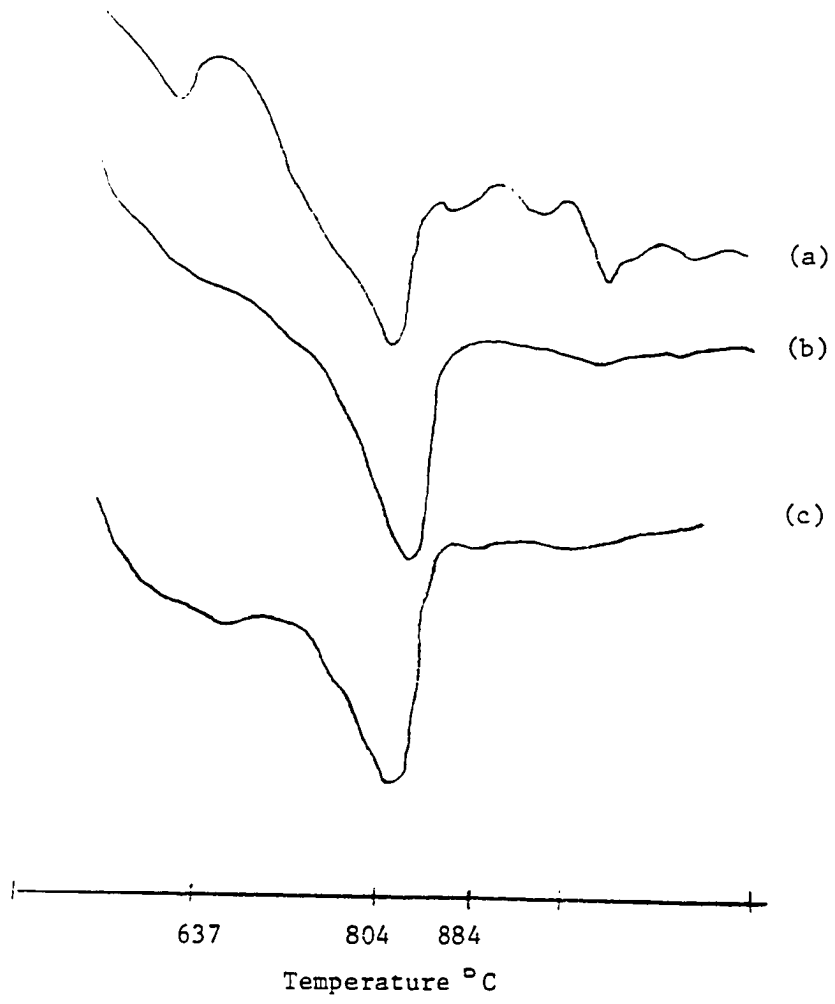
DTA results for core 1 ROS: (a) 0.5-1.0 ft. (b) 7.0-8.0 ft.
(c) 13.0-14.0 ft.



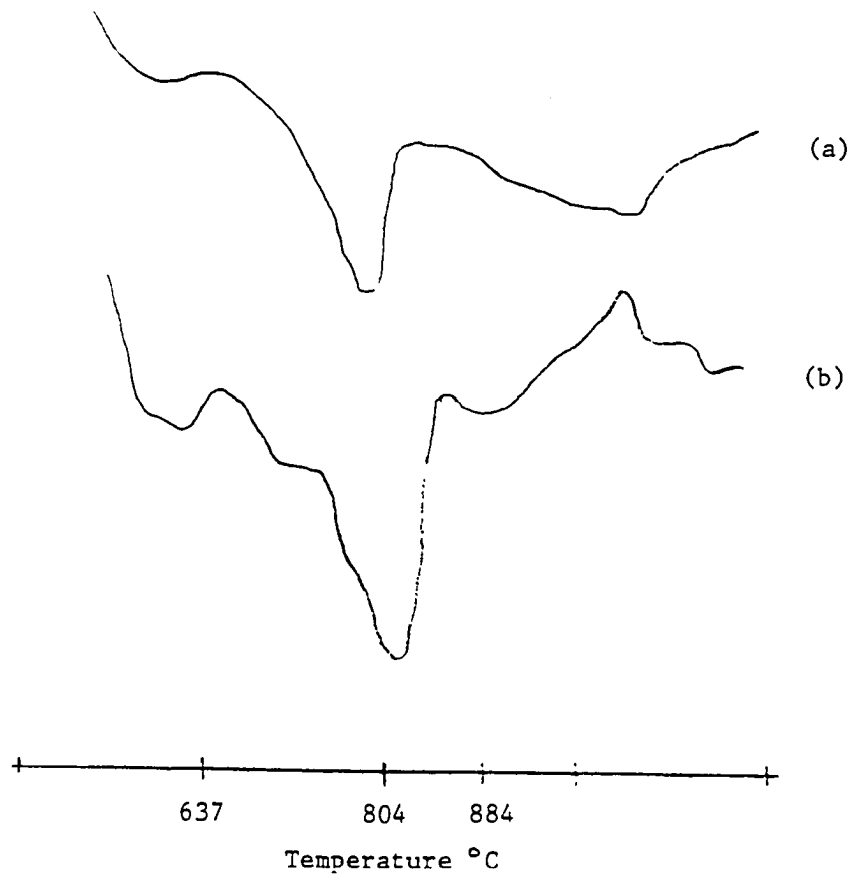
DTA results for core 2 ROS: (a) 0.3-0.8 ft. (b) 6.4-7.4 ft.
(c) 9.0-10.0 ft. (d) 12.5-13.5 ft.



DTA results for core 3 ROS: (a) 0.4-1.4 ft. (b) 5.0-6.0 ft.
(c) 13.0-13.7 ft.



DTA results for core 6 ROS: (a) 0.3-0.8 ft. (b) 14.8-15.8 ft.



Appendix C

Dissolution Rate Experiments

Rullison Site Core 2: 0.8 ft -1.2 ft
Dissolution Rate Experiment
Leachate Concentration in meq/L

Time (Min)	Na	K	Ca	Mg	pH	CO3	HCO3	NO3	SO4
0.25					6.2		0.095		
0.25					6.9		0.087		
0.50	0.161	0.100	0.135	0.061	6.2		0.121	0.039	0.096
0.50	0.113	0.115	0.140	0.061	6.4		0.095	0.029	0.108
0.75					6.5		0.154		
0.75					6.5		0.161		
1.00	0.091	0.113	0.170	0.071	6.8		0.177	0.050	0.121
1.00	0.074	0.107	0.170	0.082	6.6		0.161	0.029	0.138
2.00	0.087	0.118	0.230	0.107	6.8		0.236	0.039	0.154
2.00	0.065	0.120	0.210	0.098	7.0		0.164	0.024	0.156
5.00	0.091	0.153	0.295	0.139	7.1		0.320	0.050	0.2
5.00	0.226	0.304	0.285	0.139	6.8		0.290	0.052	0.217
10.00	0.113	0.171	0.340	0.180	7.0		0.344	0.121	0.121
10.00	0.113	0.161	0.320	0.180	6.5		0.179	0.203	0.229
30.00					7.0		0.408	0.123	0.306
30.00					6.4		0.207	0.294	0.306
60.00	0.122	0.199	0.470	0.246	6.9		0.289		
60.00	0.096	0.205	0.490	0.254	6.9		0.446		

Rulison Site Core 2: 0.8 ft -1.2 ft
 Dissolution Rate Experiment
 Leachate Concentration in meq/L

Time (Min)	Na	K	Ca	Mg
0.25	0.035	0.054	0.035	0.016
0.25	0.057	0.057	0.125	0.025
0.50	0.07	0.07	0.05	0.016
0.50	0.052	0.052	0.055	0.025
0.75	0.065	0.065	0.055	0.025
0.75	0.078	0.078	0.1	0.033
1.00	0.07	0.07	0.055	0.025
1.00	0.087	0.087	0.095	0.033
2.00	0.074	0.074	0.105	0.041
2.00	0.091	0.091	0.11	0.041
5.00	0.122	0.122	0.17	0.066
5.00	0.078	0.078	0.175	0.066
10.00	0.065	0.065	0.23	0.09
10.00	0.07	0.07	0.24	0.09
30.00	0.126	0.126	0.32	0.123
30.00	0.091	0.091	0.3	0.115
60.00	0.07	0.07	0.44	0.148
60.00	0.113	0.113	0.455	0.156

Rulison Site Core 2: 4.7 ft - 5.7 ft
 Dissolution Rate Experiment
 Leachate Concentration in meq/L

Time (Min)	Na	K	Ca	Mg
0.25	0.43	0.064	0.19	0.007
0.25	0.252	0.064	0.265	0.011
0.50	0.357	0.297	0.245	0.009
0.50	0.483	0.097	0.245	0.011
0.75	0.604	0.184	0.275	0.011
0.75	0.47	0.148	0.23	0.009
1.00	0.417	0.148	0.29	0.009
1.00	0.452	0.164	0.305	0.01
2.00	0.635	0.21	0.375	0.012
2.00	0.491	0.176	0.29	0.011
5.00	0.504	0.225	0.365	0.012
5.00	0.509	0.238	0.47	0.015
10.00	0.583	0.299	0.53	0.016
10.00	0.413	0.24	0.54	0.017
30.00	0.67	0.404	0.75	0.02
30.00	0.57	0.384	0.635	0.019
60.00	0.643	0.355	0.895	0.033
60.00	0.535	0.32	0.87	0.03

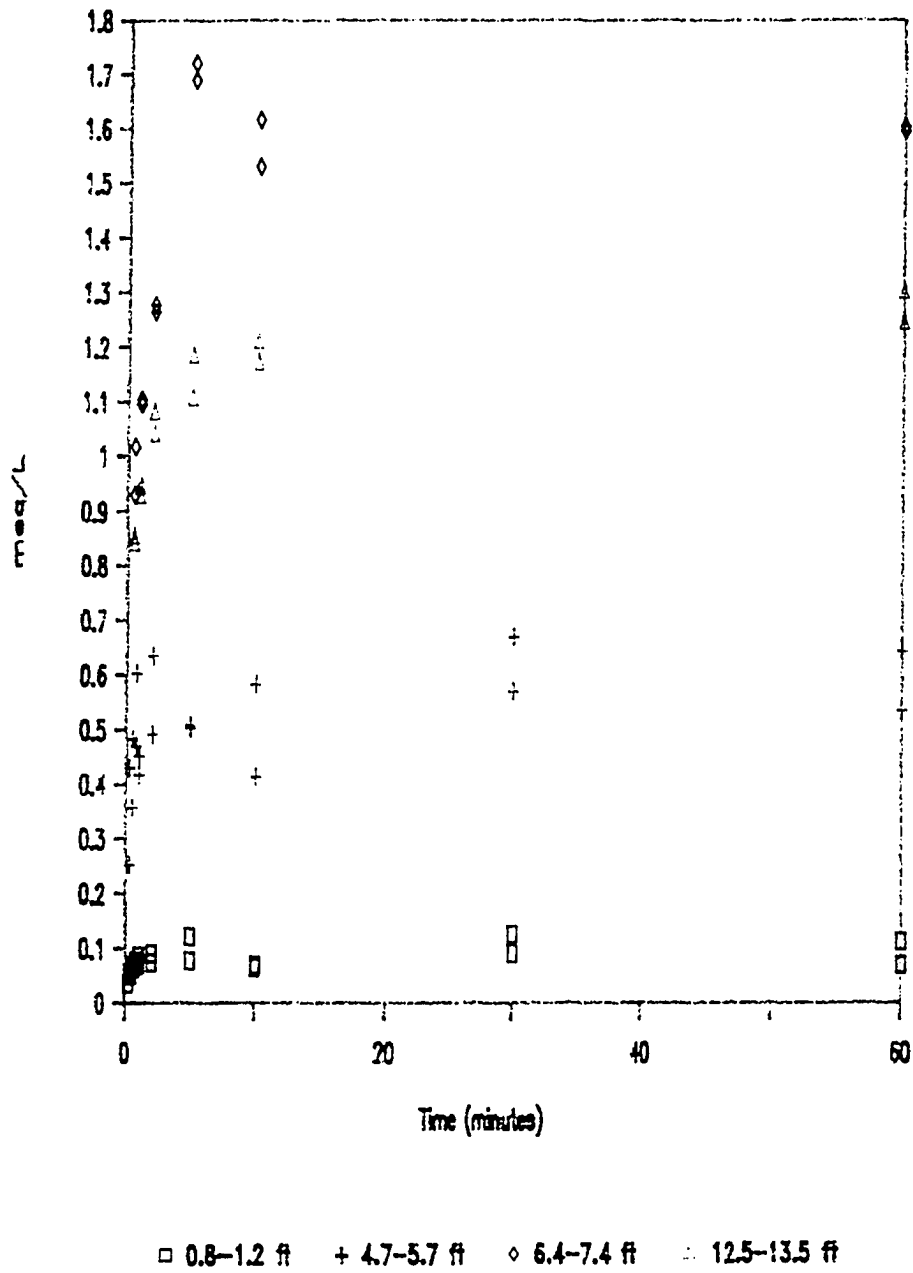
Rullison Site Core 2: 6.4 ft - 7.4 ft
Dissolution Rate Experiment
Leachate Concentration in meq/L

Time (Min)	Na	K	Ca	Mg	pH	CO3	HCO3	NO3	SO4
0.25					7.9		0.448	0.077	0.570
0.25					7.3		0.448		
0.50	1.017	0.179	0.195	0.008	9.1	0.180	0.415	0.018	0.679
0.50	0.930	0.171	0.195	0.008	7.7		0.530		0.610
0.75					9.1				
0.75					7.3		0.607	0.006	0.681
1.00	1.096	0.223	0.240	0.008	8.2	0.097	0.634	0.031	0.779
1.00	1.104	0.220	0.225	0.008	7.4		0.661		0.691
2.00	1.265	0.269	0.315	0.011	9.3	0.400	0.393	0.031	0.904
2.00	1.278	0.269	0.310	0.012	8.4	0.213	0.590	0.021	0.770
5.00	1.722	0.348	0.410	0.009	9.5	0.533	0.457	0.031	1.112
5.00	1.691	0.325	0.390	0.010	9.1	0.483	0.475	0.034	1.008
10.00	1.530	0.361	0.560	0.013	8.1	0.090	0.792		
10.00	1.617	0.386	0.550	0.014	9.3	0.793	0.280	0.053	1.400
30.00					9.5	0.713	0.292	0.300	1.606
30.00					9.4	0.680	0.249		1.229
60.00	1.604	0.430	0.650	0.015	9.4	0.463	0.280	0.108	1.523
60.00	1.596	0.412	0.665	0.013	9.2	0.647	0.233	0.019	1.623

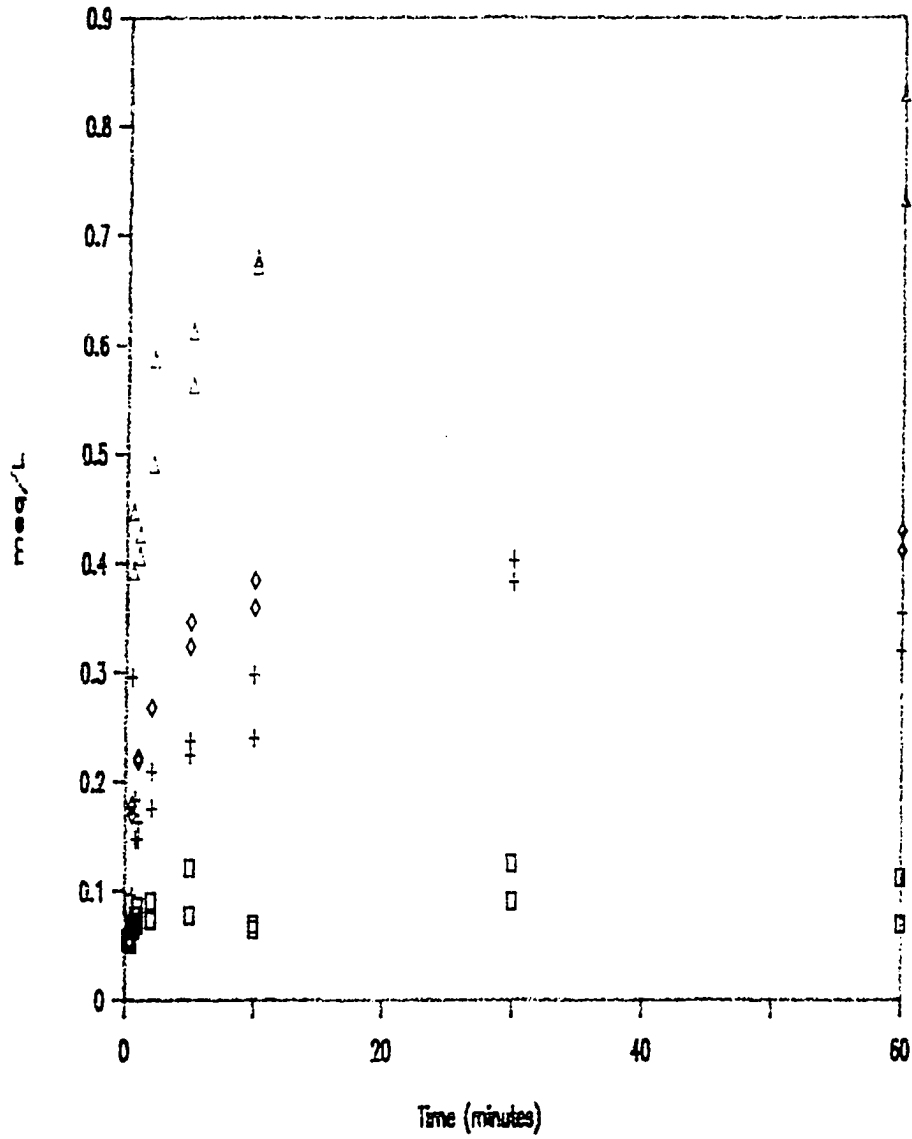
Rulison Site Core 2: 12.5 ft. - 13.5 ft.
Dissolution Rate Experiment
Leachate Concentration in meq/L

Time (Min)	Na	K	Ca	Mg	pH	CO3	HCO3	NO3	SO4
0.25					7.0		0.190		
0.25					6.9		0.192		
0.50	0.843	0.394	0.090	0.003	6.8		0.261	0.134	0.869
0.50	0.857	0.448	0.215	0.005	6.9		0.262		0.894
0.75					6.9		0.313	0.009	
0.75					6.9		0.313		
1.00	0.930	0.407	0.135	0.004	7.1		0.359		0.929
1.00	0.948	0.427	0.115	0.005	7.0		0.328	0.003	1.010
2.00	1.083	0.588	0.145	0.007	7.3		0.367	0.003	0.929
2.00	1.043	0.491	0.175	0.012	7.8	0.083	0.349	0.014	0.979
5.00	1.109	0.565	0.200	0.007	7.3		0.513	0.014	1.065
5.00	1.187	0.614	0.210	0.007	7.2		0.541	0.014	1.163
10.00	1.213	0.673	0.255	0.009	7.4		0.557	0.014	1.158
10.00	1.174	0.680	0.285	0.011	8.4	0.140	0.438	0.014	1.292
30.00					7.8	0.093	0.538	0.019	1.398
30.00					7.6		0.600	0.048	1.446
60.00	1.304	0.831	0.380	0.015	7.6		0.643		1.310
60.00	1.248	0.734	0.340	0.014	7.6		0.569	0.071	1.446

Na Dissolution Curves: Core 2 Samples

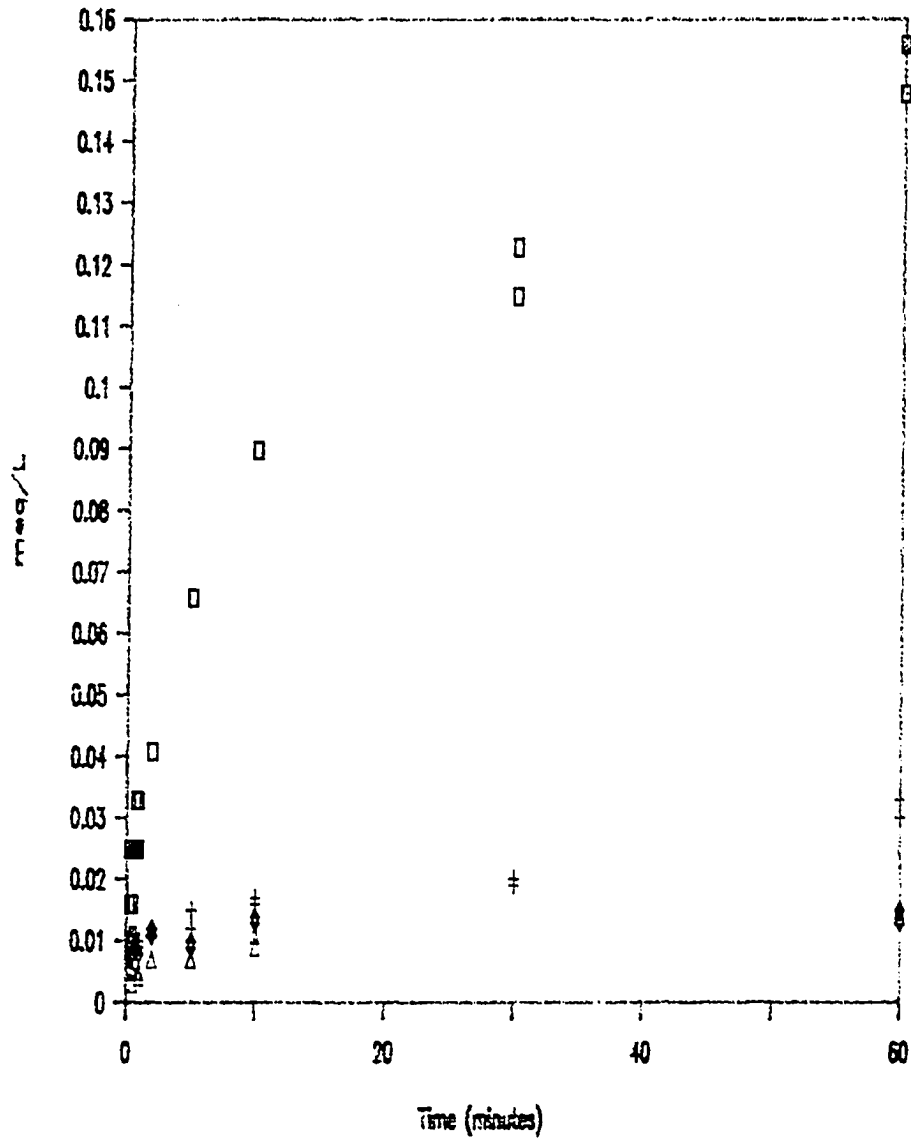


K Dissolution Curves: Core 2 Samples



□ 0.8-1.2 ft + 4.7-5.7 ft ◇ 6.4-7.4 ft △ 12.5-13.5 ft

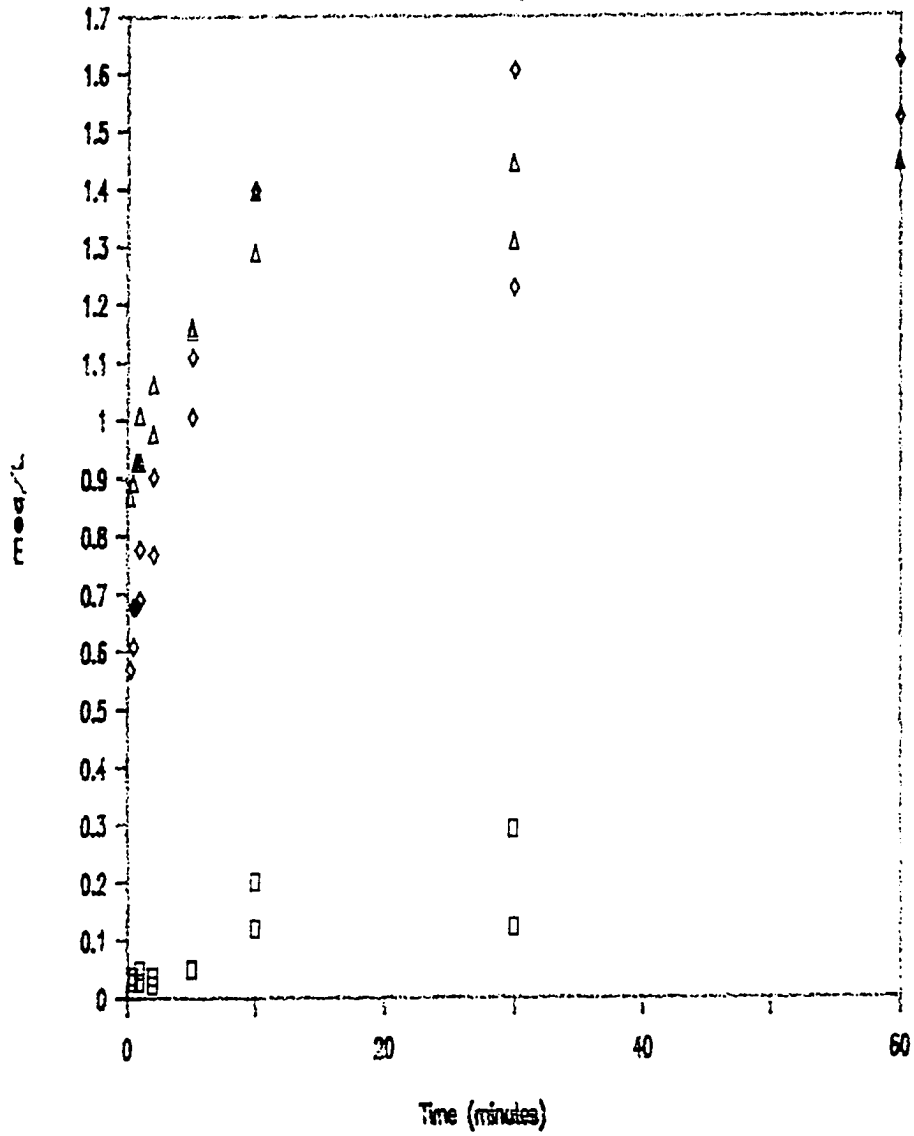
Mg Dissolution Curves: Core 2 Samples



□ 0.8-1.2 ft + 4.7-5.7 ft ◇ 6.4-7.4 ft △ 12.5-13.5 ft

Sulfate Dissolution Curves

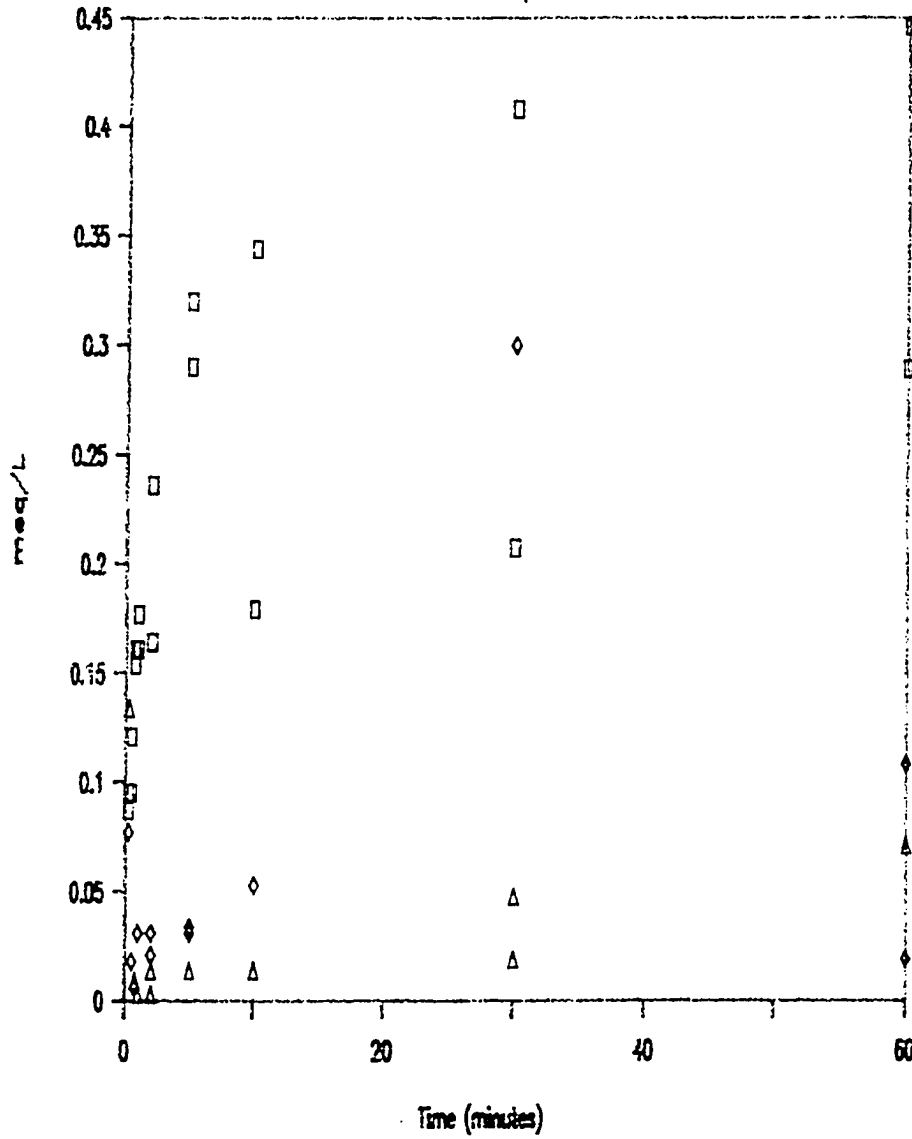
Core 2 Samples



□ = 0.8-1.2 ft + 4.7-5.7 ft ♦ 6.4-7.4 ft × 12.5-13.5 ft

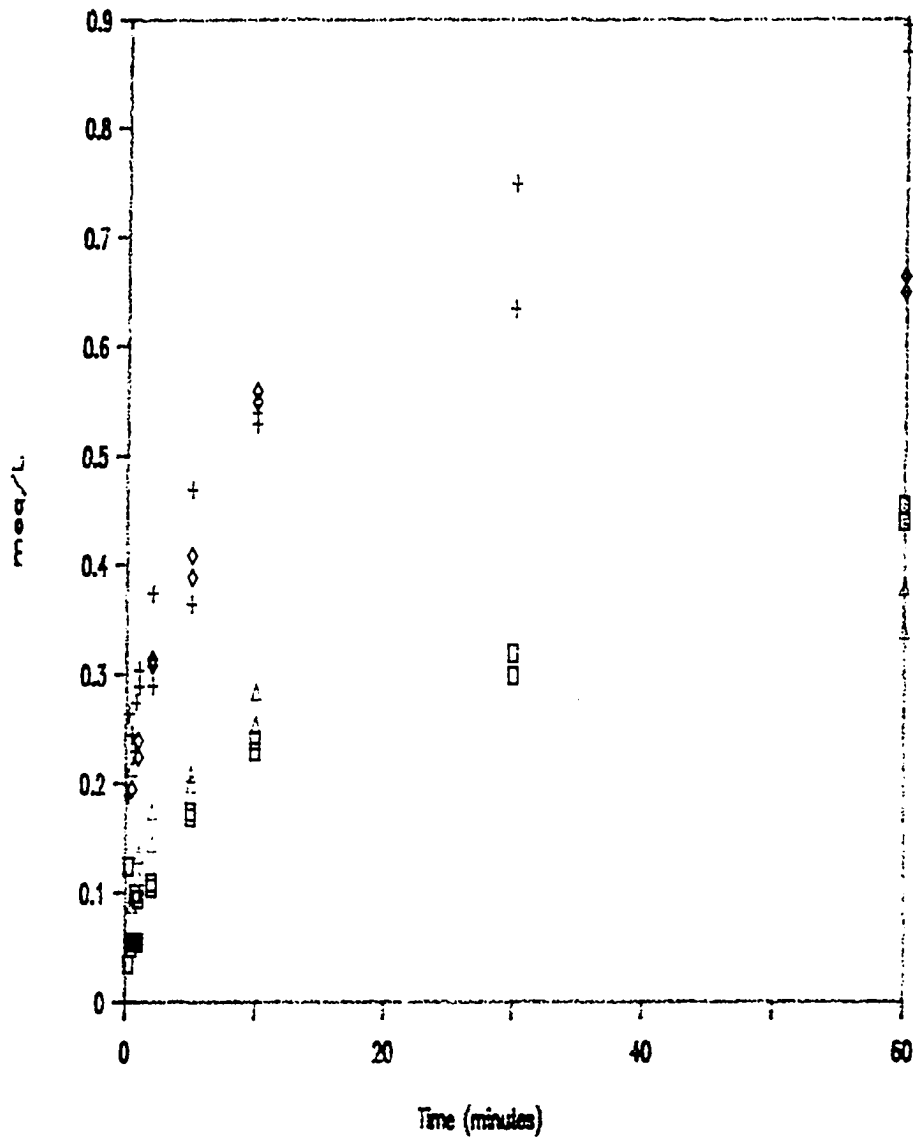
Nitrate Dissolution Curves:

Core 2 Samples



□ 0.8-1.2 ft + 4.7-5.7 ft ◇ 6.4-7.4 ft △ 12.5-13.5 ft

Ca Dissolution Curves: Core 2 Samples



□ 0.8-1.2 ft + 4.7-5.7 ft ◇ 6.4-7.4 ft △ 12.5-13.5 ft

Rulison Site Core 6: 0.3 ft. - 0.8 ft.
Dissolution Rate Experiment
Leachate Concentration in meq/L

Time (Min)	Na	K	Ca	Mg	pH	CO3	HCO3	NO3	SO4
0.25	0.087	0.041	0.026	0.039	7.9	0.037	0.095	0.055	
0.50	0.104	0.043	0.026	0.012	7.3		0.063	0.063	
0.50	0.248	0.043	0.026	0.013			0.072	0.063	0.038
0.75	0.100	0.064	0.060	0.018	6.4		0.080	0.106	
0.75	0.200	0.064	0.080	0.021				0.126	
1.00	0.191	0.164	0.060	0.023	6.6				
1.00	0.170	0.059	0.080	0.039			0.107	0.052	0.019
2.00	0.148	0.082	0.075	0.031	6.7			0.068	0.038
2.00	0.200	0.097	0.070	0.035			0.144	0.066	0.023
5.00	0.152	0.074	0.140	0.055	8.0			0.095	0.038
5.00	0.257		0.120	0.063			0.272	0.058	0.025
10.00	0.074	0.061	0.140	0.081	7.8			0.098	0.044
10.00	0.083	0.074	0.165	0.090			0.287	0.076	0.027
30.00	0.083	0.069	0.200	0.123	8.0			0.106	0.048
30.00	0.157	0.115	0.190	0.107			0.392	0.042	0.033
60.00	0.083	0.069	0.230	0.131	8.1			0.063	0.058
60.00	0.200	0.072	0.210	0.131			0.418	0.071	0.035

Rulison Site Core 6: 12.1 ft. - 12.7 ft.
Dissolution Rate Experiment
Leachate Concentration in meq/L

Time (Min)	Na	K	Ca	Mg	pH	CO3	HCO3	NO3	SO4
0.25	0.248	0.133	0.105	0.035	7.3		0.092	0.045	0.252
0.25	0.226	0.143	0.110	0.041			0.105	0.040	0.242
0.50	0.270	0.174	0.130	0.049	7.5		0.149	0.050	0.300
0.50	0.326	0.246	0.145	0.053			0.164	0.045	0.277
0.75	0.313	0.207	0.145	0.060	7.3		0.174	0.050	0.323
0.75	0.300	0.205	0.150	0.060			0.190	0.050	0.317
1.00	0.378	0.230	0.170	0.066	7.5		0.218	0.058	0.340
1.00	0.313	0.212	0.170	0.065			0.228	0.050	0.323
2.00	0.339	0.223	0.195	0.090	8.3		0.264	0.060	0.369
2.00	0.317	0.223	0.195	0.090			0.274	0.055	0.371
5.00	0.348	0.248	0.240	0.123	8.3		0.326	0.068	0.425
5.00	0.461	0.320	0.235	0.123			0.325	0.063	0.423
10.00	0.357	0.248	0.295	0.156	8.1		0.377	0.079	0.467
10.00	0.426	0.274	0.295	0.164			0.336	0.100	0.467
30.00	0.374	0.263	0.350	0.197	8.5		0.444	0.090	0.506
30.00	0.391	0.343	0.335	0.205			0.441	0.074	0.500
60.00	0.357	0.294	0.355	0.221	8.6		0.484	0.074	0.506
60.00	0.383	0.317	0.390	0.205				0.077	0.544

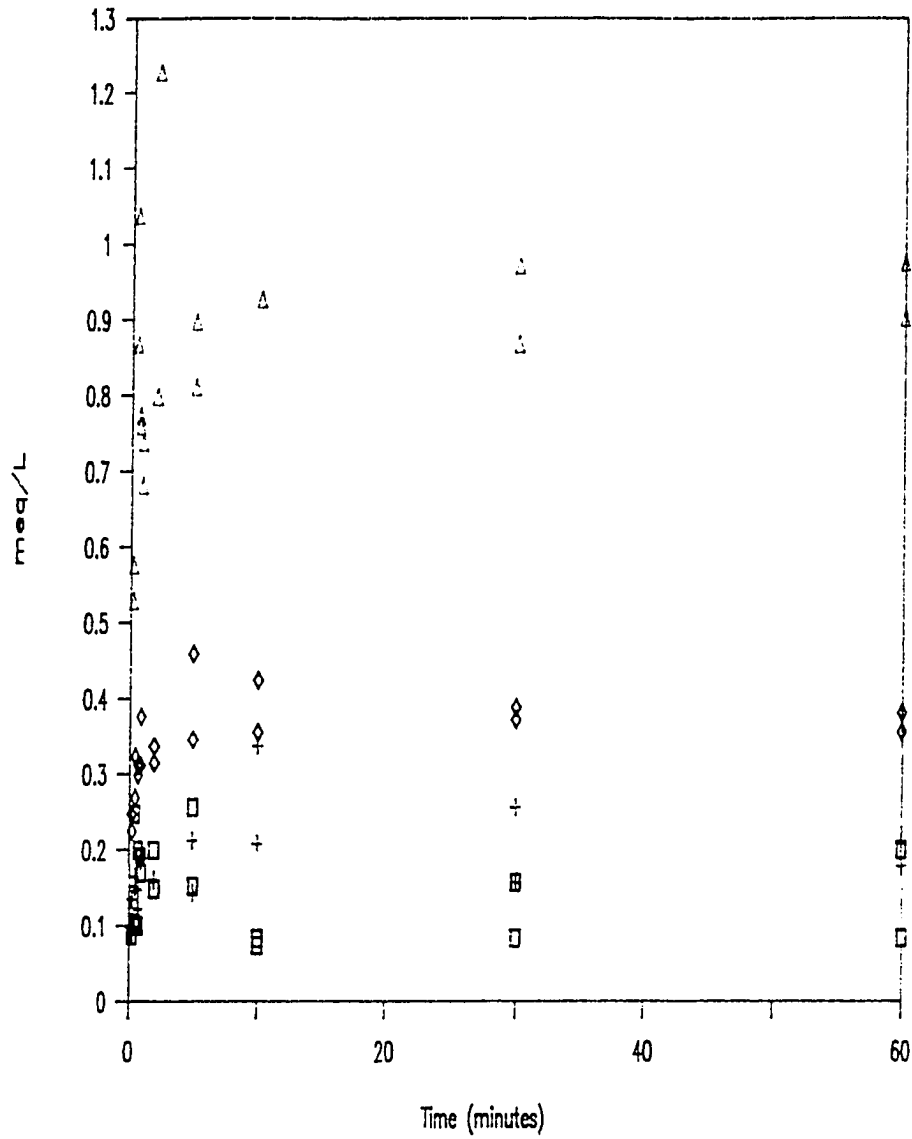
Ruilson Site Core 6: 7.1 ft. - 8.1 ft.
Dissolution Rate Experiment
Leachate Concentration in meq/L.

Time (Min)	Na	K	Ca	Mg	pH	CO3	HCO3	NO3	SO4
0.25	0.091	0.059	0.045	0.107	7.0		0.054	0.027	0.123
0.25	0.135	0.056	0.055	0.115			0.077	0.056	0.148
0.50	0.152	0.095	0.065	0.246	7.1		0.092	0.029	0.152
0.50	0.165	0.092	0.070	0.164			0.118	0.027	0.169
0.75	0.122	0.069	0.080	0.164	7.4		0.146	0.029	0.165
0.75	0.148	0.125	0.090	0.172			0.144	0.027	0.183
1.00	0.191	0.128		0.443	7.4		0.298	0.027	0.175
1.00	0.187	0.097	0.100	0.090			0.175	0.029	0.225
2.00	0.161	0.123	0.145	0.254	7.7		0.262	0.039	0.219
2.00	0.161	0.141	0.125	0.238			0.246	0.032	0.269
5.00	0.143	0.100	0.170	0.352	7.9		0.390	0.032	0.267
5.00	0.213	0.120	0.160	0.344			0.348	0.032	0.300
10.00	0.209	0.136	0.190	0.574	7.9		0.470	0.047	0.288
10.00	0.339		0.180	0.443			0.416	0.048	0.329
30.00	0.257	0.256	0.225	0.697	8.0		0.608	0.027	0.292
30.00	0.157	0.123	0.190	0.525			0.516	0.048	0.331
60.00	0.178	0.156	0.230	0.738	8.4		0.725	0.048	0.315
60.00	0.209	0.174	0.220	0.607			0.631	0.027	

Rulison Site Core 6: 13.8 ft. - 14.8 ft.
Dissolution Rate Experiment
Leachate Concentration in meq/L

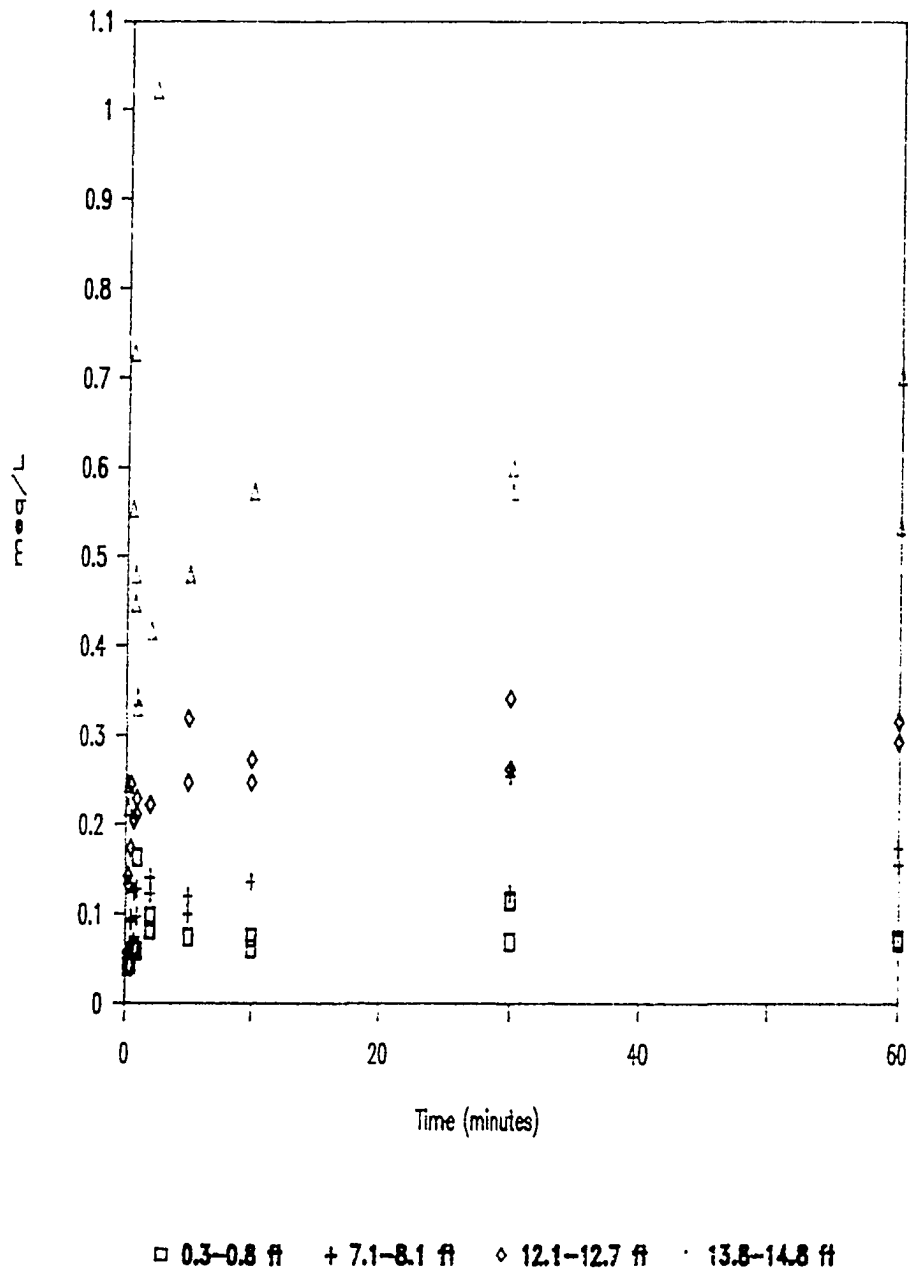
Time (Min)	Na	K	Ca	Mg	pH	CO3	HCO3	NO3	SO4
0.25	0.578	0.246	0.055	0.010	7.7		0.239	0.026	0.529
0.25	0.530	0.220	0.050	0.009			0.192	0.010	0.450
0.50	0.870	0.555	0.065	0.010	8.5		0.305	0.026	0.579
0.50	1.039	0.729	0.065	0.011			0.279	0.010	0.510
0.75	0.774	0.481	0.075	0.012	8.8		0.366	0.026	0.606
0.75	0.761	0.448	0.070	0.011		0.033	0.302	0.013	0.563
1.00	0.739	0.343	0.080	0.012	8.4	0.040	0.351	0.026	0.621
1.00	0.683	0.332	0.080	0.012			0.364	0.015	0.558
2.00	1.230	1.023	0.090	0.016	9.1	0.080	0.413	0.027	0.677
2.00	0.800	0.417	0.095	0.016		0.067	0.413	0.013	0.625
5.00	0.900	0.481	0.125	0.030	9.2	0.137	0.457	0.032	0.750
5.00	0.813	0.483	0.115	0.024		0.257	0.305	0.021	0.688
10.00	0.930	0.575	0.155	0.036	9.4	0.207	0.441	0.037	0.813
10.00	0.930	0.575	0.150	0.035		0.250	0.418	0.034	0.748
30.00	0.974	0.601	0.205	0.051	9.0	0.253	0.470	0.037	0.863
30.00	0.870	0.575	0.190	0.047		0.217	0.428	0.018	0.779
60.00	0.904	0.535	0.235	0.061	9.2	0.230	0.418	0.035	0.808
60.00	0.978	0.703	0.225	0.057		0.283	0.467	0.015	0.815

Na Dissolution Curves: Core 6 Samples

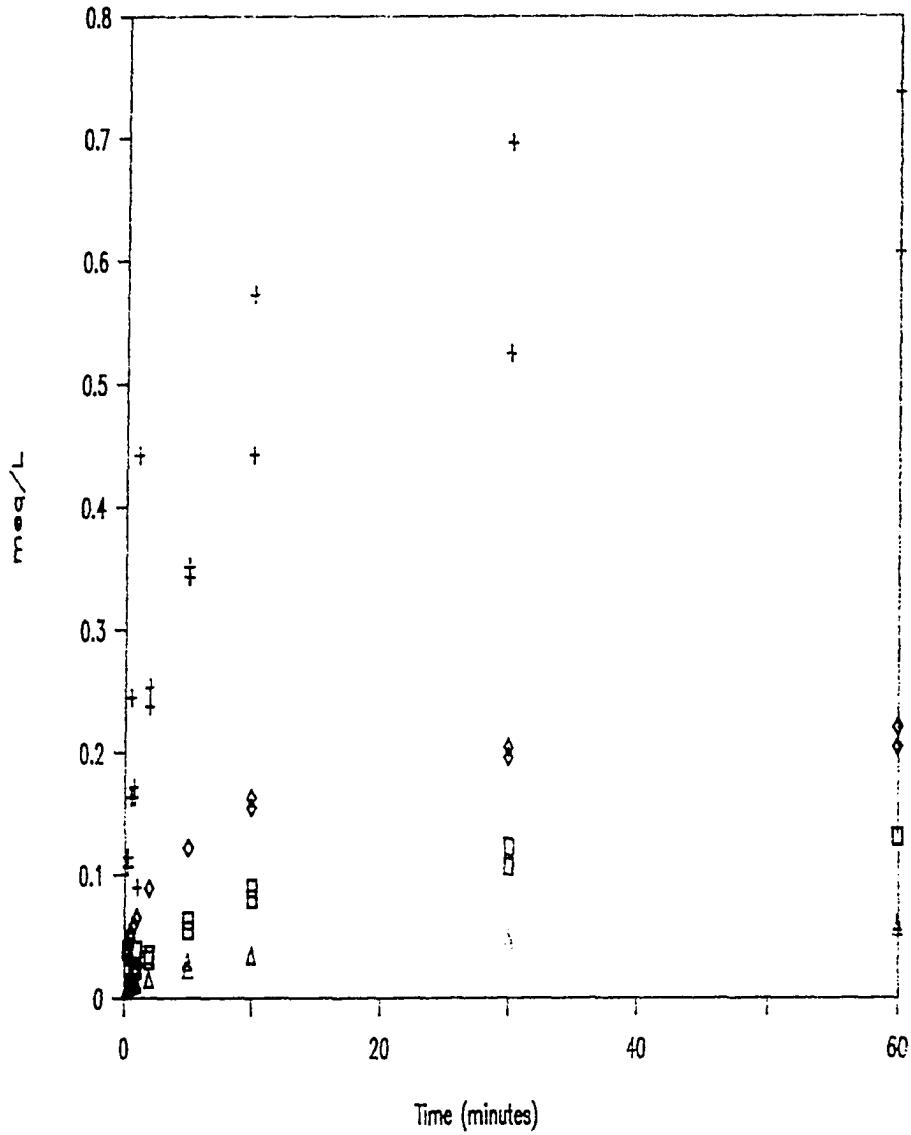


□ 0.3-0.8 ft + 7.1-8.1 ft ◇ 12.1-12.7 ft △ 13.8-14.8 ft

K Dissolution Curves: Core 6 Samples



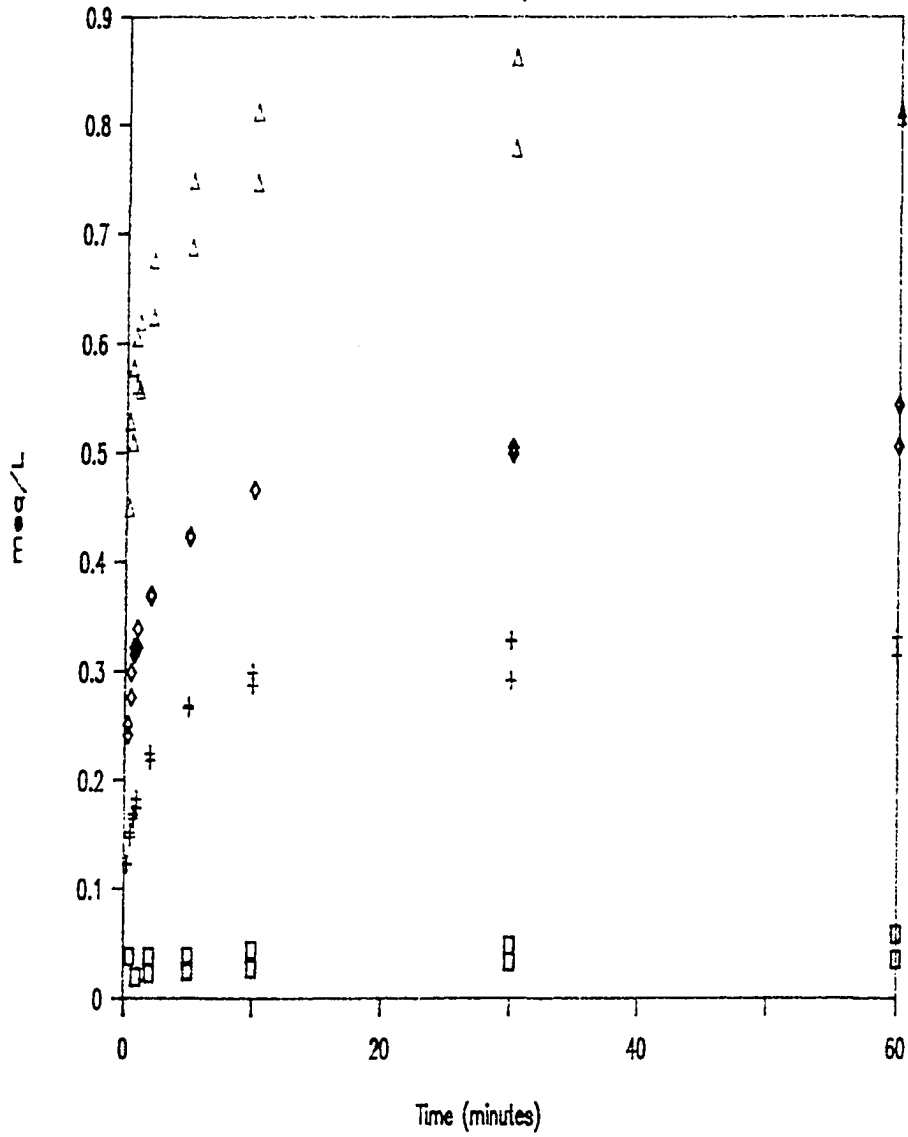
Mg Dissolution Curves: Core 6 Samples



0.3-0.8 ft + 7.1-8.1 ft ◇ 12.1-12.7 ft △ 13.8-14.8 ft

Sulfate Dissolution Curves

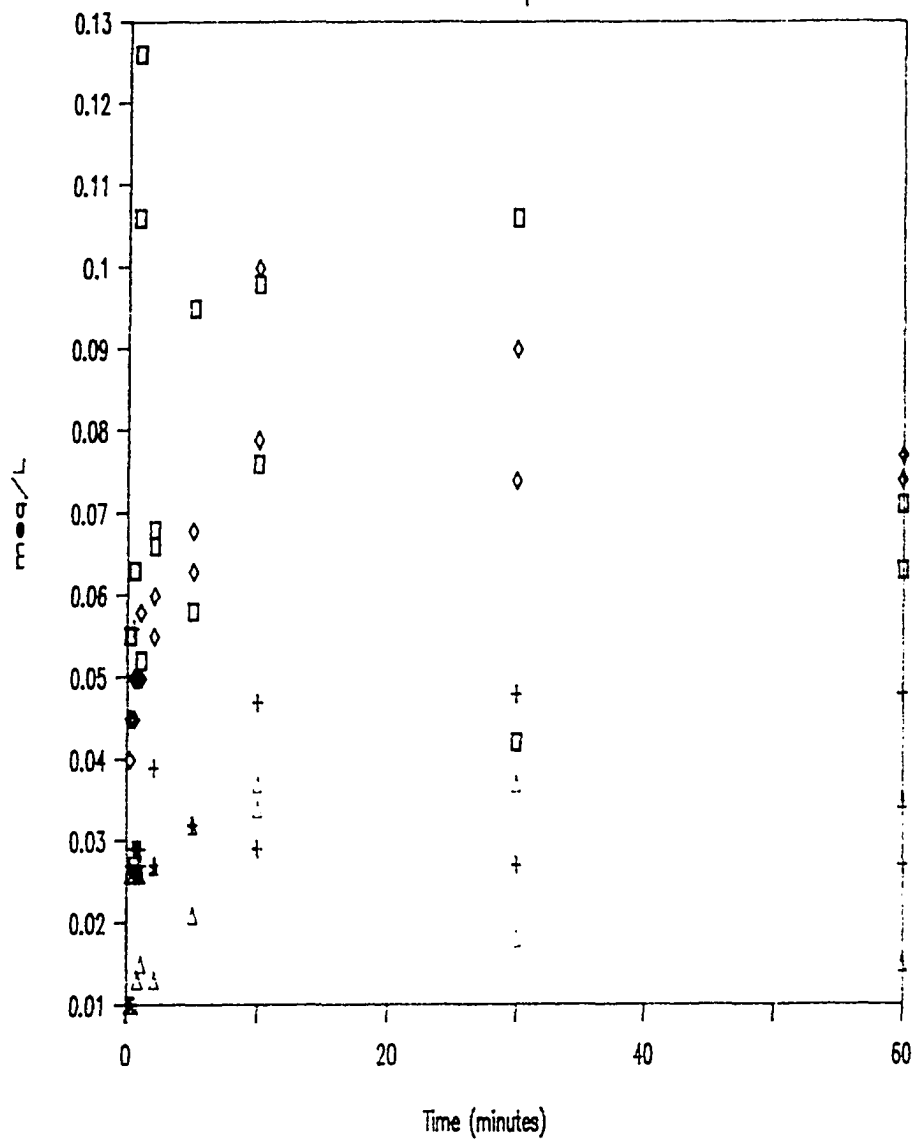
Core 6 Samples



□ 0.3-0.8 ft + 7.1-8.1 ft ◇ 12.1-12.7 ft △ 13.8-14.8 ft

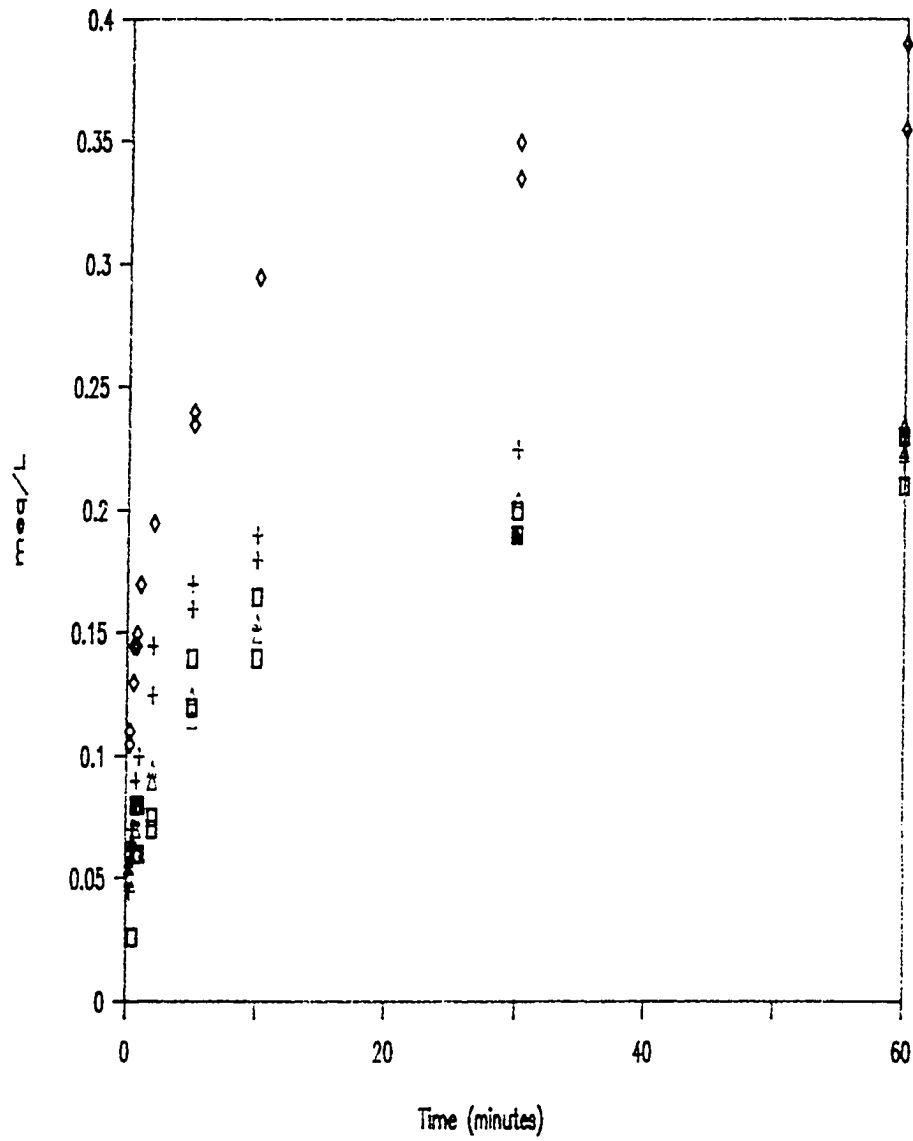
Nitrate Dissolution Curves

Core 6 Samples



□ 0.3-0.8 ft + 7.1-8.1 ft ◇ 12.1-12.7 ft △ 13.8-14.8 ft

Ca Dissolution Curves: Core 6 Samples



□ 0.3-0.8 ft + 7.1-8.1 ft ◇ 12.1-12.7 ft △ 13.8-14.8 ft

REFERENCES

Akerman, D. J. (1983) Private Communication.

American Society For Testing Materials. (1974) Selected powder diffraction data for minerals. Joint Committee on Powder Diffraction Standards, Philadelphia.

Amy, G. L., Hines, A. L., Thomas, J. F. and Selleck, R. E. (1979) Groundwater leaching of organic pollutants from in situ retorted oil shale. Environ. Sci. Technol. 14, 831-835.

Bell, P. R. F., Krol, A. A. and Greenfield, P. F. (1986) Factors controlling the leaching of major and minor constituents from processed oil shale. Water Research 20, 741-750.

Bell, P. R. F., Geronimos, G. L., Cobson, K. And Greenfield, P. F. (1982) Characteristics of leachates from Rundle shale processed in a Lurgi pilot retort. Environ. Technol. Lett. 3, 433-440.

Endersen, S. J. (1983) Chemical characterization of weathered retorted oil shale leachates: species mobility and environmental impact. Masters thesis, University of New Hampshire.

Esin, O. A., Gel'd, P. V. and Popel, S. I. (1949). Chem. Abstr. 43:7306g.

Ettinger, H. J. (1981) Industrial hygiene concerns associated with oil shale development. In Oil Shale: The Environmental Challenges (Edited by Peterson, K. K.), 64-87. Colorado School of Mines, Golden, Colo.

Feerer, J. L., Miller, A. G. and Ramirez, W. F. (1986) X-ray photoelectric spectroscopy determination of a conceptual leaching model of retorted oil shale. Environ. Sci. Technol. 20, 695-702.

Fransway, D. F. and Wagenet, R. J. (1981) Salt release and movement in processed oil shale. J. Environ. Qual. 10, 107-113.

Gavin, M. J. And Desmond, J. S. (1930) Construction And Operation of the Bureau of Mines Experimental Oil Shale Plant 1925-1927. Bulletin 315, U. S. Bureau of Mines, Washington.

Haggin J. (1985) Interest heightens in development of eastern oil shale resources. Chem. And Eng. News June 10, 17-19.

Harbert, J. P., Berg, W. A. and McWhorter, D. (1978) Vegetative stabilization of Paraho spent oil shales. Annual Report. EPA-600/7-78-021, USEPA, Cincinnati, Ohio.

Jukkola, E. E., Denilauler, H. B. and Jensen, W. I. B. (1953) Thermal decomposition rates of carbonates in oil shale. Ind. And Eng. Chem. 45, 2711-2714.

Kilkelly, M. K., Berg, W. A. and Harbert, H. P. (1982) Field studies on USBM and Tosco II retorted oil shales: vegetation, moisture, salinity, and runoff, 1977-1980. Project Summary. EPA-600/S7-81-139, USEPA, Cincinnati, Ohio.

Leenheer, J. A. and Sutber, H. A. (1981) Migration through soil of organic solutes in an oil-shale process water. Environ. Sci. Technol. 15, 1467-1475.

Loughnan, F. C. (1969) Chemical Weathering Of The Silicate Minerals. Elsevier, New York.

Okumura, M. and Kitano, Y, (1986) Coprecipitation of alkali metal ions with calcium carbonate. Geochim. Cosmochim. Acta 50, 49-58.

Park, W. C., Lindemanis, A. E. and Raab, G. S. (1979) Mineral changes during oil shale retorting. In Situ 4, 353-381.

Pereira, W. e., Rostad, C. E., Steinheimer, T. R., and Johson, S. M. (1981) Characterization of organic compounds associated with weathered, surface-retorted oil shale. J. Environ. Sci. Health A16, 571-587.

Ramirez, W. F., Ferrer, J. L., Morelli, P. J. and Peterson, W. R. (1985) Characterization of retorted oil shale and application to a model of leachate generation and transport. In Situ 9, 91-117.

Reddy, K. J. and Lindsay, W. L. (1986) The solubility relationships of calcium and magnesium minerals in processed oil shales. J. Environ. Qual. 15, 1-4.

Reddy, K. J., Lindsay, W. L., Boyle, F. W., and Redente, E. F. (1986) Solubility relationships and mineral transformations associated with recarbonation of retorted shales. J. Environ. Qual. 15, 129-133.

Richardson, S. G., McKell, C. M., George, M. R. and Gray, G. (1981) Weathering effects on some chemical and physical properties of retorted oil shale. J. Environ. Qual. 10, 221-224.

Skogerboe, R. K., Berg, W. A. and McWhorter, D. B. (1979) Field level characterization of solid residues from oil shale retorting. In Symposium On Potential Health And Environmental Effects Of Synthetic Fuel Technologies, 193-198. Oak Ridge National Laboratory, Oak Ridge, Tennessee.

Stark, J. M. and Redente, E. F. (1986) Trace element and salt movement in retorted oil shale disposal sites. J. Environ. Qual. 15, 282-288.

Stollenwork, K. G. and Runnells, D. D. (1981) Composition of leachate from surface-retorted and unretorted Colorado oil shale. Environ. Sci. Technol. 15, 1340-1346.

Tang, J. and Yen, T. F. (1979) Mining processes. In Compendium Reports On Oil Shale Technology (Slawson, G. C. and Yen, T. F., Eds.), 29-43. EPA-600/7-79-039, USEPA, Las Vegas, Nevada.

Trujillo, F. J., Grant, C. L., Taylor, H. E., Miller, M. M. and Skogerboe, R. K. (1981) Comparison of laboratory methods for studying leaching of retorted oil shale. In Proceedings Of Symposium Of Surface Mining Hydrology, Sedimentology, And Reclamation, 451-456. University of Kentucky, Lexington, KY.

Wen, C. S. and Yen, T. F. (1979) Kerogen recovery processes. In Compendium Reports On Oil Shale Technology (Slawson, G. C. and Yen, T. F., Eds.), 44-68. EPA-600/7-79-039, USEPA, Las Vegas Nevada.

Wildung, R. E. and Zachara, J. M. (1981) Geochemistry of oil shale solid waste disposal. In Oil Shale: The Environmental Challenges (Edited by Peterson, K. K.), 201-252. Colorado School of Mines, Golden, Colo.

Yen, T. F. (1979) Overview of oil shale development. In Compendium Reports On Oil Shale Technology (Slawson, G. C. and Yen, T. F., Eds.), 1-27. EPA-600/7-79-039, USEPA, Las Vegas, Nevada.